INVESTIGATIONS OF METABASITES FROM THE ASHE METAMORPHIC SUITE, EASTERN BLUE RIDGE PROVINCE, NORTH CAROLINA. ARE AMPHIBOLITES NEAR BOONE RETROGRESSED ECLOGITES?

by

Matthew Goulding Guilin

A thesis submitted to the faculty of
The University of North Carolina at Charlotte
in partial fulfillment of the requirements
for the degree of Master of Science in
Earth Science

Charlotte

2019

Approved by:

_____
Dr. Andy Bobyarchick

_____
Dr. Céline Martin

_____
Dr. Valerie Reynolds

ABSTRACT

MATTHEW GOULDING GUILIN. Investigations of metabasites from the Ashe Metamorphic Suite, Eastern Blue Ridge Province, North Carolina. Are amphibolites near Boone retrogressed eclogites? (Under the direction of DR. ANDY BOBYARCHICK)

The Ashe Metamorphic Suite in western North Carolina hosts metabasites ranging in grade from eclogite to amphibolite. To the west of the Grandfather Mountain Window (GMW) near Bakersville, retrograded eclogites, displaying primary eclogite-facies paragenesis are juxtaposed against lower-grade amphibolites. Across the GMW 65 km to the northeast near Boone, foliated amphibolites are in the same structural position have previously been interpreted to be retrograded eclogites. Their inference as retrogressed eclogites is questionable because they are not in direct contact with fresh eclogite, nor do they display any primary high-pressure relics like omphacite. In order to test the hypothesis that the foliated garnet amphibolites near Boone are retrograded eclogites, the amphibolites were investigated for high pressure features (e.g., omphacite inclusions in garnet) using quantitative major element mapping, thermobarometry, and petrography. Additionally, a series of samples from Bakersville displaying varying degrees of altered eclogite were similarly investigated to better understand their metamorphic evolution. Results from the Boone amphibolites show that garnet inclusions contain sodic plagioclase and lack omphacite which suggests that they are not eclogite relics. This finding, along with no observations of matrix omphacite relics suggests that these rocks are not retrogressed eclogites, which is in disagreement with previous studies. New late retrograde P-T estimates for the Boone metabasites straddle granulite and amphibolite facies ranging from 9-5 kbars and 750-600 °C. For the Bakersville samples, new P-T estimates based on symplectite formation adjacent to primary omphacite range from 700-550 °C and 16-6 kbar which is in general agreement with previous studies. New P-T estimates based on spongy CPX with the same assemblage of symplectites after omphacite suggest a hotter decompression path ranging from 800-565 °C and

16-4.5 kbar. Finally, new estimates of kelyphite formation range from 10-5.5 kbar and 825-625 °C and suggest an influx of heat along the decompression path.

TABLE OF CONTENTS

LIST OF TABLES

LSIT OF FIGURES

LIST OF EQUATIONS

LIST OF ABBREVIATIONS

[]	Cation Vacancy
Ab	Albite
Al	Aluminum
Alm	Almandine Garnet
AM	Amphibole/Amphibolite Facies
AM-EC	Amphibolite Eclogite Facies
AMP	Amphibole
AMS	Ashe Metamorphic Suite
An	Anorthite
Ca	Calcium
CPX	Clinopyroxene
Cr	Chromium
Di	Diopside
EBR	Eastern Blue Ridge
EP-AM	Epidote Amphibolite Facies
EPMA	Electron Probe Microanalysis
Fe	Iron
GMW	Grandfather Mountain Window
GR	Granulite Facies
Grt	Garnet
Grs	Grossular Garnet
GS	Greenschist Facies
Hbl	Hornblende
HGR	High-Pressure Granulite Facies

HP	High-Pressure (Metamorphism)
Jd	Jadeite
K	Potassium
Kbar	Kilobar
Km	Kilometer
Ma	Million Years Ago
Mg	Magnesium
Mn	Manganese
Na	Sodium
NAM	Nominally Anhydrous Mineral
OPX	Orthopyroxene
Pl	Plagioclase Feldspar
PPL	Plane-polarized light
Prp	Pyrope Garnet
Qtz	Quartz
SGS	Sub-greenschist Facies
Si	Silicon
Sps	Spessertine Garnet
Ti	Titanium
UHP	Ultra High-Pressure (Metamorphism)
WBR	Western Blue Ridge
WDS	Wavelength Dispersive Spectroscopy
XPL	Cross-polarized light

1: INTRODUCTION

Metabasites (i.e., mafic metamorphic rocks) of different grades (e.g., eclogite, amphibolite, granulite) are commonly found next to each other. This can be explained by faulting or metamorphic alteration of one to the other. Unraveling the relationship yields important insights into our understanding of exhumation mechanisms (Bridgeman, 2015) and deep crustal processes (Austreim, 1987). In western North Carolina, high-grade metabasites occur in the Ashe Metamorphic Suite at the base of the Eastern Blue Ridge Province (Fig 1). West of the Grandfather Mountain Window (GMW) and near Bakersville, eclogite and amphibolite occur within the same outcrop (Fig 1). 65 km to the northeast near Boone, NC, foliated garnet amphibolites have been interpreted to be retrogressed eclogite based because they are in the same structural position as the Bakersville eclogites and because they display microtextures known as symplectites, which have been widely recognized as evidence of previous high-pressure conditions. The peak metamorphic conditions experienced by the latter rocks are ambiguous considering they are not in contact with any known unaltered eclogite body and don't display any primary eclogite-facies phases like omphacite pyroxene. If the amphibolites near Boone are altered eclogite, then it would be expected that they contain eclogite relics like omphacite as inclusions in garnet unless the eclogites experienced complete reequilibration. To understand the metamorphic evolution of high-grade metabasites from Boone and retrograde alteration of eclogite from Bakersville, samples from each outcrop were investigated using high-resolution quantitative EPMA element maps obtained by electron probe microanalysis (EPMA) in addition to petrography and thermobarometry.

1.1 Microtextures in Metabasites

High-grade metabasites (e.g., eclogites, high-pressure granulites) commonly display evidence of retrogression such as transformations occurring during exhumation like reaction textures and chemical zoning. Examples are symplectite and kelyphite, which serve as important indicators for the evolution of the chemistry, pressure, and temperature (X, P, T) of subducted lithosphere during its exhumation (Schmädicke et al., 1992; Janák et al., 1996; Lanari et al., 2013; Martin, 2018) in addition to exhumation rates (Anderson and Moecher, 2009).

Symplectites are fine-grained intergrowths of multiple minerals and when found within eclogites and high-pressure granulites, have been interpreted as evidence for retrograde metamorphic overprinting (Eskola, 1921; Abbot and Greenwood, 2001; Shervais et al., 2003; Anderson and Moecher, 2007). The formation of symplectites was first attributed to decompression. Symplectites composed of diopside and sodium-rich plagioclase (Di-Pl symplectite) were first observed in Norwegian Caledonian eclogites and their formation has been explained by the breakdown of unstable jadeite component in omphacite upon decompression during exhumation (Eskola, 1921).

Additionally, symplectites may indicate temperature changes in exhumation environments. In a study of eclogites from the Central Scandinavian Caledonides, symplectites at the grain-edges of omphacite occurred as two distinct grain sizes (Boland and van Roermund, 1983). It was determined that the two different grain sizes recorded two distinct stages of cooling wherein the coarser-grained symplectitc domains formed at higher temperatures than the finer-grained symplectitc domains (Boland and van Roermund, 1983).

Recently, it has been shown that water plays a role in symplectite formation (Martin and Duchene, 2015; Spruzeniece et al., 2017). Experiments that subjected feldspar-rich samples to brines enriched in ^{18}O under heat and pressure for varying periods of time revealed that radial symplectic microtextures formed at grain boundaries around the rims of samples, and showed that a water-facilitated dissolution-precipitation mechanism involving multiple phases was responsible for the reaction (Spruzeniece et al., 2017). Additionally, in a study of eclogites from the Western Gneiss Region (WGR) of Norway, it was determined that the formation of anhydrous symplectites was facilitated by available water that was freed from the breakdown of the hydrous mica-mineral phengite (Martin and Duchene, 2015).

Similar to symplectites, kelyphites are fine-grained polymineralic intergrowths that surround garnet and radiate outwardly from its surface. They are the result of a decomposition reaction involving garnet and nearby minerals upon decompression (Obata, 1994). Examples in olivine-bearing garnet peridotites derived from the mantle exhibit anhydrous assemblages (e.g., spinel + pyroxene (Obata, 1994) while those in subducted metabasites like eclogite, exhibit hydrous assemblages (e.g., plagioclase + amphibole) that formed in amphibolite facies conditions from an influx of external fluid (Martin, 2018). Similarly, amphibole-bearing symplectites after omphacite also exist (Anderson and Moecher, 2007; Lanari et al., 2013; Martin, 2018). In studies of eclogites from the Himalayas and Norway, it was found that hydrous symplectites formed continuously from the onset of plagioclase stability though granulite facies and ending in amphibolite facies conditions (Lanari et al., 2013; Martin, 2018).

Sources of water for the formation of these microtextures can be described as either *internal* or *external.* Internal sources associated with the formation of symplectites include localized fluid released from the breakdown of hydrous minerals like phengite (Martin and Duchêne, 2015), fluid inclusions trapped during prograde metamorphism (Vallis and Scambelluri, 1996), and nominally anhydrous minerals (NAM) like omphacite (Anderson and Moecher, 2007). In the case of omphacite, it is thought that hydroxyl ions stored in cation vacancies (Smyth, 1991) are the source of water.

External sources are associated with a late stage of retrogression involving the formation of hydrous symplectic assemblages from earlier stage anhydrous assemblages (Yang, 2004). In high-grade metabasites, kelyphites have been associated with influxes of external fluid (Martin, 2018), which may come from the dehydration of surrounding rocks (Austreim, 1987).

In the Eastern Blue Ridge Province of the southern Appalachians, microtextures (e.g., symplectites) have been instrumental in unraveling the PT-conditions and tectonics of subducted slabs. In high-grade metabasites near Boone, NC, post-peak eclogite PT-conditions were estimated using reintegrated compositions of symplectite in the absence of available omphacite (Abbot and Greenwood, 2001). Furthermore, Anderson and Moecher (2007) correlated textural differences in symplectite to differences in exhumation rate. In a comparison between vermicular (i.e., worm-like texture) symplectites from the WGR, and lamellar symplectites of the EBR, it was determined that the former resulted from a high degree of overstepping (i.e., the degree to which the rocks experienced conditions beyond their stability fields) associated with rapid

exhumation, while the latter resulted from a lower degree of overstepping associated with slower exhumation (Anderson and Moecher, 2007).

1.2 Geologic Setting and Previous Work

In western North Carolina the Appalachian Blue Ridge complex records the accretion of various terranes onto the Laurentian (i.e., ancient North America) margin associated with the closure of the Iapetus Ocean (Hatcher, 2010). The Western Blue Ridge (WBR) is represented by Grenville-aged (Middle Proterozoic) basement gneisses and metasediment cover sequences of the Laurentian margin that are juxtaposed against accreted terranes of the Central and Eastern Blue Ridge (EBR) Provinces (Hatcher, 2010). West of the Grandfather Mountain Window, that exposes Laurentian basement rocks and Late Proterozoic rift facies sedimentary and volcanic cover sequences, the WBR-EBR boundary is marked by the Devonian dextral strike-slip Burnsville fault (Trupe et al., 2003). High-grade metamorphic rocks within shear zones adjacent to this fault include unaltered and retrograded eclogites and amphibolites close to the GMW near Bakersville (Willard and Adams, 1994), and garnet-granulites further to the southwest at Winding-Stair Gap (Moecher et al., 2004). North of the GMW, the WBR-EBR boundary is marked by the northwest-verging, Taconic-aged Gossan-Lead fault (Abbot and Raymond, 1984) that shows kinematic evidence of strike-slip motion preceding thrusting, and that it is a continuation of the Burnsville fault (Levine et al., 2018). Within close vicinity to this fault, banded garnet metabasites north of Boone, NC have been interpreted as retrograded eclogites.

The aforementioned eclogites and amphibolites belong to the Ashe Metamorphic Suite, an accretionary mélange (Willard and Adams, 1994; Page et al., 2003; Anderson,

2009) made up of metabasites, metapelites, and minor ultramafic rocks (McSween et al., 1989; Misra and Conte, 1991). At the WBR-EBR boundary, high-grade metabasites of the AMS have MORB-like bulk chemistries (Misra and Conte, 1991; Abbot and Greenwood, 2001) and record Taconic-aged (Middle Ordovician) prograde metamorphism, in addition to Acadian (Silurian-Devonian), and Alleghenian (Carboniferous-Permian) retrograde overprints (Stewart et al., 1995; Goldberg and Dallmeyer, 1997; Miller et al., 2010). In North Carolina, two locations of retrograde eclogite have been described (Fig 1): West of the GMW, in Bakersville, and north of the GMW, near Boone (Willard and Adams, 1994; Abbot and Greenwood, 2001; Anderson and Moecher, 2009).

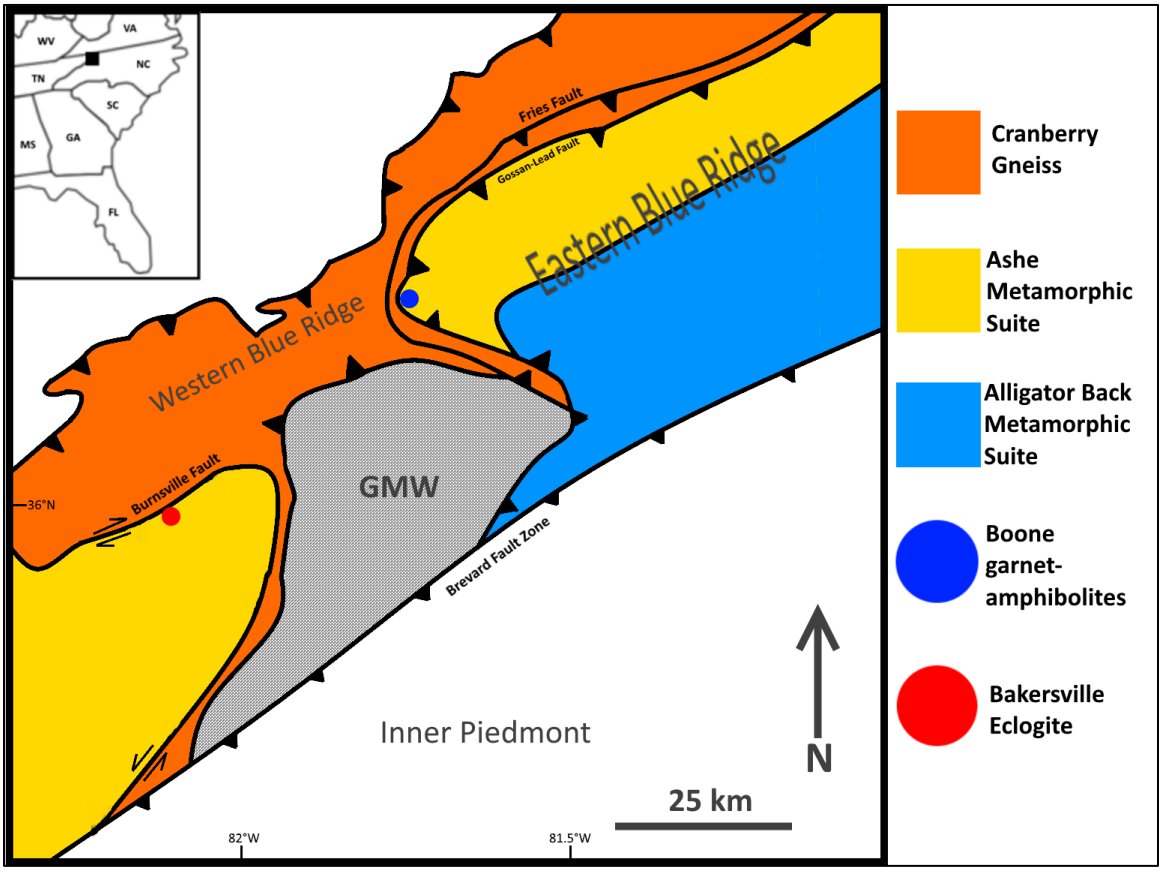

Figure 1: Simplified map(modified after Page et al., 2003) showing locations of Boone and Bakersville eclogites.

Bakersville outcrops display fresh and partially retrograded eclogites (Willard and Adams, 1994) that retain a metamorphic peak assemblage made of omphacite pyroxene, garnet, quartz, and rutile. This paragenesis is overprinted by retrograde Di-Pl symplectite, hornblende, plagioclase, titanite, and epidote (Anderson and Moecher, 2009). The PT evolution of these rocks has been developed iteratively by many workers and resembles a hairpin-shaped clockwise path (Fig 2) that starts in amphibolite facies, peaks at eclogite facies and decompresses nearly isothermally through granulite facies. (Willard and Adams, 1994; Page et al., 2003; Anderson and Moecher, 2009). Peak pressures are not well-constrained, but a lack of coesite and little-to no Calcium Eskola (CaEs) component in reintegrated peak pyroxenes suggest that these rocks have not experienced ultrahigh pressures (≥2.5 GPa) (Page et al., 2005) that could have been associated with the subduction of continental crust (Liou et al., 2004). Finally, a study by Bridgeman (2015) found that differential zircon ages between eclogite and surrounding amphibolite suggest that the former were emplaced into the latter as part of circulatory flow exhumation within a subduction channel. A summary of P-T estimates is presented in Table 1.

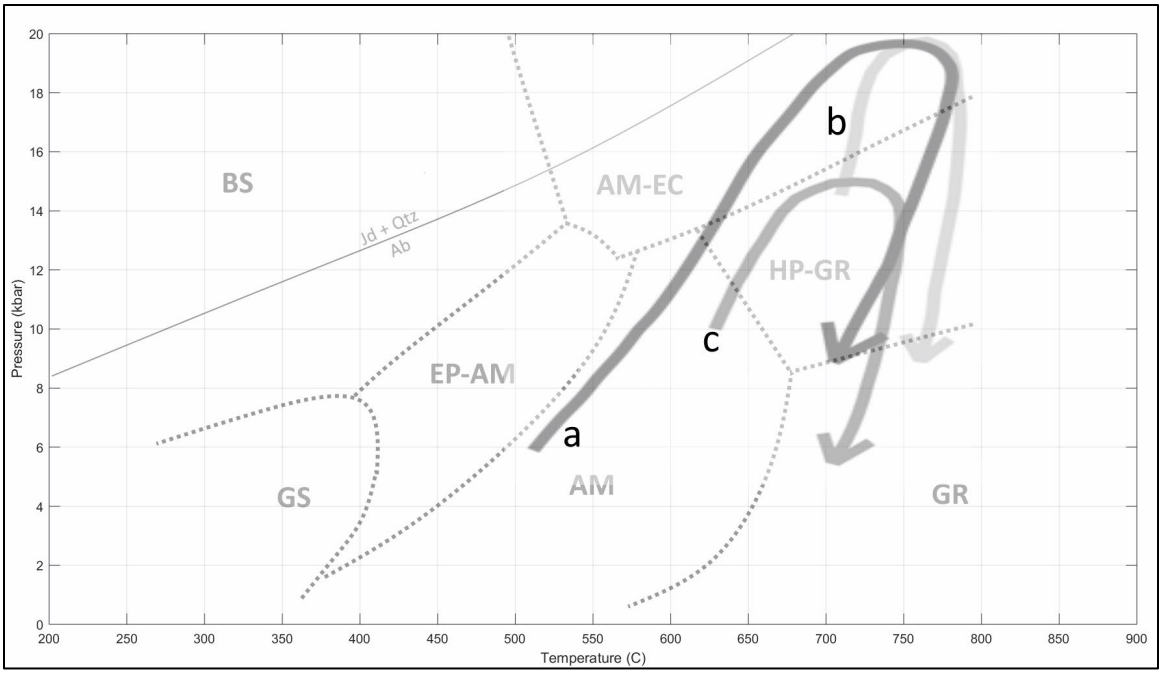

Figure 2: Suggested P-T paths modified from Anderson and Moecher, 2009. a) Bakersville partially retrograded eclogite; b) garnet amphibolites ("retrogressed eclogites") from near Boone; c) Dellwood garnet granulites. Metamorphic facies abbreviations are as follows: AM amphibolite; AM-EC amphibole eclogite; BS blueschist; EP-AM epidote amphibolite; GR granulite; GS greenschist; HP-GR high pressure granulite

Table 1: Summary of PT estimates for Bakersville (Lick Ridge) retrograde eclogite. Thermocalc and TWQ are multi-equilibrium phase modelling applications.

	Assemblage	Method	Estimates	Reference
Prograde	Inclusions in garnet: clinozoisite, titanite, rutile, quartz	Thermocalc	6-12 kbar 400-680°C	Page et al., 2003
Prograde	Inclusions in garnet: Hornblende, biotite, quartz	Thermocalc	13-16 kbar 630-680°C	Page et al., 2003
Peak*	Garnet-pyroxene	Thermocalc Thermometry (Ravna, 2000a)	17 kbar at 700–750°C	Page et al., 2003
Retrograde	Garnet rim, hornblende, plagioclase, quartz	TWQ	13-15 kbar 725-800°C	Anderson and Moecher, 2009
Retrograde	Hornblende, cpx, plagioclase symplectite	Hbl-Pl Barometry (Holland and Blundy, 1994) TWQ	16 – 9 kbar 690 –775°C	Anderson and Moecher, 2009
Retrograde	Grt, Cpx, Opx, Qtz, Pl	Thermocalc	700 – 760 °C 11- 16 kbar	Page et al., 2003

The Boone outcrop is characterized by amphibole-bearing garnet granulites, designated as retrograded eclogites by Abbot and Greenwood (2001). They display calcic hornblende, garnet grains rimmed by plagioclase, and Di-Pl ± Am symplectites in suspected replacement of omphacite grains (Abbott and Greenwood, 2001). Their PT evolution follows a clockwise path that goes through amphibolite facies, peaks at eclogite

facies, and decompresses nearly isothermally through granulite facies (Fig 2). A summary of estimates is presented in Table 2.

Table 2: Summary of PT estimates for Boone retrograde eclogite

	Assemblage	Method	Estimates	Reference
Prograde	Inclusions in garnet: Hornblende, quartz	TWQ	14-17 kbar 625-750°C	Anderson and Moecher, 2009
Peak*	Omphacite (reconstructed from Di-Pl symplectite), garnet	TWQ	18 kbar 775°C	Anderson and Moecher, 2009
Retrograde	Garnet rim, hornblende, plagioclase	TWQ	10-13 kbar 725-825°C	Anderson and Moecher, 2009

2: METHODS

Element mapping of high-grade metabasites has been shown to elucidate localized polymetamorphic patterns that can be linked to large-scale processes (Lanari et al., 2013). In order to gain a better understanding of the exhumation-related evolution of the Eastern Blue Ridge, a combination of high-resolution quantitative element mapping and geothermobarometry was applied to variably retrogressed eclogites to obtain new pressure-temperature (PT) estimates of the metabasites.

2.1 Sampling Strategy

Samples of retrogressed high-grade metabasite belonging to the EBR were collected from two locations (Fig 3):

(1) Area north of Boone, NC (hereby referred to as Boone metabasite)

(2) Bakersville, NC

Eleven samples of Boone metabasite (garnet amphibolite) were selected from loose blocks on two distinct outcrops located approximately 3.5 km NNW of Boone, North Carolina: four from the northern outcrop (Howard's Creek Rd just east of Tater Hill Rd) and seven from the southern outcrop (on Junaluska Rd. 1.5 mile SSE from northern outcrop) In order to study sources of fluid on the effects of retrograde metamorphic reactions, efforts were made to sample pieces with and without apparent hydrothermal features (e.g., veins). Of the eleven initial samples collected, nine areas were selected for *in situ* major element mapping by electron probe microanalysis (EPMA). Eight representative samples, four from each outcrop, were selected for whole-rock analysis for major and trace elements by inductively coupled plasma mass spectrometry (ICP-MS).

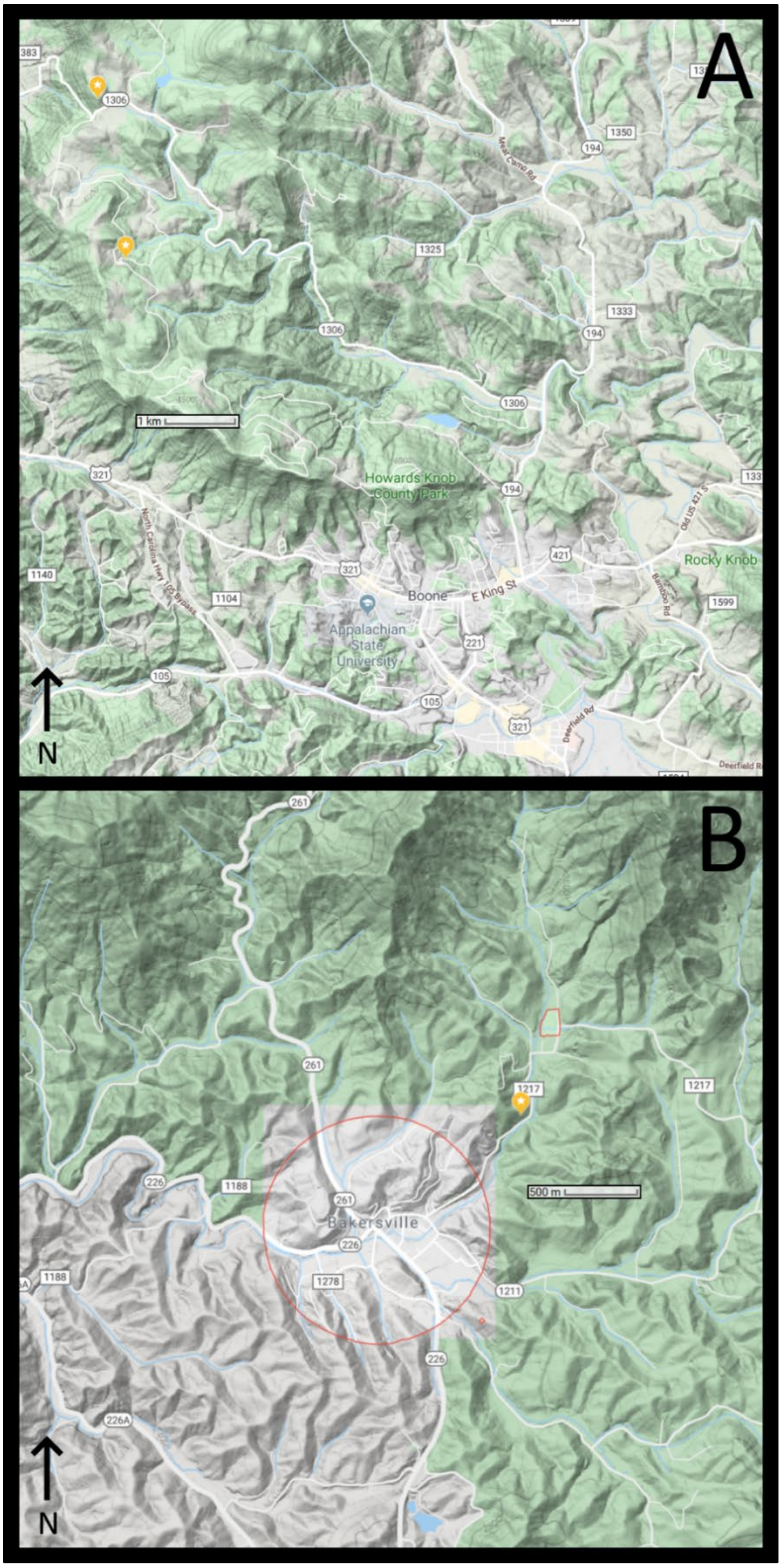

Figure 3: Sample locations. A) Map showing two outcrops (yellow markers) near Boone, NC where metabasites were collected. B) Map showing location (yellow marker) where metabasite samples were collected at Bakersville, NC.

At Bakersville, five samples were collected from a roadside outcrop on McKinney Cove Road where relatively pristine eclogite grades to amphibolite approaching a small (~ 6cm) felsic vein. At the outcrop scale, the contacts and relationships among different lithologies are largely indistinguishable due to substantial surficial weatheing and vegetative obstruction. Efforts were made to collect samples close-to and away-from the felsic intrusion to see it's affects on alteration. Of the five samples, twelve thin sections were made, wherein four representative areas were mapped. Four bulk samples were selected for whole-rock major and trace element ICP-MS analysis.

2.2 Quantitative Element Mapping

EPMA X-ray mapping for major elements was carried-out using a Cameca SX100 microprobe at the American Museum of Natural History in New York City, NY. The elements analyzed and their respective calibration standards are as follows: Na, Al (jadeite); Mg, Si, Ca (Wakefield diopside); K (potassium feldspar); Ti (synthetic rutile); Cr (magnesiochromite); Mn (rhodonite); Fe (synthetic fayalite).

The production of quantitative maps can be generally described by a two-step process. First, semi-quantitative element intensity maps are obtained using wavelength dispersive spectrometry with an electron beam voltage of 15 KeV, current of 80 nA, and a spot dwell time of around 200-300 ms. In order to accommodate analysis of ten major elements, two scanning passes are required, each for the analysis of five different elements. Na and K were analyzed in the first pass due to their sensitivity to the electron beam and tendency to migrate. Second, transects of quantitative spot analyses (profiles) are conducted within each mapped area with efforts to capture the composition of each phase. Compared to the semi-quantitative analysis, these require the same voltage (15 KeV), less current (10-20 nA), and a much longer dwell time (~40s). The quantitative analyses are used as internal standards to produce major element oxide percentages of each semi-quantitative analysis (pixel) of the map. This two-step process allows

for the acquisition of quantitative chemical maps in the fraction of the time than it would using high-dwell time spot analyses to construct element maps alone.

The processing and map standardization were carried-out using the MATLAB-based software XMapTools 2.5.2 (Lanari et al., 2014). Processing begins with the classification of pixels into corresponding mineral phases. This is done using a semi-automatic grouping function that requires user selection and identification of mineral phases. Next, borders between mineral phases are *masked* (i.e., removed) in order to avoid erroneous signals caused by mixing. From there, the positions of the internal standards are checked to make sure they match with corresponding phases and are adjusted accordingly. Then the semiquantitative *background* compositional values are manually calibrated, element by element, to the internal standards using linear regression, resulting in maps of element oxide weight percentages. After that, structural formulae (i.e., end-member components) are calculated for each classified pixel and appropriate geothermobarometers may be applied.

2.3 Thermobarometry

The XMapTools function *map mode* allows for the application of user-selected thermometers, barometers, or combinations of each to appropriately classified pixels. This method was applied to amphibole pixels interpreted to be in equilibrium with plagioclase and quartz using a combination of the thermometer of Holland and Blundy (1994) and the barometer of Schmidt (1992). The function calculates estimates based on the formula compositions of classified plagioclase and amphibole pixels that have been interpreted to be in equilibrium. The composition of plagioclase that is used remains as a fixed albite component percentage, inputted by the user, while amphibole formula composition is taken automatically from amphibole pixels. In this manner, variations in pressure-temperature estimates are dependent on variations in amphibole formula compositions and can be mapped to amphibole pixels accordingly.

The amphibole-plagioclase thermometer of Holland and Blundy (1994) is suitable to use on calcic amphiboles, like the ones of this study. The equilibrium assemblage on which it's based, and corresponding formula are as follows:

Edenite + 4 quartz = tremolite + albite

$NaCa_2Mg_5Si_4(AlSi_3)O_{22}(OH)_2 + 4SiO_2 = Ca_2Mg_5Si_8O_{22}(OH)_2 + NaAlSi_3O_8$

$$T = \frac{-76.95+0.79P+Y_{ab}+39.4X_{Na}^{A}+22.4X_{K}^{A}+(41.5-2.89P)*X_{Al}^{M2}}{-0.0650-R*ln\left(\frac{27*X^{A}\,X_{Si}^{T1}*X_{ab}^{plag}}{256*X_{Na}^{A}*X_{Al}^{T1}}\right)} \quad (1)$$

Where Y_{ab} is given by: for $X_{ab} > 0.5$ then $Y_{ab}=0$, otherwise $Y_{ab}=12.0(1-X_{ab})^2-3.0$ kj (Holland and Blundy, 1994)

The crystallographic sites in amphibole and corresponding cations are as follows (Table 3)

Table 3: Crystallographic sites in amphibole

Amphibole						
Crystallographic Site	A	M4	M13	M2	T2	T1
Cations	K, Na, []	Ca, Na, Mn, (Fe^{2+}, Mg)	Mg, Fe^{2+}, (Mn)	Al^{vi}, Fe^{3+}, Ti, Cr, +(Mg, Fe^{2+})	Si, Al^{iv}	Si

The XMapTools function *spot mode* allows pressure-temperature estimates to be calculated from two adjacent phases in chemical equilibrium. After selecting the appropriate thermometer, areas in corresponding phases were used to calculate average temperature

estimates. This method was applied separately to amphibole-garnet and clinopyroxene-garnet pairs. The garnet-hornblende thermometer of Ravna (2000a) is based on the exchange of Fe^{2+} and Mg between garnet and hornblende. The relationship between temperature and element partitioning between the two phases is as follows:

$$T(℃) = \frac{1504+1784(X_{Ca}^{Grt}+ X_{Mn}^{Grt})}{\ln K_{D(Fe^{2+}/Mg)}^{Grt-Hbl}+0.720} - 273 \quad (2)$$

Where

$$K_{D(Fe^{2+}/Mg)}^{Grt-Hbl} = \frac{(Fe^{2+}/Mg)^{Grt}}{(Fe^{2+}/Mg)_{M1-M3}^{Hbl}}$$

$$X_{Ca}^{Grt} = \frac{Ca}{Ca + Mn + Fe^{2+} + Mg} in\ garnet$$

$$X_{Mn}^{Grt} = \frac{Mn}{Ca + Mn + Fe^{2+} + Mg} in\ garnet$$

The garnet-clinopyroxene thermometer of Ravna (2000b) is based on the exchange of Fe^{2+} and Mg between garnet and clinopyroxene at equilibrium. The relationship between temperature and element partitioning between the two phases is as follows:

$$T(℃) = \frac{\left(1939.9+3270X_{Ca}^{Grt}-1396\left(X_{Ca}^{Grt}\right)^2+3319X_{Mn}^{Grt}-3535\left(X_{Mn}^{Grt}\right)^2+1105X_{Mg\#}^{Grt}-3561\left(X_{Mg\#}^{Grt}\right)^2+2324\left(X_{Mg\#}^{Grt}\right)^3+169.4\ P(GPa)\right)}{(lnK_D+1.223))} - 273 \quad (3)$$

Where

$$K_D = \frac{(Fe^{2+}/Mg)^{Grt}}{(Fe^{2+}/Mg)^{Cpx}}$$

$$X_{Ca}^{Grt} = \frac{Ca}{Ca + Mn + Fe^{2+} + Mg} in\ garnet$$

$$X_{Mn}^{Grt} = \frac{Mn}{Ca + Mn + Fe^{2+} + Mg} in\ garnet$$

$$X_{Mg\#}^{Grt} = \frac{Mg}{Mg + Fe^{2+}} in\ garnet$$

$$Mg\# = \frac{100 * Mg}{Mg + Fe^{2+}}$$

(Ravna, 2000b)

The barometer of Schmidt (1992) is based on the total amount of Al (Al^{tot}) in hornblende and relies on the *Tschermak*-exchange ($^{VI}Mg^{2+}\ ^{IV}Si^{4+} <\!\!-\!\!> {}^{VI}Al^{3+}\ ^{IV}Al^{3+}$). Based on experiments on amphibole-bearing tonalites, it was shown that with increasing pressure, Al content in amphibole increases while Mg content decreases. Despite the lithological differences between amphibole-bearing tonalites and amphibolites, the late retrograde assemblage (am-pl-qtz) found in amphibolites is similar to that of amphibole-bearing tonalites.

$$P(\pm 0.6\ kbar) = -3.01 + 4.76\ Al_{hbl}^{tot} \quad (4)$$

(Schmidt, 1992):

3: SAMPLE DESCRIPTIONS

3.1 Boone Hand Samples

Samples from both outcrops display variable millimetric dark-colored layers of black amphibole, dark-green Di-Pl symplectite and garnet and, more rarely, millimetric felsic layers composed of quartz and plagioclase (Fig 4A, B). Where quartz layers exist, they are bounded by sub-millimetric garnet aggregate (Fig 4B). Euhedral to subhedral garnets up to a millimeter in diameter are distributed evenly throughout the matrix and locally as millimetric garnet aggregate layers (Fig 4C, D). Accessory phases include epidote and titanite-rimmed ilmenite and anhedral pyrite.

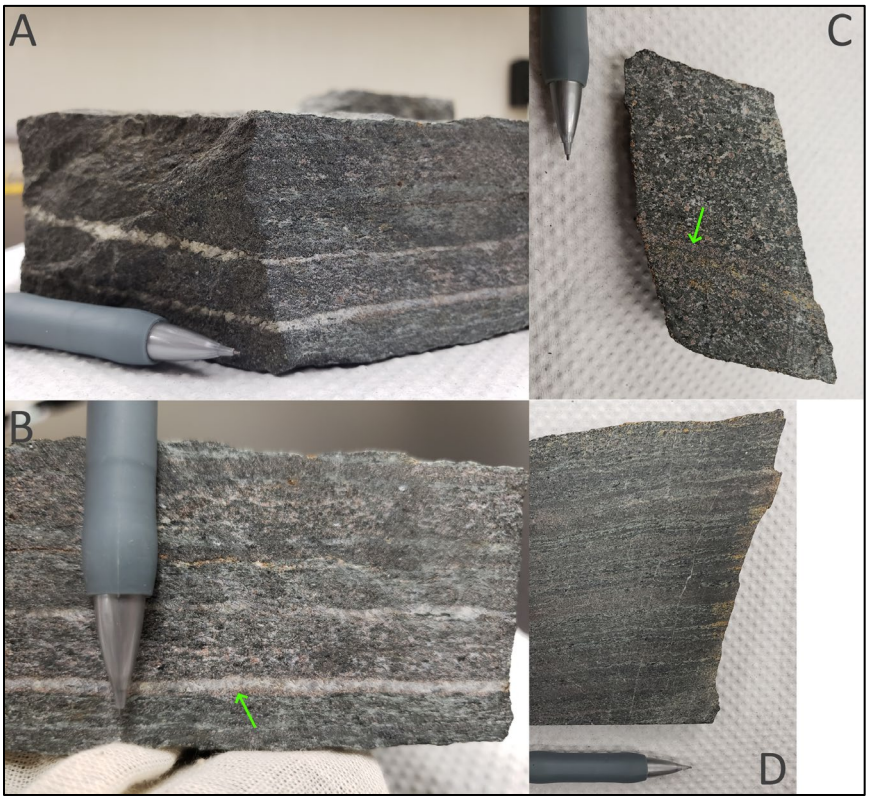

Figure 4: Macroscopic description of samples from near Boone. A) Isometric view of sample from the southern outcrop (bjm418) with millimetric quartz layers. B) Close view of quartz layers outlined by aggregates sub-millimetric garnet (green arrow) (sample bjm418). C) A representative sample from the northern outcrop showing euhedral garnets up to a millimeter in diameter with white plagioclase coronas. Green arrow points to garnet aggregate layer. D) Another sample from the southern outcrop(bjm618) shows pronounced millimetric layering of black amphibole, green Di-Pl symplectite, and pink garnet aggregates.

3.2 Boone Petrography

Samples from both outcrops display variable layering with near identical mineralogy, with the difference being that the northern outcrop displays abundant matrix epidote.

In a representative sample (bhcm418) from the northern outcrop, weak layering is defined by concentrations in either sub-millimetric anhedral garnet, medium-grained elongated patches of Di-Pl symplectite, medium-grained anhedral epidote, or green medium-grained anhedral-to-subhedral hornblende (Fig 5). Relatively large millimetric euhedral-to-subhedral garnets are surrounded by thin rims of plagioclase (Fig 5) while smaller anhedral examples are resorbed with thicker plagioclase coronas or medium-grained kelyphites of plagioclase and hornblende (Fig 6).

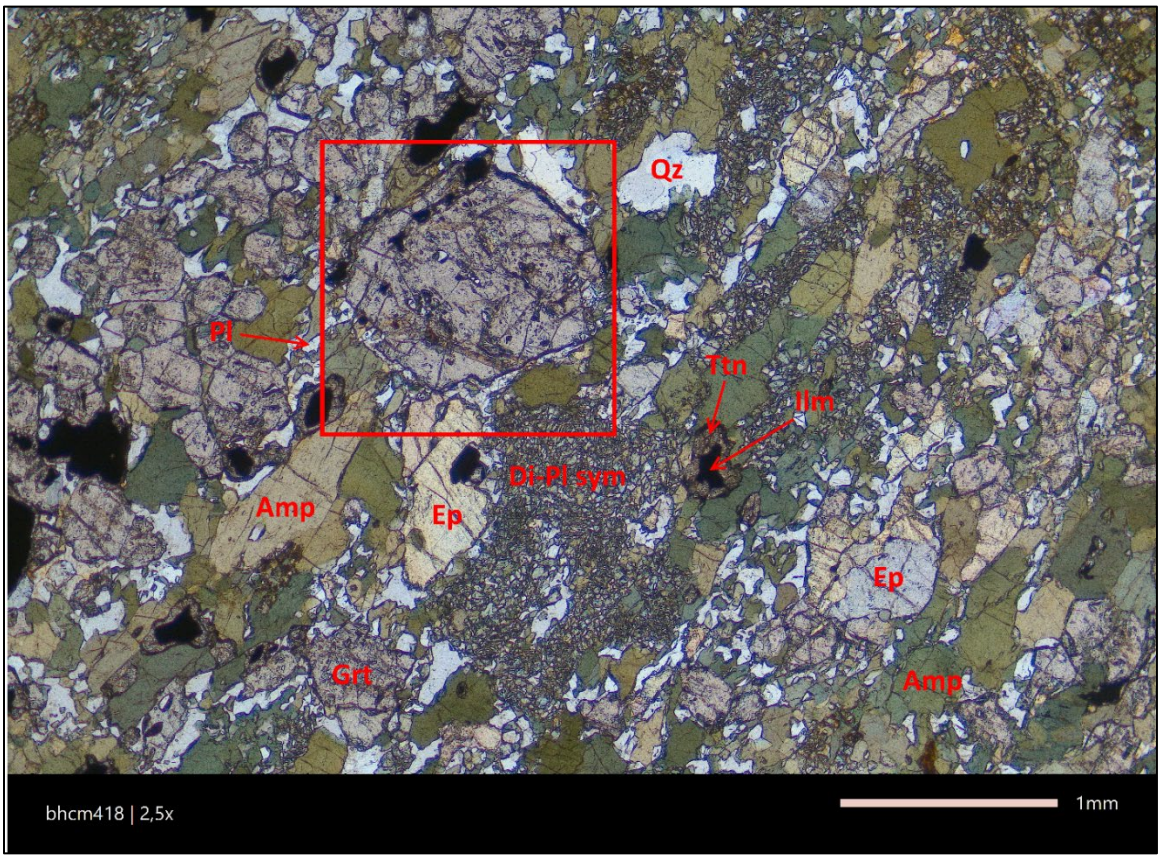

Figure 5: Photomicrograph of sample bhcm418m2 in PPl. Layers are defined by concentrations of various minerals including garnet, amphibole, di-pl symplectite, and epidote. Red outline shows area subjected to EPMA mapping (bhcm418m2). Abbreviation are as follows: Qz=quartz; Ttn=titanite; Grt=garnet; Amp=amphibole; Ep=epidote/zoisite; Ilm=ilmenite; Pl=plagioclase; Di-Pl sym=diopside-plagioclase symplectite.

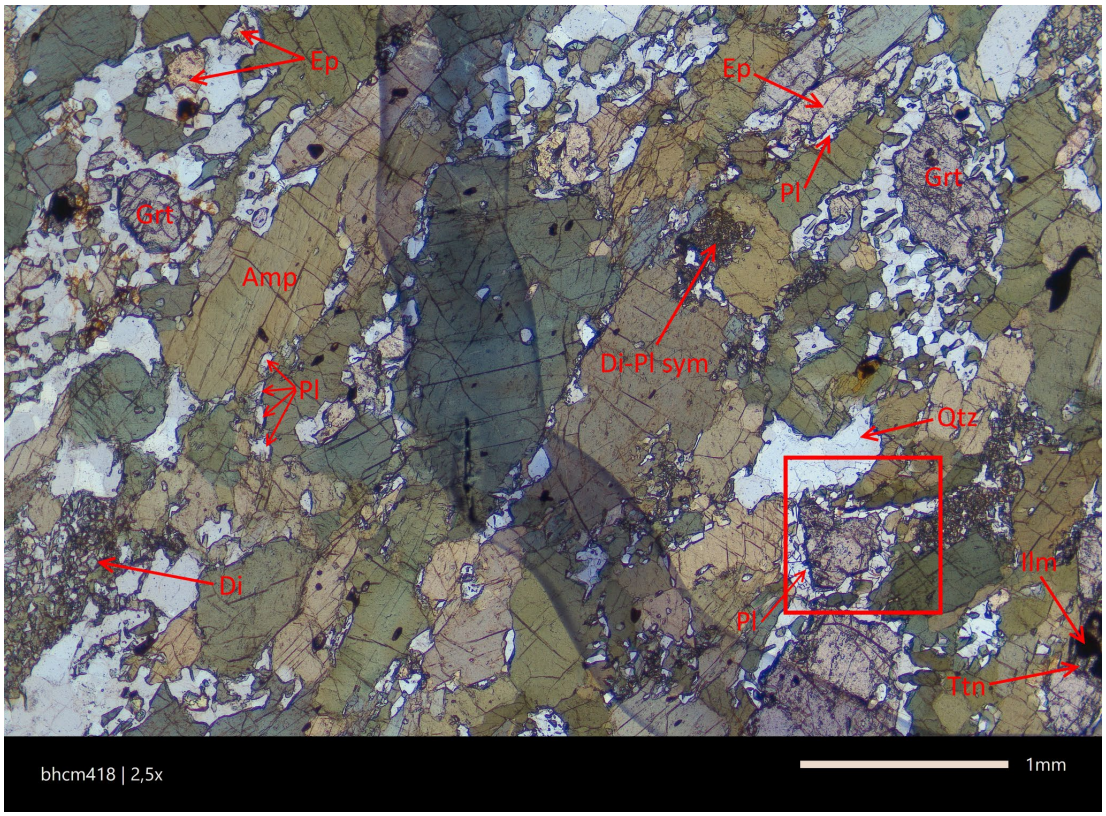

Figure 6: Photomicrograph of sample bhcm418m1 in PPL. Partially resorbed garnets are surrounded by thick plagioclase coronas and plagioclase-amphibole kelyphites (upper right). Beaded chains of plagioclase exist between amphibole grains. Red square depicts area subjected to EPMA mapping (bhcm418m1). Note dark semicircle at center of image is identification marker and does not represent natural color of sample. Grt=garnet; Amp=amphibole; Pl=plagioclase feldspar; Qtz=quartz; Ilm=ilmenite; Ttn=titanite; Di=diopside; Di-Pl sym=diopside-plagioclase symplectite; Ep=epidote.

A representative sample (bjm518) from the southern outcrop displays a change in texture and reduction in grain size leading up to a quartz layer (Fig 7). Away from the quartz layer, mineralogy consists of green medium-grained anhedral hornblende and sub-millimetric (100-300 µm) euhedral-to subhedral garnets that are frequently separated by thin slivers of plagioclase. Less frequent constituents include fine-grained ilmenite rimmed with titanite and medium-grained patches of quartz ± plagioclase. Approaching the quartz layer, hornblende is replaced by fine-grained vermicular symplectite of clinopyroxene, plagioclase, and hornblende while garnets ± ilmenite are concentrated in a tightly spaced aggregate parallel to the quartz layer. Fragments of the aforementioned symplectite are entrained within the quartz layer in addition to medium grained epidote rimmed with plagioclase and anhedral pyrite.

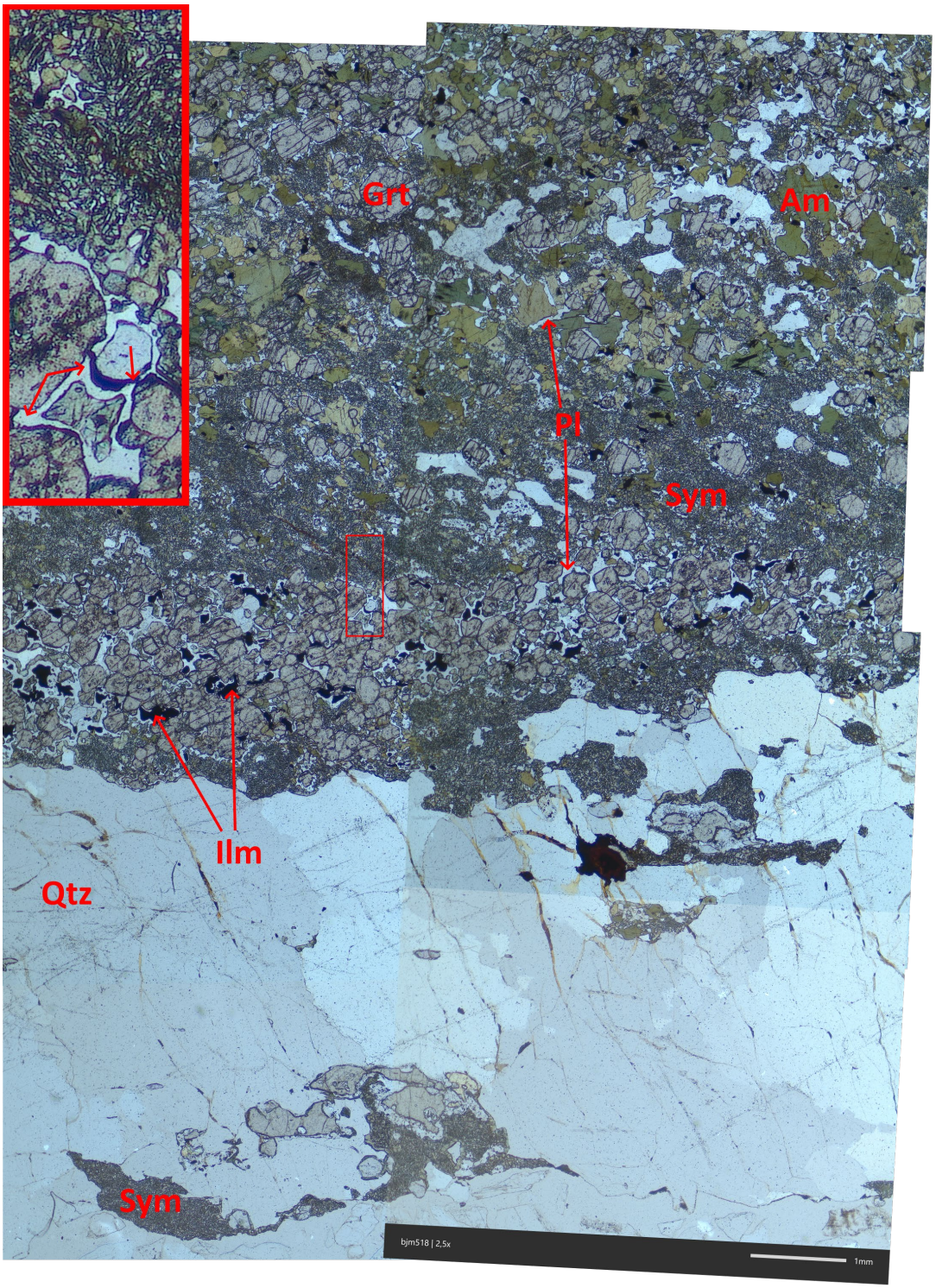

Figure 7: Photomicrograph mosaic of sample bjm518 from which two areas were sampled for quantitative mapping. A quartz layer is associated with garnet aggregate ± ilmenite that is adjacent to a domain of vermicular Di-Pl-Amp symplectite. Fragments of the surrounding symplectite have been entrapped within the quartz layer. Inset shows detailed texture. Arrows point to highly cuspate plagioclase. Map bjm518m1 is within garnet aggregate and bjm518m2 is within adjacent symplectite domain (actual locations not shown). Grt=garnet; Amp=amphibole; Pl=Plagioclase feldspar; Ilm=ilmenite; Sym=symplectite.

In addition to occurring as vermicular symplectite, clinopyroxene also takes the form of distinct medium-sized subhedral-to-anhedral grains hosting fine-grained lamellar inclusions of plagioclase and hornblende. These altered pyroxene grains are found in sample bjm218b (Fig 8).

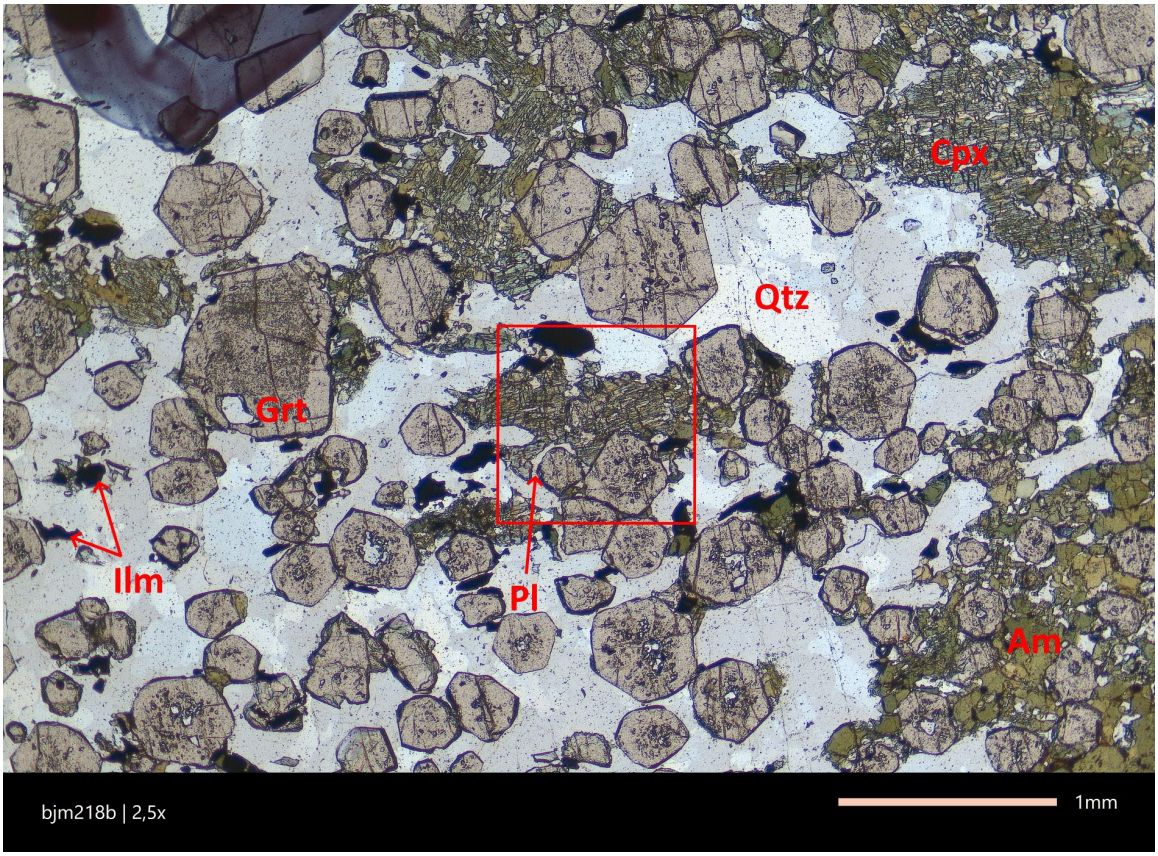

Figure 8: photomicrograph of sample bjm218b in PPL. Red outline is area subjected to element mapping. Grt=garnet; Qtz=quartz; Cpx=clinopyroxene; Am=amphibole.

3.3 Bakersville Hand Samples

Five samples were collected from a roadside outcrop where relatively pristine eclogite grades to amphibolite approaching a small (~ 6cm) felsic intrusion. The lithologies' decrease in metamorphic grade is reflected by a diminishing abundance of clinopyroxene and garnet accompanied by an increasing abundance of amphibole and plagioclase. The highest grade sample (bkmc0118a) is mostly made up of red millimetric euhedral garnets (30%) in a matrix of pale blue-green medium-grained subhedral omphacite (63%). Small patches of black amphibole

(4%) and rare plagioclase (2%) dot the matrix as well as accessory rutile (1%) (Fig 9A). Samples bkmc0218 and bkmc0518 represent moderately altered eclogite. Both display red millimetric euhedral garnets (20-25%) in a matrix of pale green medium-grained subhedral clinopyroxene (50-55%) and a greater abundance of black fine-grained amphibole (15%). The latter is maked by a greater abundance of plagioclase (15%) that occurs intergranularly (Fig 9B,C). Samples bkmc0418 and bkmc0318 represent advanced retrogression and are marked by little-to-no clinopyroxene content (0-15% respectively) and an abundance of amphibole. Sample bkmc0418 is made-up of red millimetric eudhedral garnets (25%) surrounded by thin plagioclase coronas (7%) in a matrix of fine-to-medium grained black amphibole (45%) dotted with small patches of quartz (7%) (Fig 9D). Sample bkmc0318 displays the lowest grade mineral assemblage. It is made up of millimetric euhedral-to-subhedral plagioclase pseudomorphs (20%) after garnet in a matrix of black fine-to-medium grained amphibole (80%) (Fig 9E).

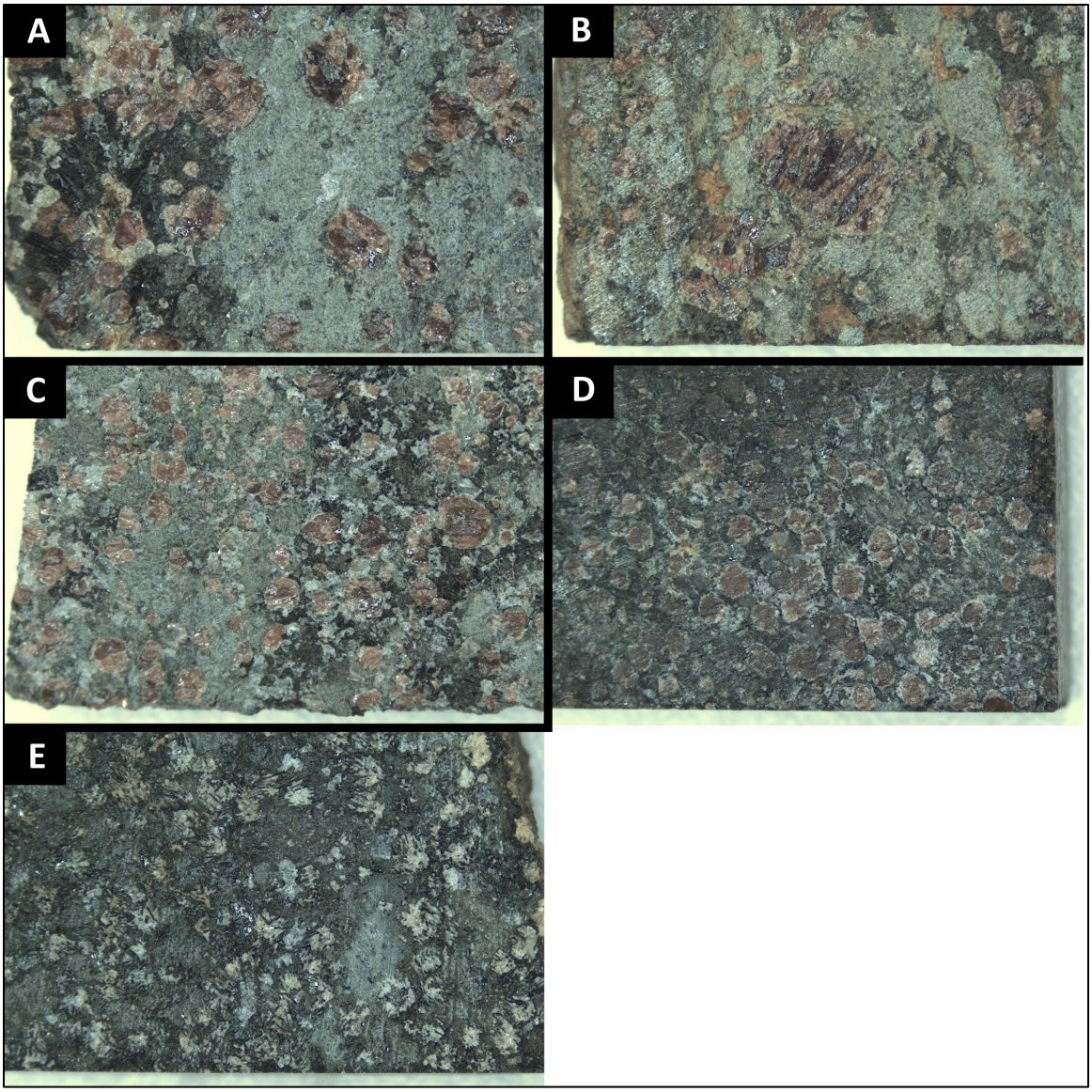

Figure 9: Macroscopic description of samples from Bakersville. Cut-surfaces show mineralogy and texture associated with decreasing metamorphic grade (A-E) Short edges are approximately 1.5 cm. (A) bkmc0118; (B) bkmc0218; (C) bkmc0518; (D) bkmc0418; (E) bkmc0318

3.4 Bakersville Petrography

The least altered sample (bkmc0118) is sourced farthest from the felsic intrusion and displays the peak assemblage of pale blue-green medium-grained anhedral-to-subhedral omphacite, red millimetric euhedral garnets, and accessory rutile. Garnets have few inclusions

that include fine-grained rutile and quartz. Other phases include poikiloblastic Cpx, fine-grained retrograde plagioclase and green amphibole that occur intergranulaly (Fig 10).

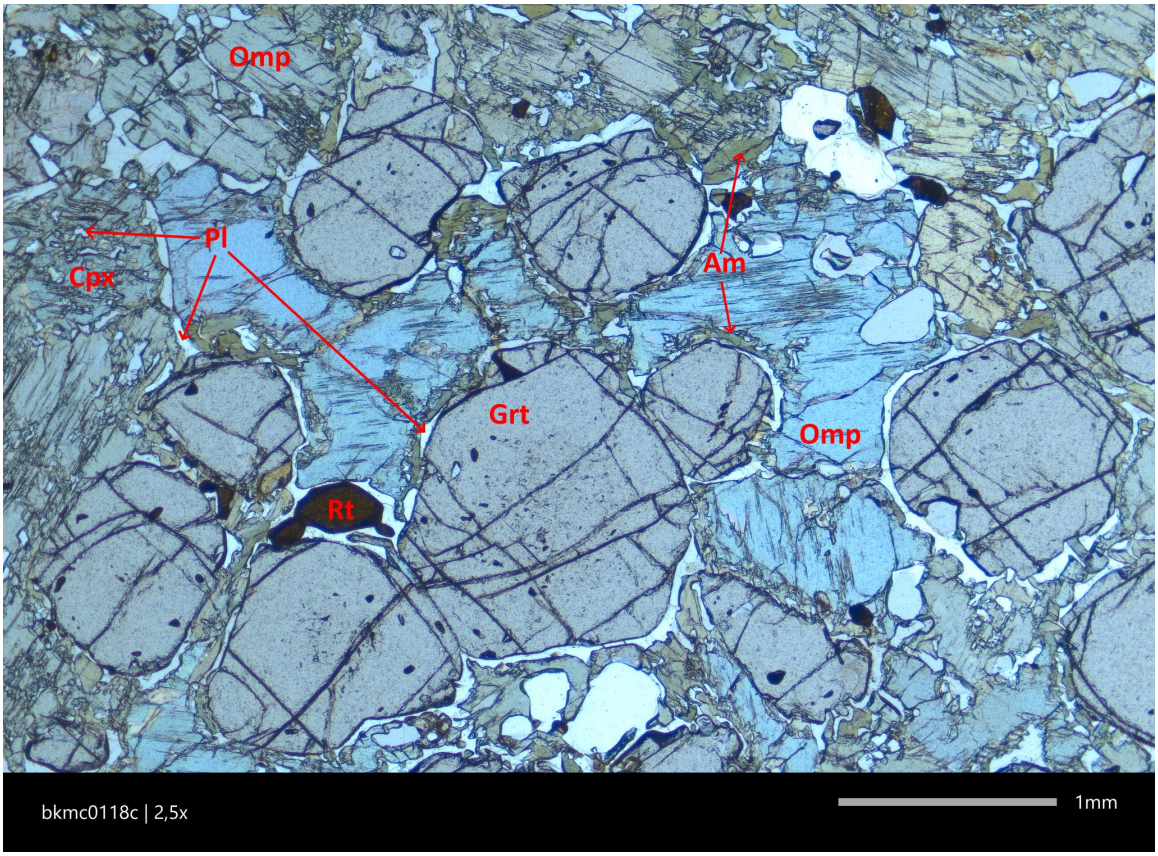

Figure 10: Photomicrograph of sample bkmc0118c in PPL. Grt=garnet; Omp=omphacite; Am=amphibole; Rt=rutile; Pl=plagioclase; Cpx=clinopyroxene

In moderately altered samples (bkmc0218; bkmc0518) most of the clinopyroxene consists of medium-to-coarse grained spongy poikiloblasts with inclusions of plagioclase and amphibole. Garnets have partially reacted to form circular to semi-circular fine grained intergrowths of plagioclase and amphibole (kelyphites) at their edges and from within. Amphibole occurs as medium grains in the matrix and as rims on clinopyroxene (Fig 11).

.

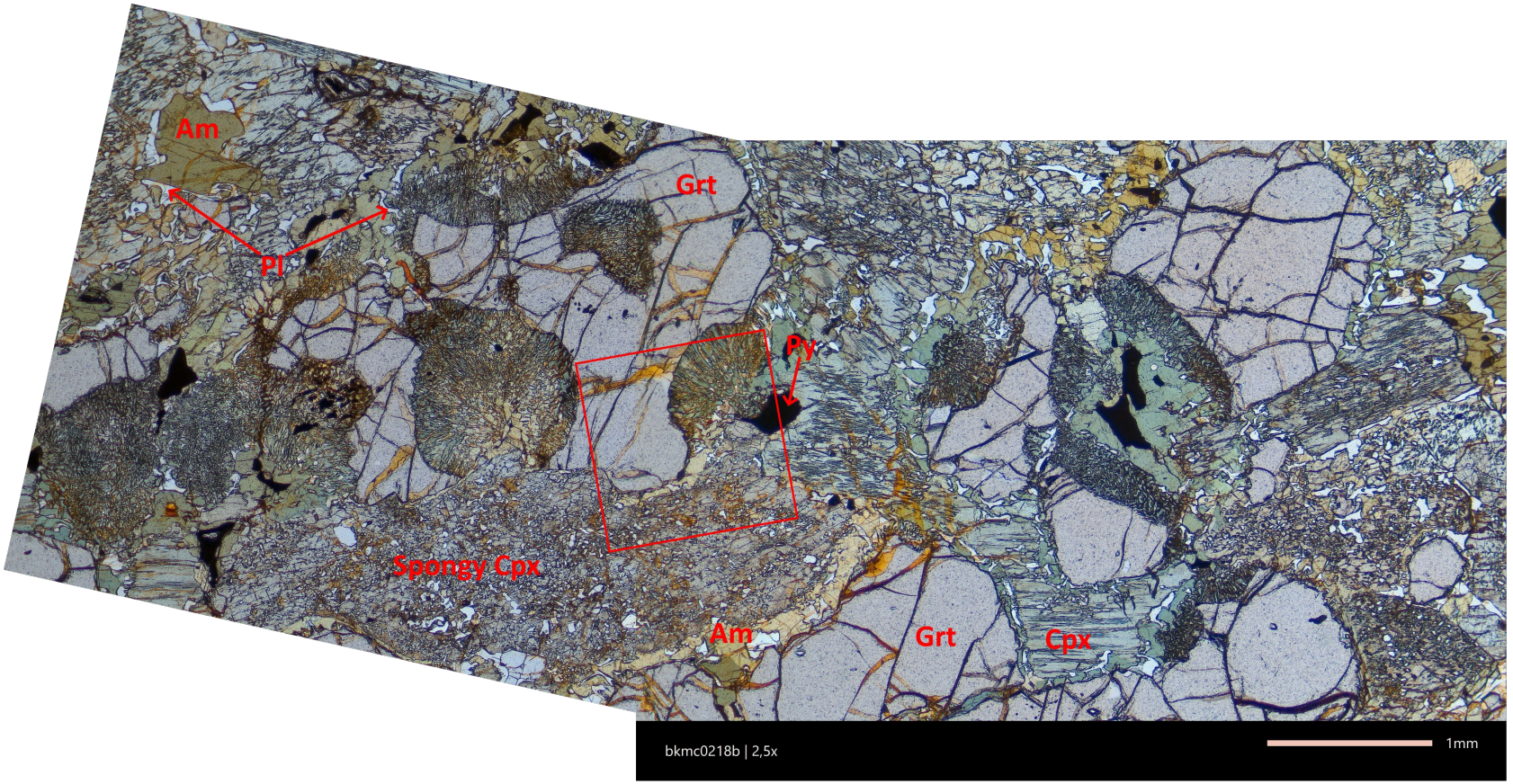

Figure 11: Photomicrograph mosaic of sample bkmc0218b in PPL. Red Outline shows area subjected to element mapping. Am=amphibole; Grt=garnet; Cpx=clinopyroxene; Pl=plagioclase; Py=pyrite

Samples bkmc0418 and bkmc0318 represent a series of advanced retrogression to amphibolite. Sample bkmc0418 displays the assemblage garnet-amphibole-quartz-plagioclase ± cpx ± rutile. Millimetric subhedral-to-anhedral garnets are surrounded by thin rim-assemblages of green amphibole and plagioclase that appear to jaggedly cut into the garnet. Locally, the aforementioned partially altered garnets are surrounded by patches of medium-grained quartz and/or medium-grained poikiloblastic amphibole with quartz inclusions (Fig 12A). In sample bkmc0318, garnets have been completed replaced by medium-grained circular pseudomorphic aggregates of plagioclase intergrown with needles of green amphibole. (Fig 12B).

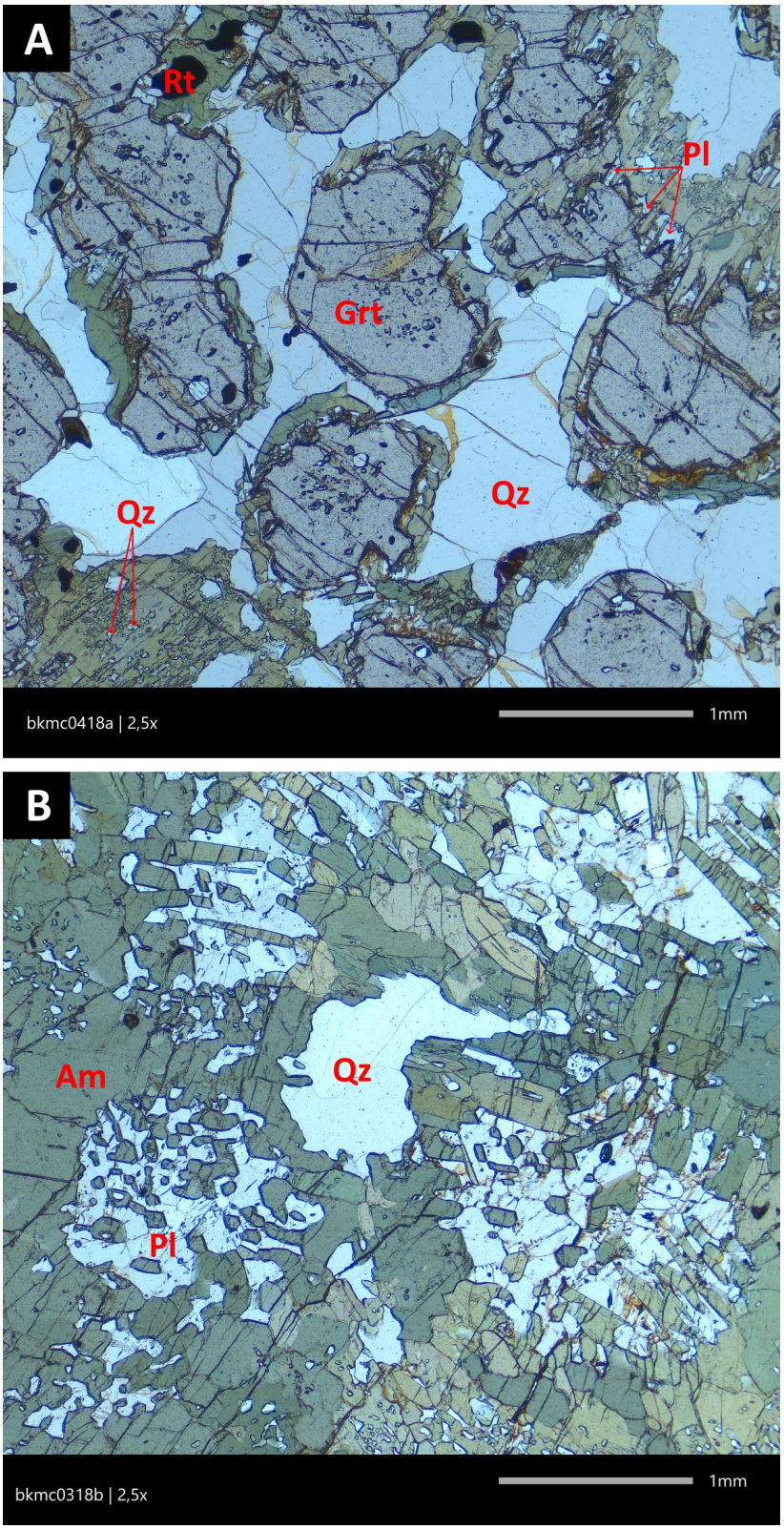

Figure 12: Photomicrographs in plane polarized light of samples displaying advanced retrogression. (A) bkmc0418; (B) bkmc0318. Am=amphibole; Qz=quartz; Pl=plagioclase; Grt=garnet; Rt=rutile

4 ANALYTICAL RESULTS

4.1 Bulk Chemistry

Bulk samples from Bakersville and north of Boone plot as tholeiitic mid-ocean-ridge basalt (T-MORB) (Fig 13), which is in agreement with previous studies of similar metabasites of the AMS (Abbot and Raymond, 1984; Abbot and Greenwood, 2001). For the Boone granulites, northern samples are slightly richer in Fe compared to southern samples.

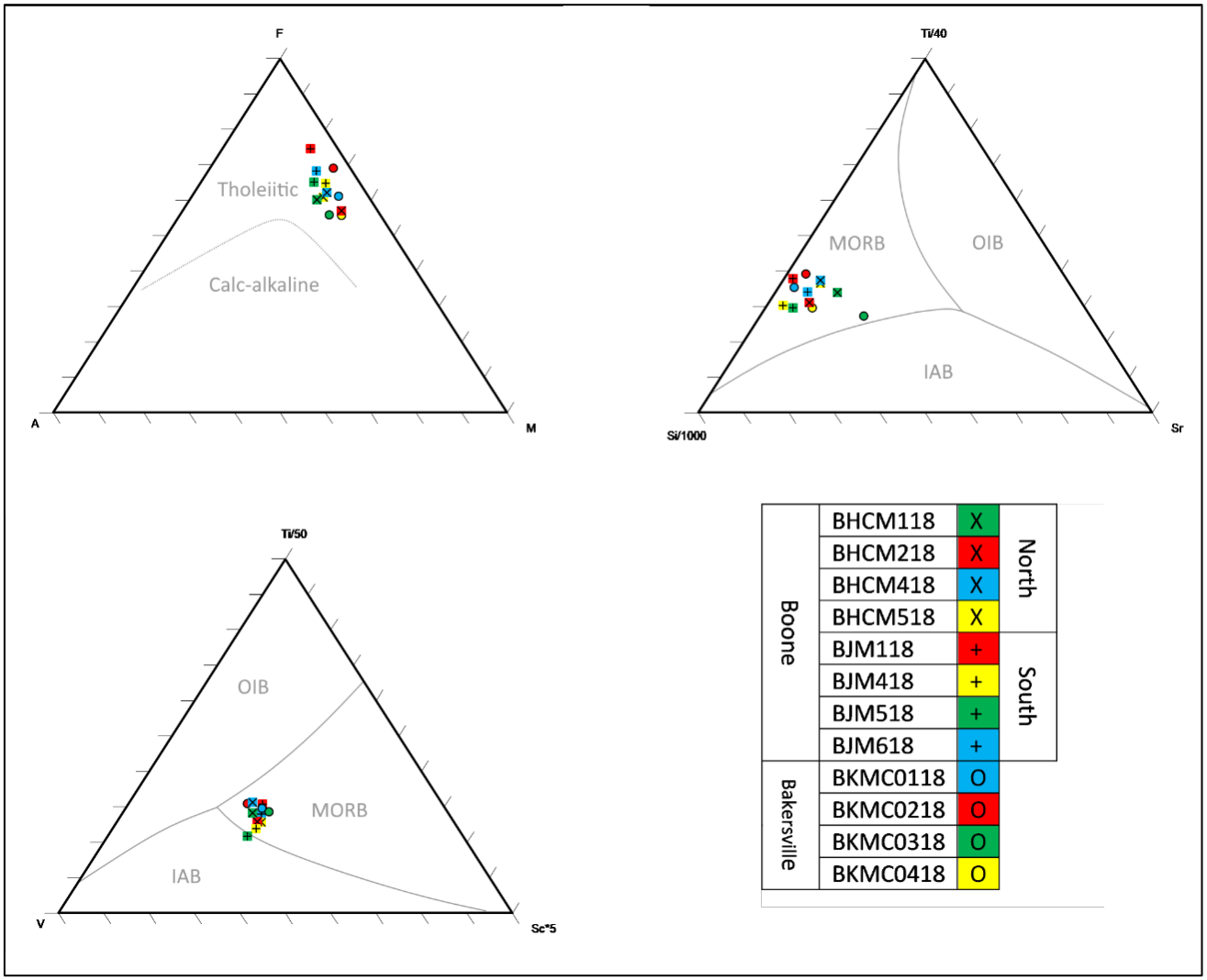

Figure 13: Bulk chemistry plotted in AFM and those of Vermeesch (2006) demonstrating MORB characteristics of metabasites from the AMS. Abbreviations: MORB= mid-ocean ridge basalt; OIB=oceanic island basalt; IAB=island arc basalt

4.2 Mineralogy of Boone Samples

The map acquired on sample bjm518bm1 (Fig 14A) shows tightly clustered sub-millimetric subhedral-anhedral garnet with inclusions of quartz, epidote and plagioclase. Garnet is mostly surrounded by smooth-edged plagioclase and less commonly, spaces between garnet grains in close proximity are occupied by hornblende. Diopside occurs as both fine-grained symplectite with plagioclase and hornblende, and together with plagioclase as highly cuspate patches adjacent irregular patches of quartz. Two types of ilmenite occur as accessory matrix phases. Ilmenite 1 has a slightly higher Fe/Ti ratio than ilmenite 2.

The map acquired on sample bjm618b (Fig 14B) shows a prehnite vein cutting across a matrix of coarse-grained hornblende, fine-grained Di-Pl symplectite, and fractured garnet. Garnet fragments are surrounded by plagioclase and are seldomly in contact with matrix hornblende. Two types of ilmenite occur as accessory matrix phases. Ilmenite 1 has a slightly higher Fe/Ti ratio than ilmenite 2. Other accessory phases include quartz and one very fine grain of potassium feldspar that is in contact with Di-Pl symplectite.

The map acquired on sample bhcm418bm2 (Fig 14C) shows a euhedral millimetric garnet with inclusions of quartz, rutile, plagioclase, epidote, hornblende, titanite, ilmenite, and biotite. Within the outer rim, a coarse polymineralic inclusion of ilmenite rimmed with titanite and minor biotite extends to the outside matrix where other titanite-rimmed ilmenite grains occur. Surrounding garnet, a thin plagioclase rim is fragmented and discontinuous in areas, leaving the garnet in direct contact with matrix hornblende. Other matrix phases include fine-grained vermicular Di-Pl symplectite as well as coarse-grained quartz and epidote.

The map acquired on sample bjm218b (Fig 14D) shows sub-millimetric garnets with inclusions of quartz, titanite, and rutile. One garnet has a discontinuous plagioclase rim with smooth edges, while others are in direct contact with diopside, hornblende, other garnet. Poikiloblastic diopside has lamellar inclusions of plagioclase, hornblende, and quartz. Quartz

occurs as both coarse grains in the matrix and large continuous areas. Ilmenite occurs as coarse subhedral grains and small fragments in the matrix.

The map acquired on sample bjm518bm2 (Fig 14E) shows a region of fine-grained vermicular diopside-plagioclase-hornblende symplectite. An anhedral garnet within the symplectite matrix is in contact with all three symplectite components at different places.

The map acquired on sample bjm318m1 (Fig 14F) shows millimetric euhedral garnet with inclusions of quartz, rutile, titanite, hornblende and plagioclase. It is in contact with matrix hornblende, diopside-plagioclase symplectite, quartz, and plagioclase. Ilmenite occurs as an accessory phase in the matrix.

The map acquired on sample bhcm418m1 (Fig 14G) shows a submillimetric anhedral garnet with inclusions of epidote, rutile, quartz, titanite, and hornblende. It is mantled by a highly fractured plagioclase rim up to ~200 μm thick that contains pieces of titanite and has an irregular boundary where it comes in contact with matrix hornblende. Fine grained symplectite of diopside and plagioclase occurs within the hornblende matrix, as well as quartz ~500 μm in diameter.

The map acquired on sample bjm318bm2 shows two textures (Fig 14H). The top of the map is dominated by fine-grained symplectite made of diopside, plagioclase, and hornblende and minor quartz. A subhedral garnet within this zone of symplectite is rimmed by continuous plagioclase and contain inclusion of titanite. Smaller anhedral garnets in this zone have irregular, discontinuous plagioclase rims and are in contact with matrix hornblende in places. The bottom of the map is dominated by coarse hornblende matrix with subhedral garnet included with titanite and rimmed by irregular, discontinuous plagioclase rims.

The map acquired on sample bjm718 (Fig 14I) shows a 700 μm diameter euhedral garnet with inclusions of quartz, titanite, plagioclase, hornblende, and epidote, some of which are polymineralic quartz + plagioclase. The garnet is rimmed by irregular discontinuous plagioclase

and comes in contact with matrix hornblende at places. Fine-grained symplectite of diopside and plagioclase occurs in hornblende matrix, as well as linear ilmenite between garnet grains.

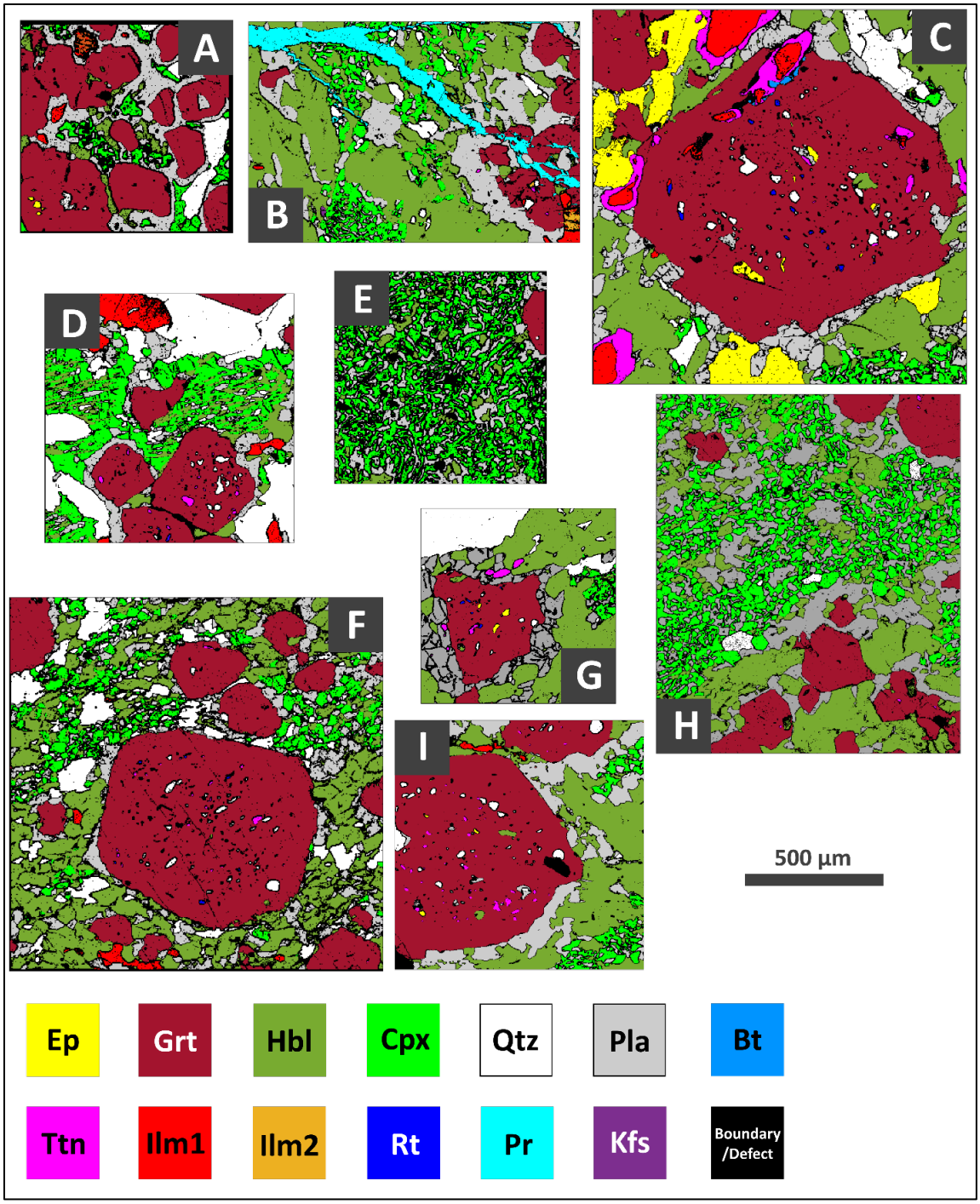

Figure 14: Mineralogy of non-contiguous areas subjected to EPMA mapping from samples north of Boone. A) bjm518m1; B) bjm618b; C) bhcm418m2; D) bjm218b; E) bjm518bm2; F) bjm318bm1; G) bhcm418m1; H) bjm318bm2; I) bjm718 Ep=epidote; Grt=garnet; Hbl=hornblende; Cpx=clinopyroxene; Qtz=quartz; Pla=plagioclase feldspar; Bt=biotite; Ttn=titanite; Ilm=ilmenite; Rt=rutile; Pr=prehnite; Kfs=potassium feldspar

4.3 Mineral Chemistry of Boone Samples

4.3.1 Garnet

Rim-to-rim zoning profiles from representative garnets of each outcrop are flat overall with subtle variation within and between each. A representative sample from the northern outcrop (bhcm418m2) has a homogenized composition except for a distinct change in the outer rim (approx. 100 um thick) where Ca markedly increases at the expense of Fe and Mg. The very outer edge shows a very minor increase in Mn (Fig 15). The inner bulk has the average composition $Alm_{57}\,Grs_{25}\,Prp_{13}\,Adr_{2.6}\,Sps_{1.6}$) and the outer region has the average composition $Alm_{55}\,Grs_{29}\,Prp_{13}\,Adr_{2.6}\,Sps_{1.3}$.

Conversely, a representative sample from the southern outcrop (bkm718) shows an overall core-to-rim increase in Fe, Mg, oscillatory Ca, and a Mn-rich core that decreases outwards (Fig 16). The inner core has the average composition $Alm_{52}\,Grs_{30}\,Prp_{9.4}\,Adr_{3.9}\,Sps_{5.2}$ while the region surrounding it is enriched in Ca with an average composition $Alm_{51}\,Grs_{34}\,Prp_{9.3}\,Adr_{3.2}\,Sps_{2.6}$. The outer edge displays a distinct increase in Mg and decrease in Ca ($Alm_{52}\,Grs_{29}\,Prp_{13}\,Adr_{3.5}\,Sps_{2.4}$).

Overall, garnets from both outcrops have nearly identical almandine-rich compositions and opposite growth patterns (Fig 17). A resorbed northern sample (bhcm418m1) displays a limited compositional range that is depleted in Ca compared to the other described garnets.

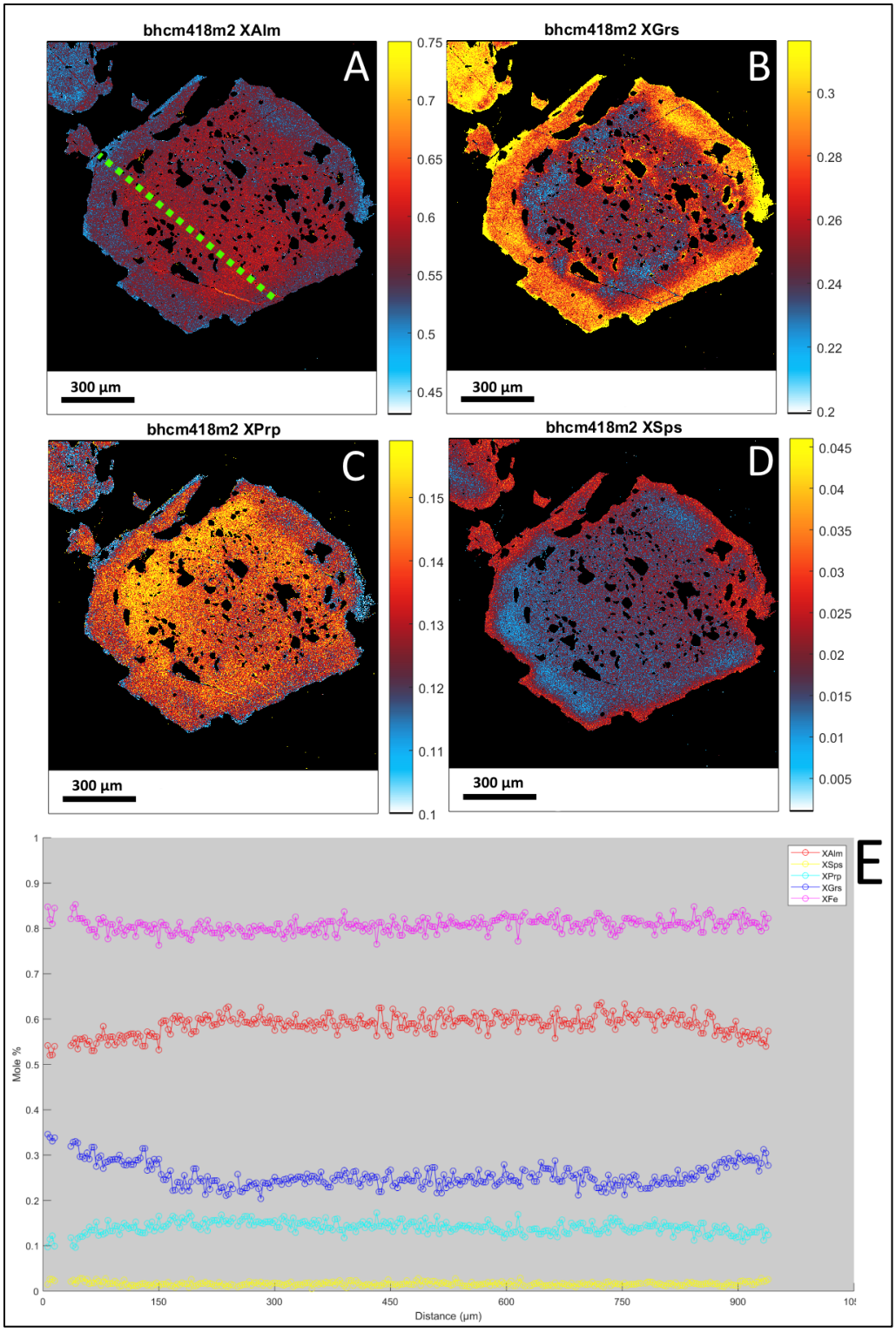

Figure 15: Garnet zoning maps and profiles for sample bhmc418m2. (A) almandine component (B) grossular component (C) pyrope component (D) spessartine component (E) component profiles corresponding to dashed green line in (A). Fuchsia= XFe; Red=XAlm; Blue=XGrs; Cyan=XPrp; Yellow=XSps

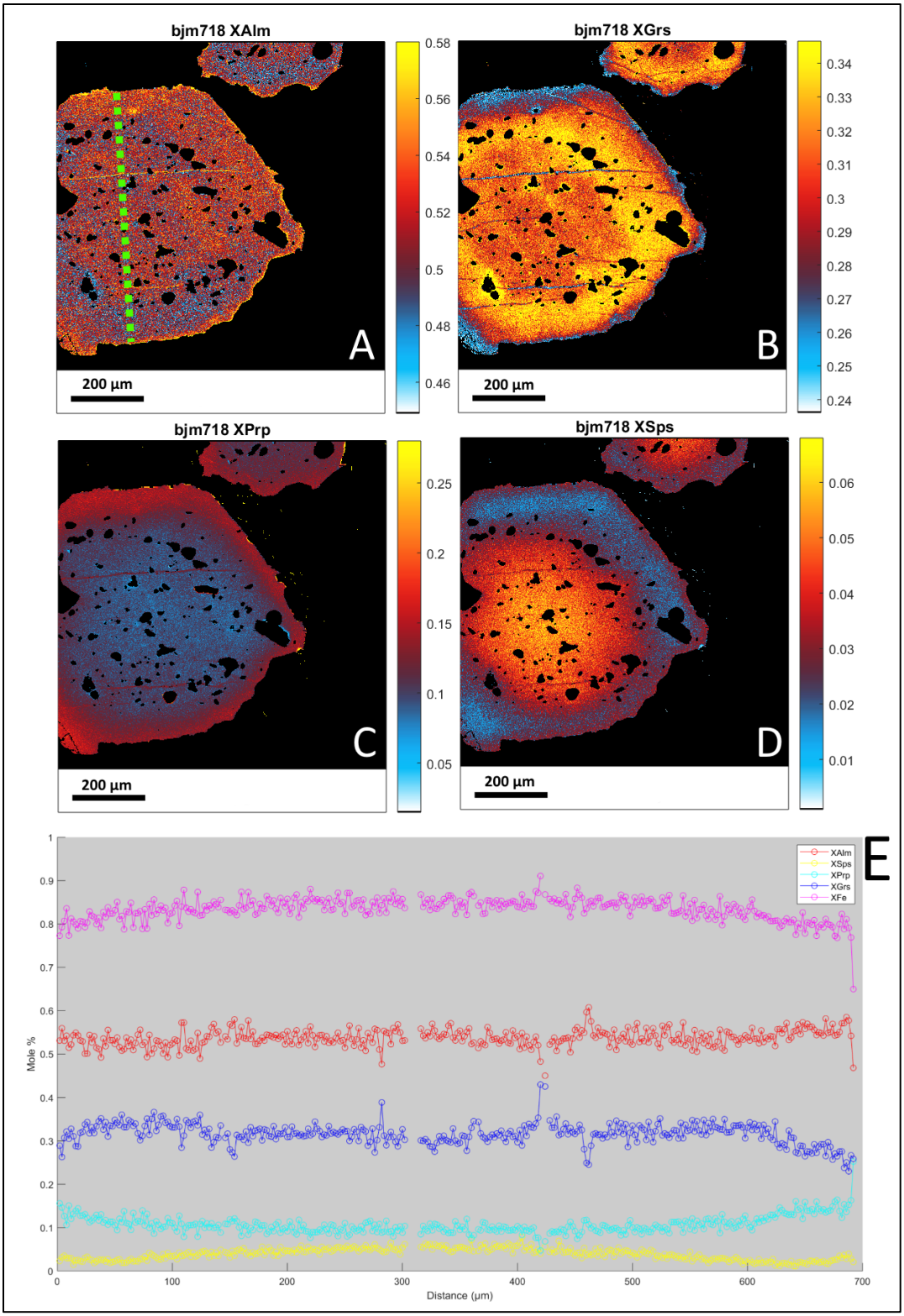

Figure 16: Garnet zoning maps and profiles for sample bjm718. (A) almandine component (B) grossular component (C) pyrope component (D) spessartine component (E) component profiles corresponding to dashed green line in (A). Fuchsia= XFe; Red=XAlm; Blue=XGrs; Cyan=XPrp; Yellow=XSps

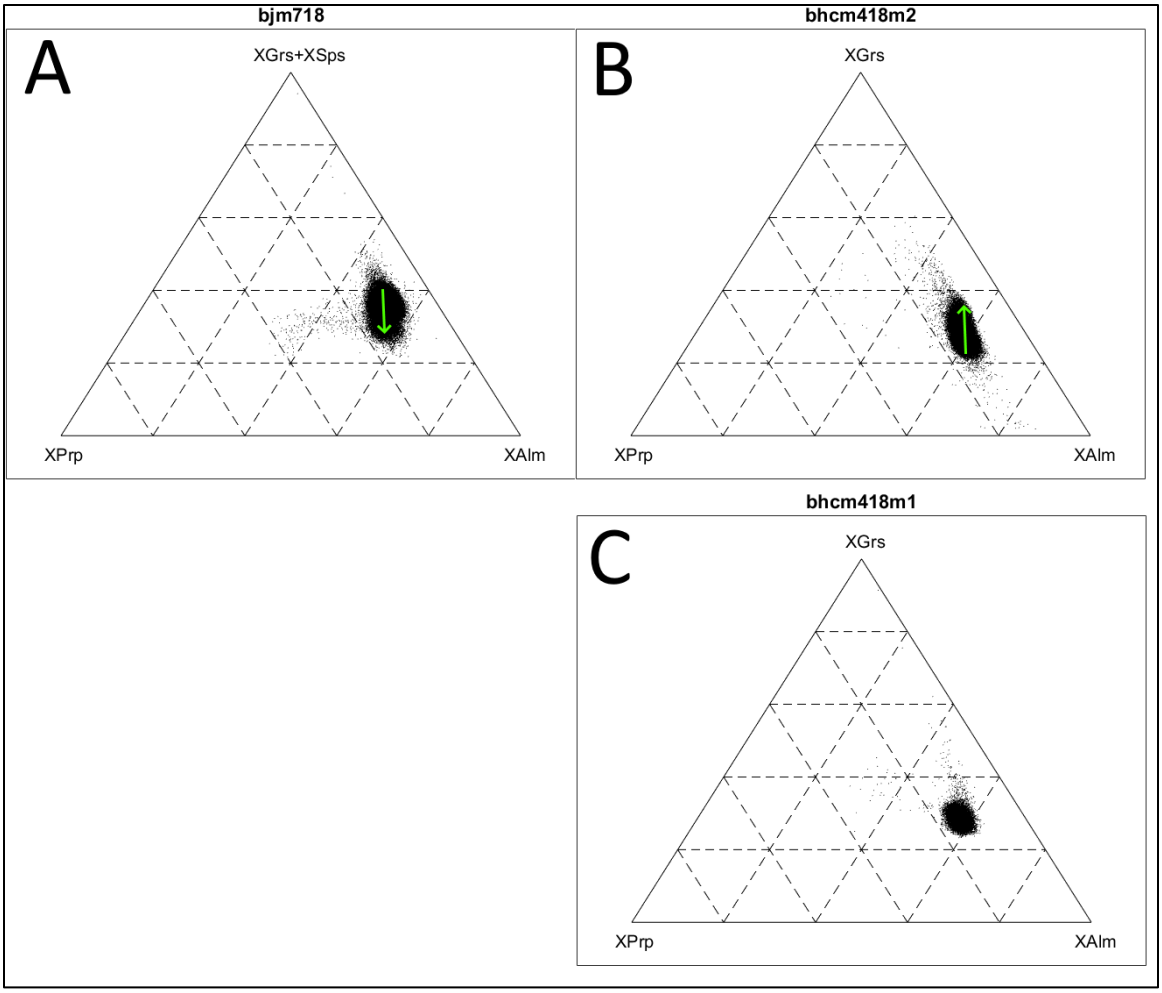

Figure 17: Representative garnet compositions for Boone metabasites. Green arrows show general core-to-rim progression. (A) garnet from south (bjm718) (B) garnet from north (bhcm418m1) (C) resorbed garnet from north (bhcm418m2).

4.3.2 Pyroxene

Symplectitc clinopyroxene from northern samples bhcm418m1 and bhcm418m2 have the average compositions $Di_{64}Hd_{28}Jd_{03}Ae_{03}Cats_{02}$ and $Di_{65}Hd_{27}Jd_{03}Ae_{03}Cats_{02}$ respectively. Altered clinopyroxene grain from sample bjm218 has the average composition $Di_{64}Hd_{28}Jd_{04}Ae_{04}Cats_{02}$. Mapped clinopyroxene from samples bjm518m1,m2 have the average compositions $Di_{64}Hd_{31}Jd_{04}Ae_{04}Cats_{02}$ and $Di_{65}Hd_{28}Jd_{04}Ae_{04}Cats_{02}$ respectively. Mapped clinopyroxene from sample bjm318m1,m2 could not be quantified. Mapped clinopyroxene from sample bjm618b has

the average composition $Di_{68}Hd_{27}Jd_{04}Ae_{03}Cats_{02}$. Mapped clinopyroxene from sample bjm718 has the average composition $Di_{65}Hd_{28}Jd_{03}Ae_{03}Cats_{02}$

Fine-grained symplectitc clinopyroxene with sodic plagioclase ± hornblende (bhcm418m1, bhcm418m2, bjm518m1, bjm518m2, bjm618, bjm718) and apparently altered clinopyroxene grains with inclusions of plagioclase and hornblende (bjm218) are all diopsidic with very small Na-content (XJd <=04) and little variation among all samples analyzed (Fig 18).

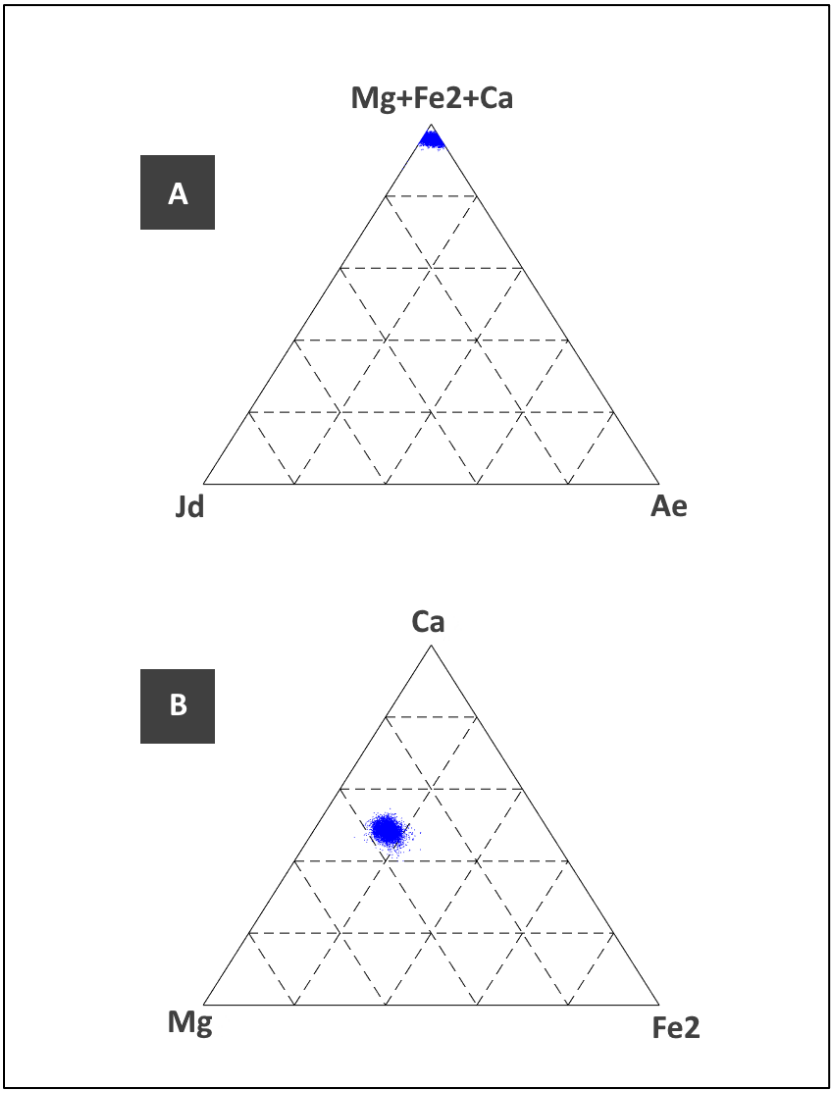

Figure 18: Representative pyroxene composition (sample bjm518m2). (A) ternary diagram with endmembers Jd=jadeite component, Ae=aegirine component, Mg+Fe2+Ca= 'quad'component. (B) 'quad' ternary diagram.

4.3.3 Amphibole

Mapped amphibole from samples bhcm418m1, bhcm418m2, bjm218, bjm318m1, bjm318m2, bjm518m1, bjm618, and bjm718 are calcic, magnesium-rich hornblende that vary in composition between edenite, magnesiohastingsite, and hastingsite (Fig 19). A hornblende inclusion in garnet from northern sample bhcm418m2 classifies as magnesiohastingsite and has a narrower compositional range with a lower overall Si/Al ratio compared to matrix hornblende from the same sample. A hornblende inclusion in garnet from southern sample bjm718 classifies between hastingsite and magnesiohastingsite and has a similar, yet smaller compositional range compared to matrix hornblende from the same sample. Sample bjm518m2 has a greater Si/Al ratio and classifies as edenite (Fig 19B), however this result may be unreliable because standardization was based on only two spot analyses. In sample bhcm418m1, concentrations in Al and depletions in Ca and Mg occur around garnet and as secondary fractures (Fig 20).

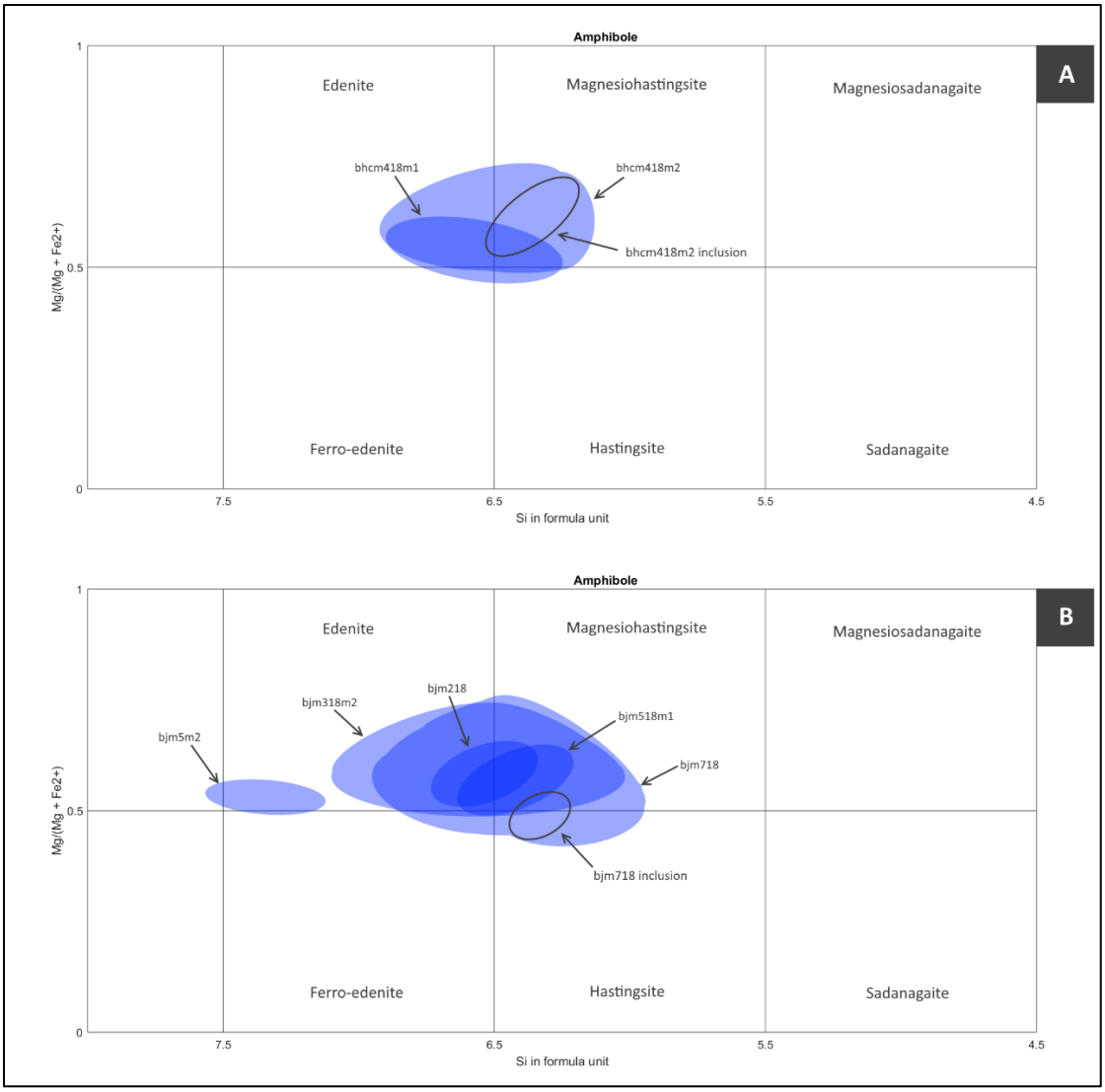

Figure 19: Amphibole nomenclature diagrams showing compositional ranges for northern and southern outcrops.(A) Northern amphiboles range from magnesiohastingsite to edenite. Black ellipse represents inclusion in garnet from sample bhcm418m2 and lies mostly within the magnesiohastingsite field. (B) Southern amphiboles range from magnesiohastingsite to edenite. Black ellipse represents inclusion in garnet from sample bjm718 that varies between hastingsite and magnesiohastingsite. Sample bjm518 is mostly edenite and represents symplectitc amphibole with diopside and sodic plagioclase that is found adjacent to a layer of garnet aggregate.

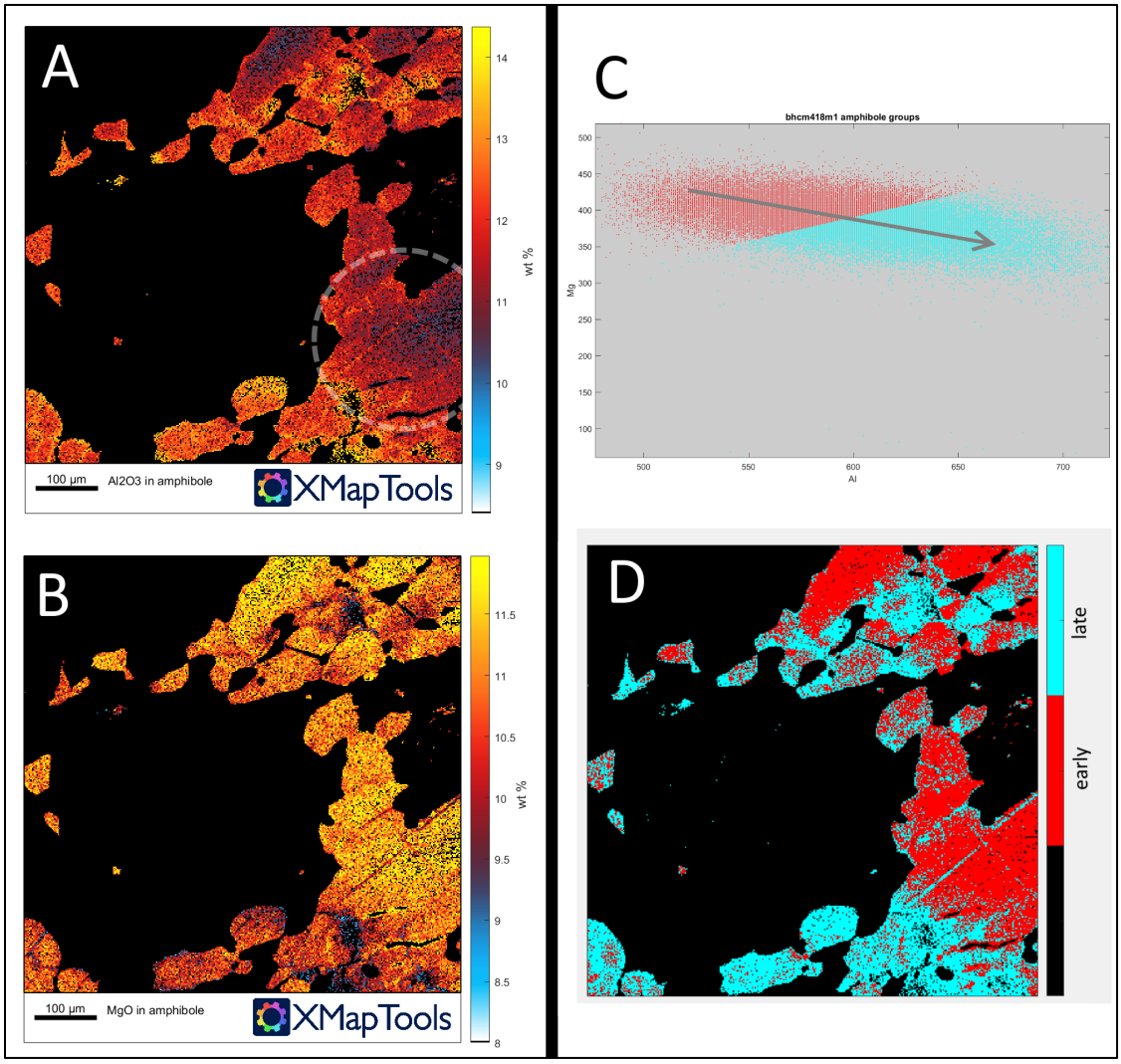

Figure 20:Chemical variation in amphibole from sample bhcm418m1. A) Amphibole map of Al2O3 weight percent. Dashed semi-circle encloses fractures. B) Amphibole Map of MgO weight percent. C) and D) Early (red) and late (cyan) amphibole groups. Early group is located at amphibole core and inclusion in garnet while late is located along lineations and adjacent to garnet.

4.3.4 Feldspar

Among all the mapped samples coming from north of Boone, three groups of sodic plagioclase feldspar were recognized (Fig 21). Samples from the northern outcrop are the most calcic with the average composition $Ab_{62}An_{38}Or_{00}$ and classify as andesite plagioclase while those from the southern outcrop have the average composition $Ab_{72}An_{28}Or_{00}$ and classify as oligoclase plagioclase. Albite ($Ab_{91}An_{08}Or_{00}$) and a small grain of potassium feldspar, for which no quantitative data was obtained, occur in sample bjm618b that is cut by a localized fine-grained prehnite vein network. Representative samples from the northern and southern outcrops (bhcm418m2, bjm718) display patchy zoning overall (Fig 22).

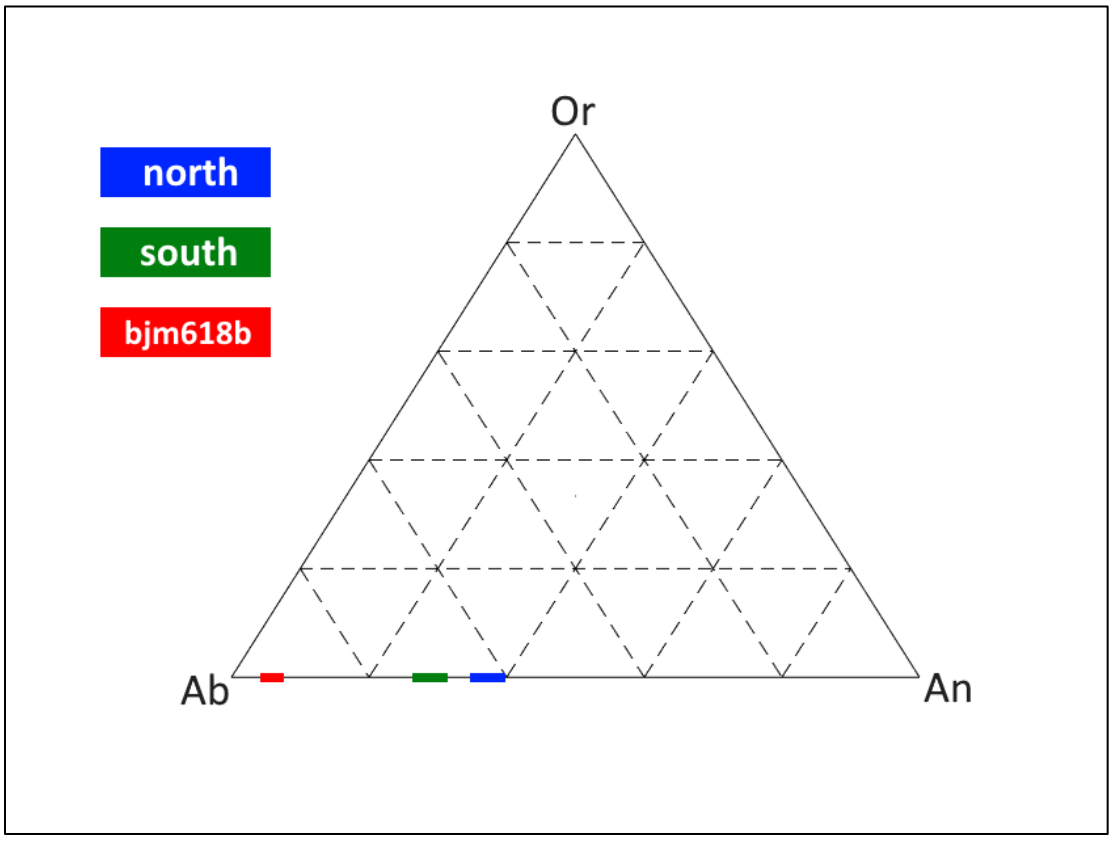

Figure 21: Summary of feldspar compositions for Boone metabasites. Abbreviations are as follows: Ab=albite; An=anorthite; Or=orthoclase

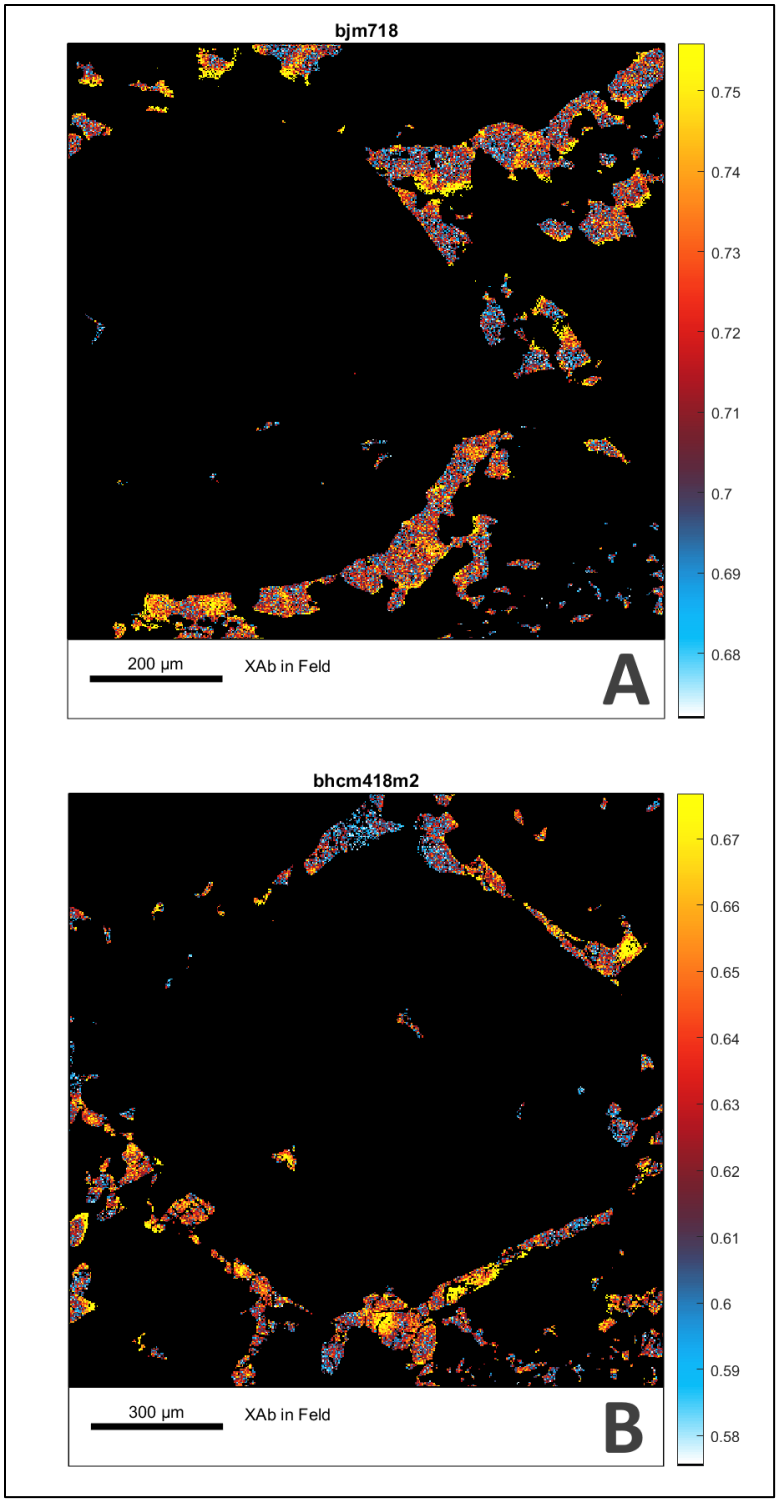

Figure 22: Feldspar maps showing ranges in albite component percentage. A) Mapped albite component of sample bjm718 ranges from Ab_{68} to Ab_{75}. B)) Mapped albite component of sample bhcm418m2 ranges from Ab_{58} to Ab_{67}.

4.3.5 Epidote

Epidote occurring both as a matrix phase and inclusions in garnet among the two outcrops exists as a solid solution between epidote and clinozoisite (Fig 23). Epidote from a representative northern sample has similar compositions between matrix ($Ca_2Al_{2.35-2.55}Fe_{0.45-0.65}(Si_2O_7)(SiO_4)O(OH,O)$) and garnet-inclusion phases ($Ca_2Al_{2.42-2.58}Fe_{0.42-0.58}(Si_2O_7)(SiO_4)O(OH,O)$). Compared to the north, southern epidote is slightly richer in iron ($Ca_2Al_{2-2.35}Fe_{0.65-1}(Si_2O_7)(SiO_4)O(OH,O)$). Matrix epidote from the north (sample bhcm418m2) displays zoning wherein rims are enriched in iron compared to the core (Fig 24).

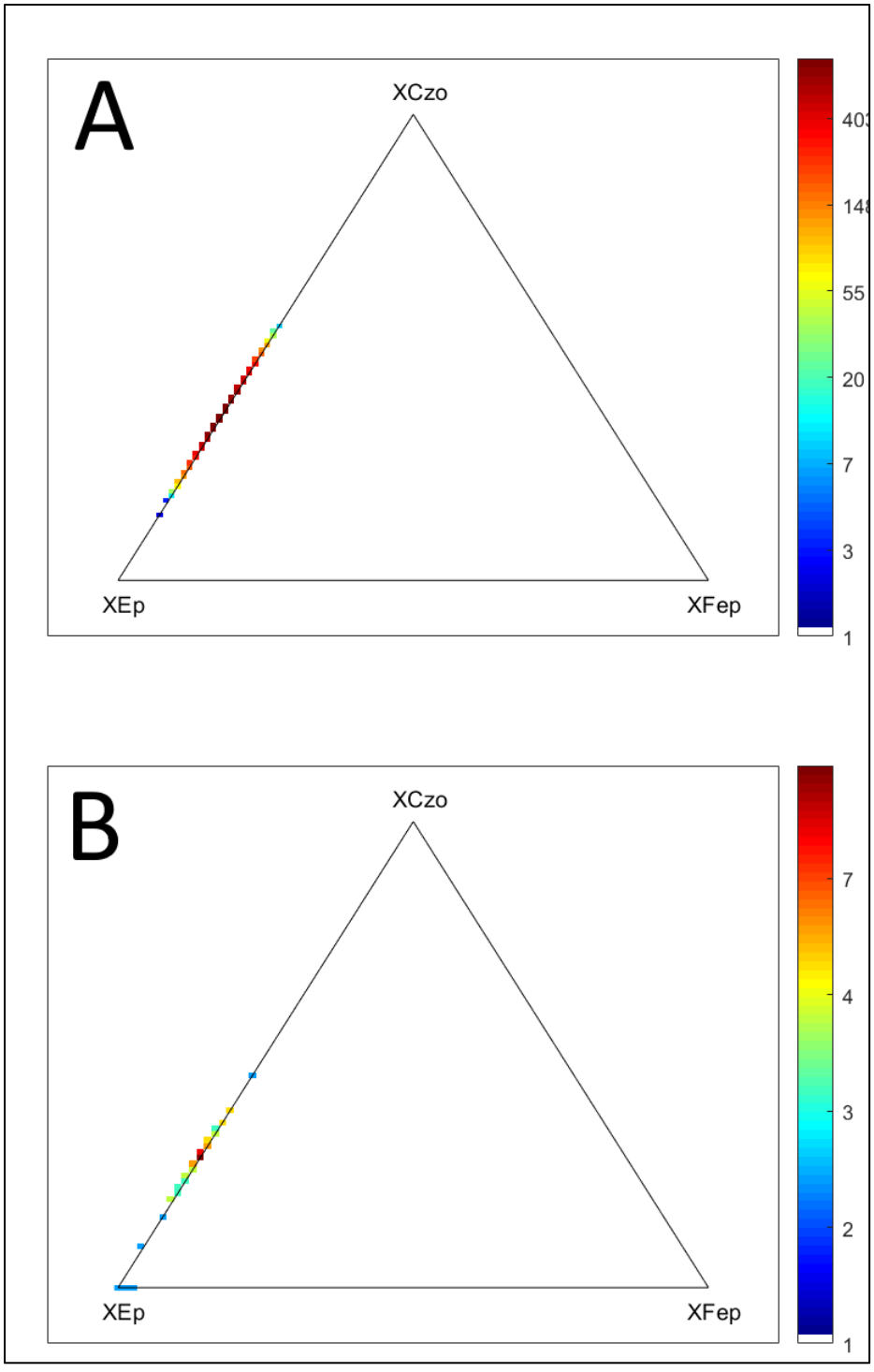

Figure 23: A)Pixel densities for epidote inclusions in garnet and matrix epidote. From sample bhcm418m2 plotted in ternary diagram. B) Pixel densities for epidote inclusions in garnet from sample bjm718. Ep=epidote; Czo=clinozoisite; Fep=ferriepidote

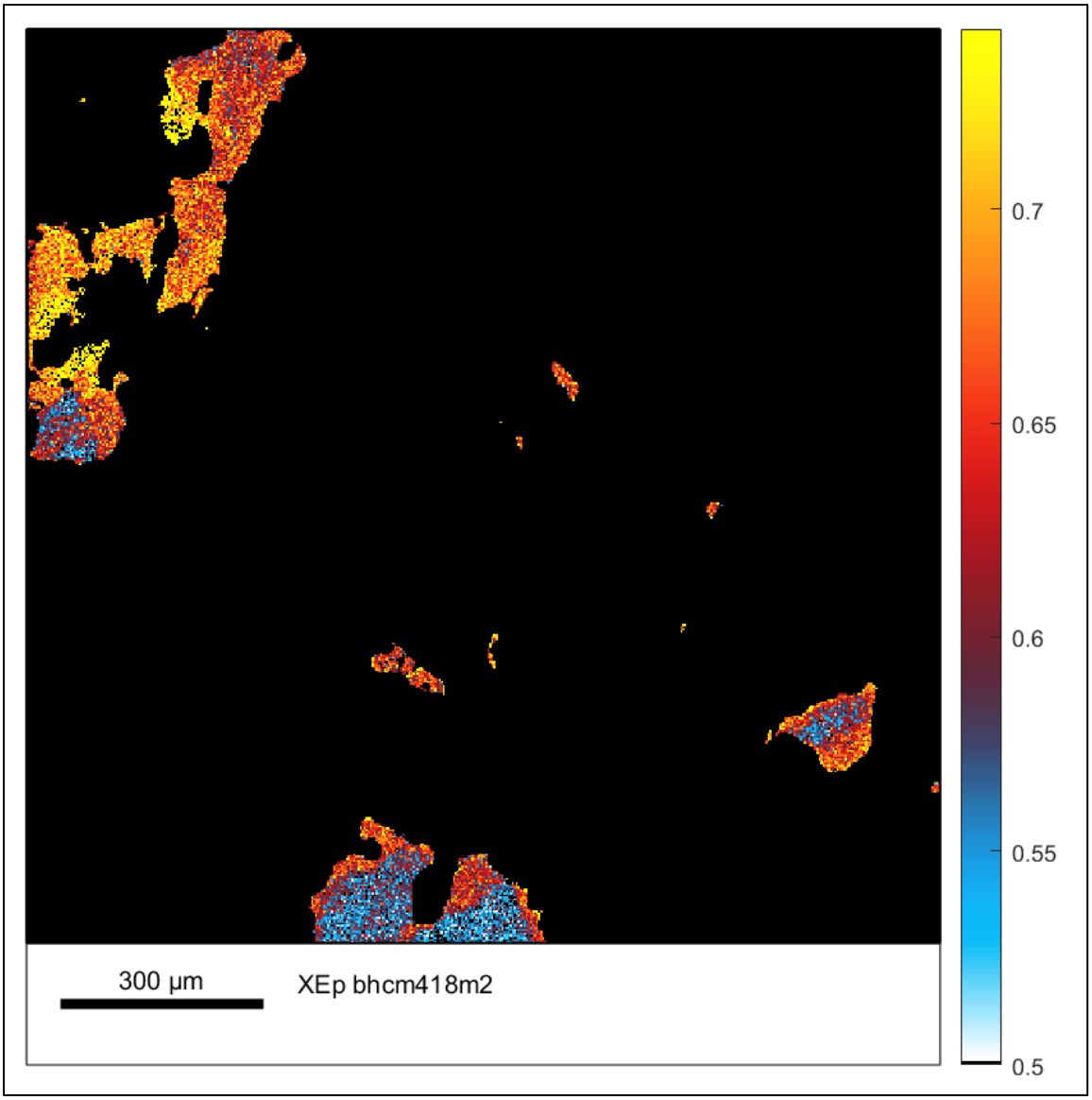

Figure 24: Map of Epidote component percent in epidote from sample bhcm418m2 reflects iron-content. Subhedral grain at bottom has a rim enriched in Fe compared to the core.

4.3.6 Ilmenite

Two groups of ilmenite are recognized in samples bjm618b and bjm518m1. Based on X-ray intensity values, ilmenite 1 has a slightly higher Fe/Ti ratio compared to ilmenite 2 (Fig 25).

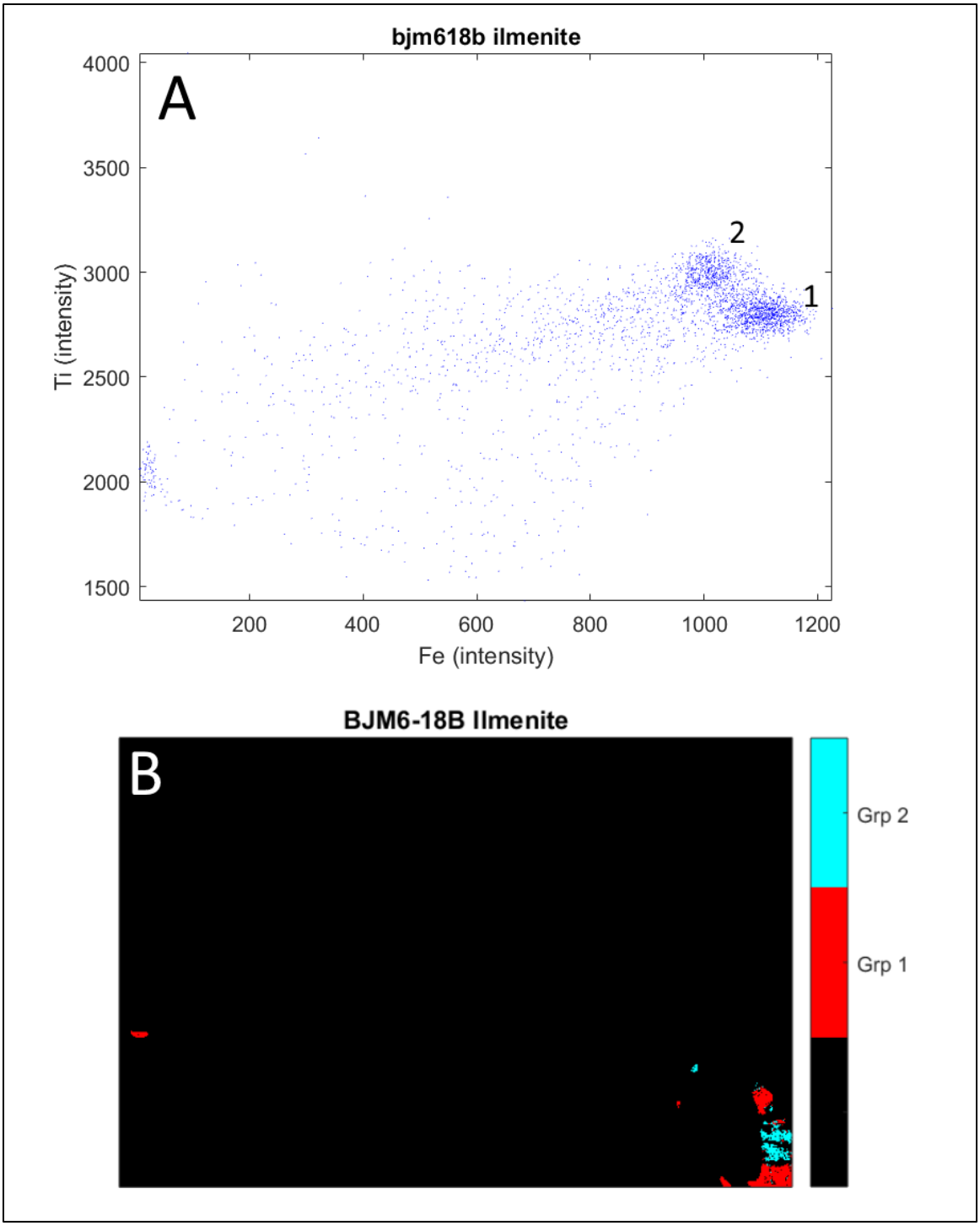

Figure 25: (A) Two groups of Ilmenite pixels plotted in Fe-Ti intensity space (bjm618b). (B) Corresponding map of ilmenite groups from sample bjm618b.

4.3.7 Prehnite

Prehnite within the vein network found on sample bjm618b consists mostly of Si, Ca, and Al (wt% oxide = 93) with a small amount of Fe (FeO wt% = 1.5) and approximately 6% is unaccounted for by major element analysis (Table 4). Two groups of prehnite are recognized (Fig 26A) that are discernable from each other by sharp polygonal boundaries that correspond to differences in Fe content (Fig 26B). These boundaries are similarly visible in cross-polarized light (Fig 26D).

Table 4: Average wt% oxides of prehnite from sample bjm618b.

Oxide	Weight percent
Al_2O_3	22.7786
CaO	26.9500
Cr_2O_3	0.0106
FeO	1.4878
K_2O	0.0026
MgO	00139
MnO	0.0197
Na_2O	0.0142
SiO_2	42.8337
TiO_2	0.0513
SUM	94.1624

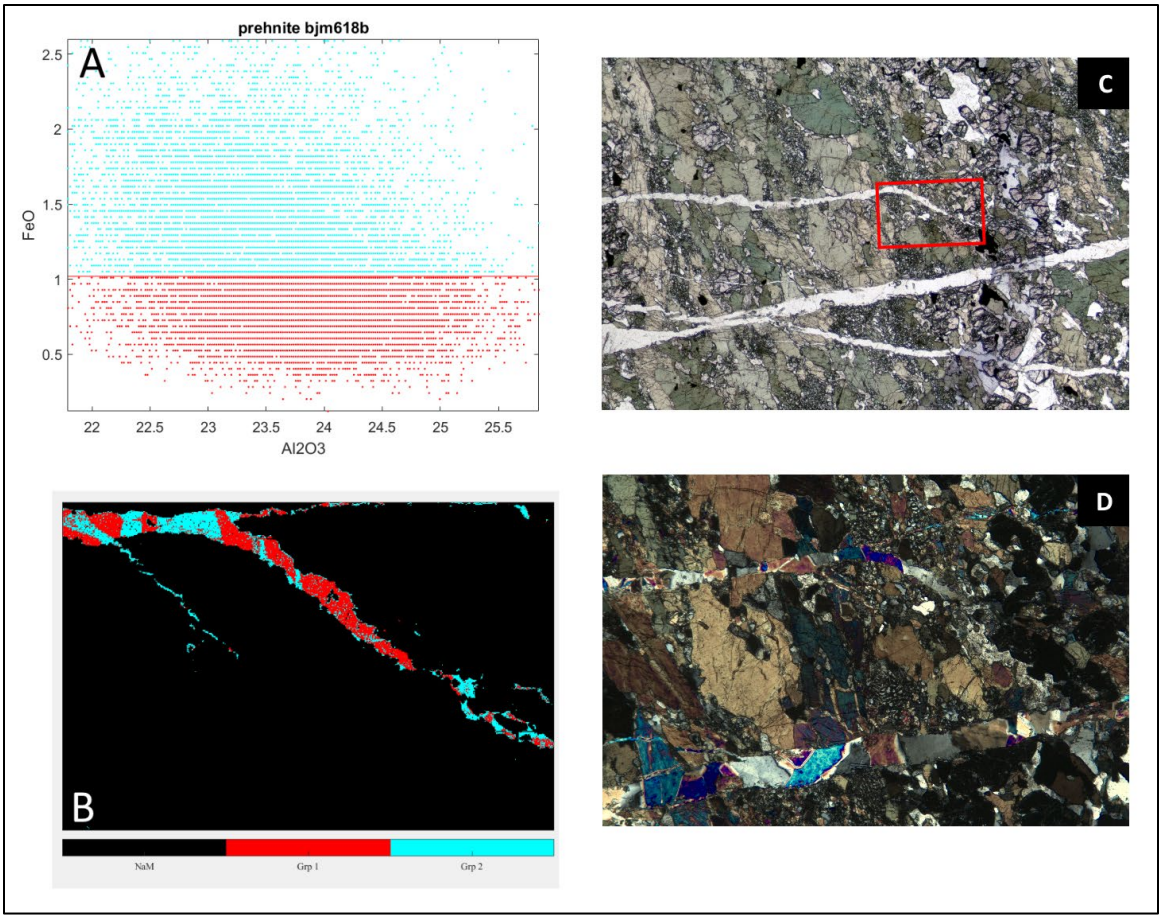

Figure 26: (A) Plot of prehnite pixels in Al-Fe-oxide space showing two groups. Group 1 has lower Fe-content compared to group 2. (B) Corresponding map of prehnite groups displaying polygonal shapes and sharp boundaries. (C) Photomicrograph in plane-polarized light of sample bjm618 with mapped area outlined in red. (D) Detailed view of prehnite veins in cross-polarized light.

4.4 Mineralogy of Bakersville Samples

The map acquired on sample bkmc0118a (Fig 27A) shows a millimetric subhedral garnet with inclusions of rutile and quartz. Adjacent to the garnet is coarse-grained polygonal clinopyroxene with a primary omphacitic core and retrograde diopsidic rim. A second type of diopsidic clinopyroxene occurs as coarse poikiloblastic grains with lamellar inclusions of hornblende and plagioclase. Plagioclase occurs between grains of pyroxene with hornblende and minor quartz and between pyroxene and garnet.

The map acquired on sample bkmc0218b (Fig 27B) shows millimetric anhedral garnet that has been partially replaced by fine-grained kelyphite of calcic plagioclase and hornblende with a semi-circular shape that intrudes into the garnet. The hornblende of this kelyphite extends as a partial rim around the garnet and separates it from spongy clinopyroxene containing blebs of sodic plagioclase, hornblende, and rarely quartz. Coarse-grained pyrite occurs adjacent to the kelyphite distal to garnet.

The map acquired on sample bkmc0418a (Fig 27C) shows millimetric anhedral garnet with an irregular jagged boundary that has inclusions of quartz and rutile and is in direct contact with another garnet. The garnet is surrounded by a very thin polymineralic rim of plagioclase feldspar and an unidentified phase containing Si, Al, Ca, and Fe. The matrix consists of a broad area of quartz as well as amphibole with a sieve-like texture occupied by quartz. Coarse-grained polygonal rutile occurs as an accessory phase.

The map acquired on sample bkmc0518a (Fig 27D) shows a subhedral grain of allanite (250 μm diameter) rimmed with plagioclase that occurs as an inclusion within spongy clinopyroxene that has blebs of plagioclase and hornblende. Medium-grained patches of plagioclase completely surround medium-grained euhedral rutile and partially surround garnet.

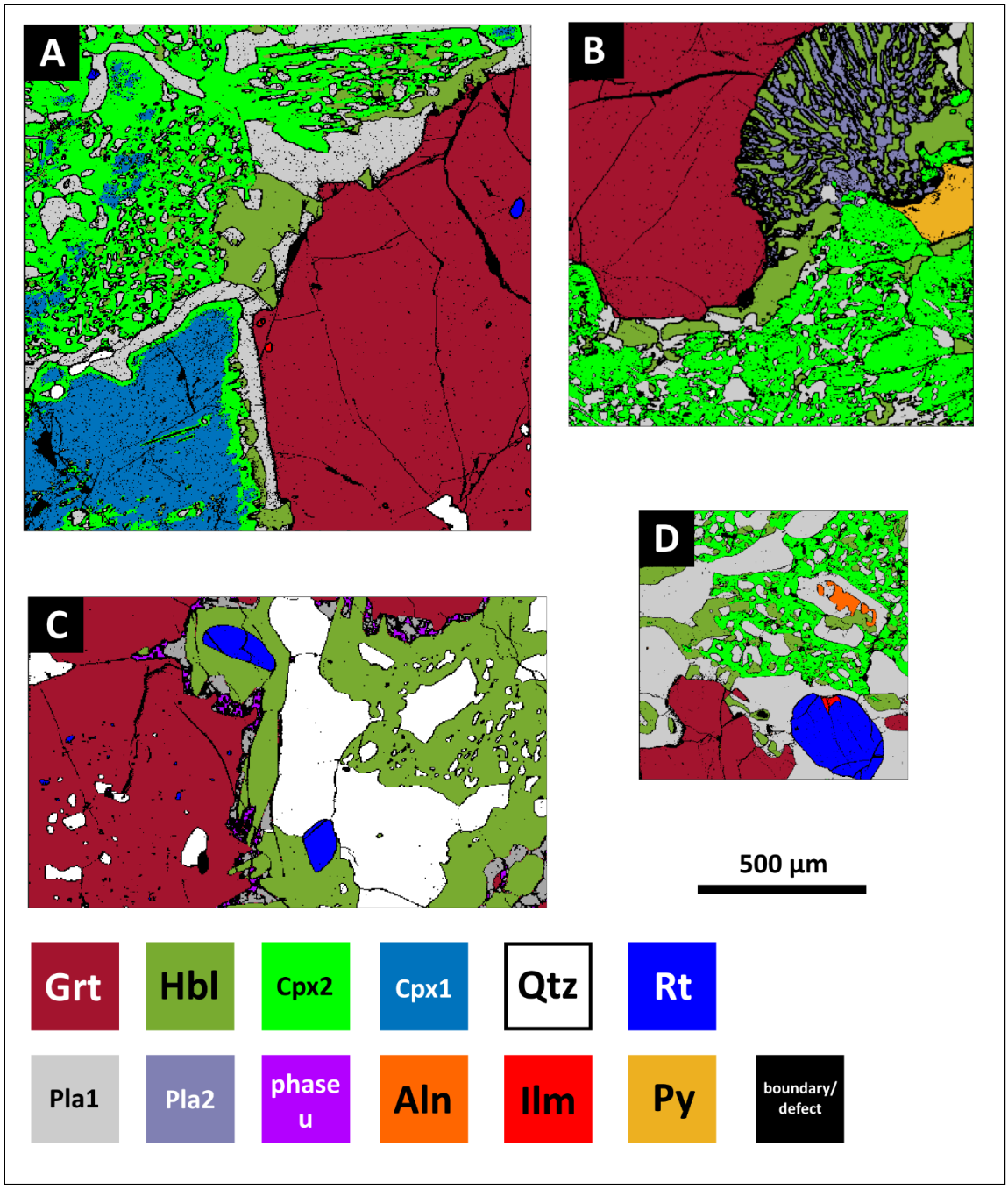

Figure 27: Mineralogy of retrograde eclogites from Bakersville. Each mineral map is from a separate sample and are noncontiguous with one another. A) bkmc0118a; B) bkmc0218b; C) bkmc0418a; D) bkmc0518a. Grt=garnet; Hbl=hornblende; Cpx2=diopsidic clinopyroxene; Cpx1=omphacitic clinopyroxene; Qtz=quartz; Rt=rutile; Pla1=sodic plagioclase; Pla2=calcic plagioclase; phase u=unidentified phase; Aln=allanite; Ilm=ilmenite; Pr=pyrite

4.5 Mineral Chemistry of Bakersville Samples

4.5.1 Garnet

In sample bkmc0118a, the core ($Alm_{53}Grs_{24}Prp_{20}Sps_{03}$) is enriched in Mn and displays decreasing Fe and increasing Mg approaching the rim ($Alm_{46}Prp_{31}Grs_{22}Sps_{01}$). A zone of slight Ca enrichment approximately 150 um thick occurs intermediately between the core and rim (Fig 28).

In sample bkmc0218b the core ($Alm_{47}Prp_{28}Grs_{24}Sps_{01}$) is enriched in Mn and displays decreasing Fe and increasing Mg approaching the rim ($Alm_{43}Prp_{33}Grs_{24}Sps_{00}$). The outermost 100 um of rim ($Alm_{46}Prp_{28}Grs_{24}Sps_{02}$) displays a marked increase in Mn and Fe and a decrease in Mg (Fig 29).

Sample bkmc0418a has a core composition $Alm_{48}Grs_{26}Prp_{26}Sps_{01}$ and a rim composition $Alm_{53}Grs_{24}Prp_{21}Sps_{02}$. Profiles are mostly flat except for the rim in which Fe, Ca, and Mn increase while Mg decreases (Fig 30).

Core-to-rim variances in sample bkmc0518a display an increase in Fe and a decrease in Mg. Near the core the composition is $Alm_{44}Prp_{31}Grs_{24}Sps_{01}$ and at the rim the composition is $Alm_{49}Prp_{26}Grs_{24}Sps_{01}$ (Fig 31)

Garnets are mostly almandine with lesser pyrope and grossular components and little to no spessartine components with most of the variation occurring between Fe and Mg (Fig 32). The core-to-rim evolution coming from the most pristine eclogite, sample bkmc0118a, shows a shift from almandine to pyrope accompanied by increasing-then-decreasing grossular component (Fig 32). Conversely, the evolution coming from a retrograded sample, bkmc0418a, shows a shift from pyrope to almandine accompanied by decreasing-then-increasing grossular component (Fig 32C).

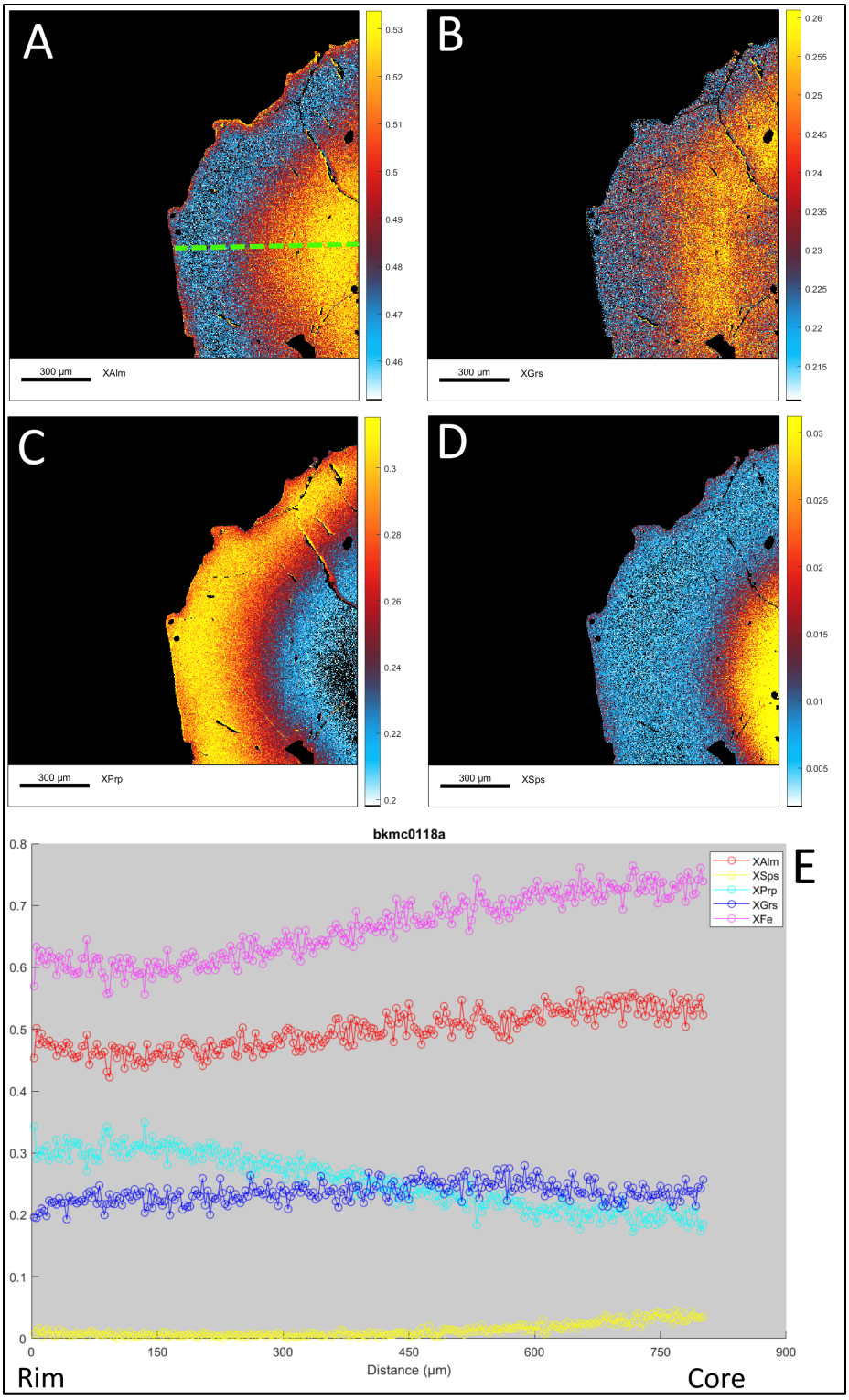

Figure 28: A-D) Garnet zoning maps and profiles from sample bkmc0118a. (A) almandine component (B) grossular component (C) pyrope component (D) spessartine component (E) component profiles corresponding to dashed green line in (A). Fuchsia= XFe; Red=XAlm; Blue=XGrs; Cyan=XPrp; Yellow=XSps

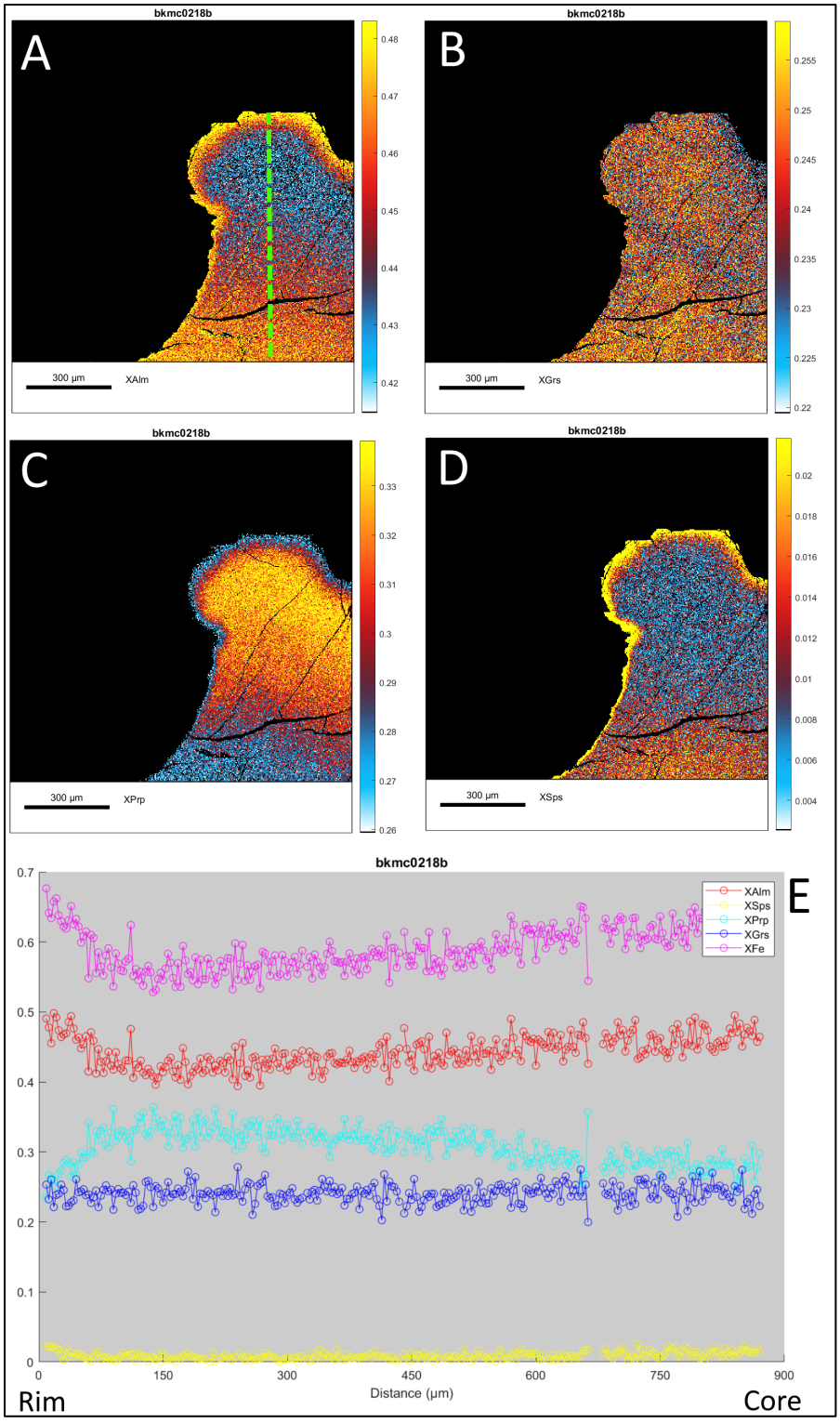

Figure 29: Garnet zoning maps and profiles for sample bkmc0218b. (A) almandine component (B) grossular component (C) pyrope component (D) spessartine component (E) component profiles corresponding to dashed green line in (A). Fuchsia= XFe; Red=XAlm; Blue=XGrs; Cyan=XPrp; Yellow=XSps

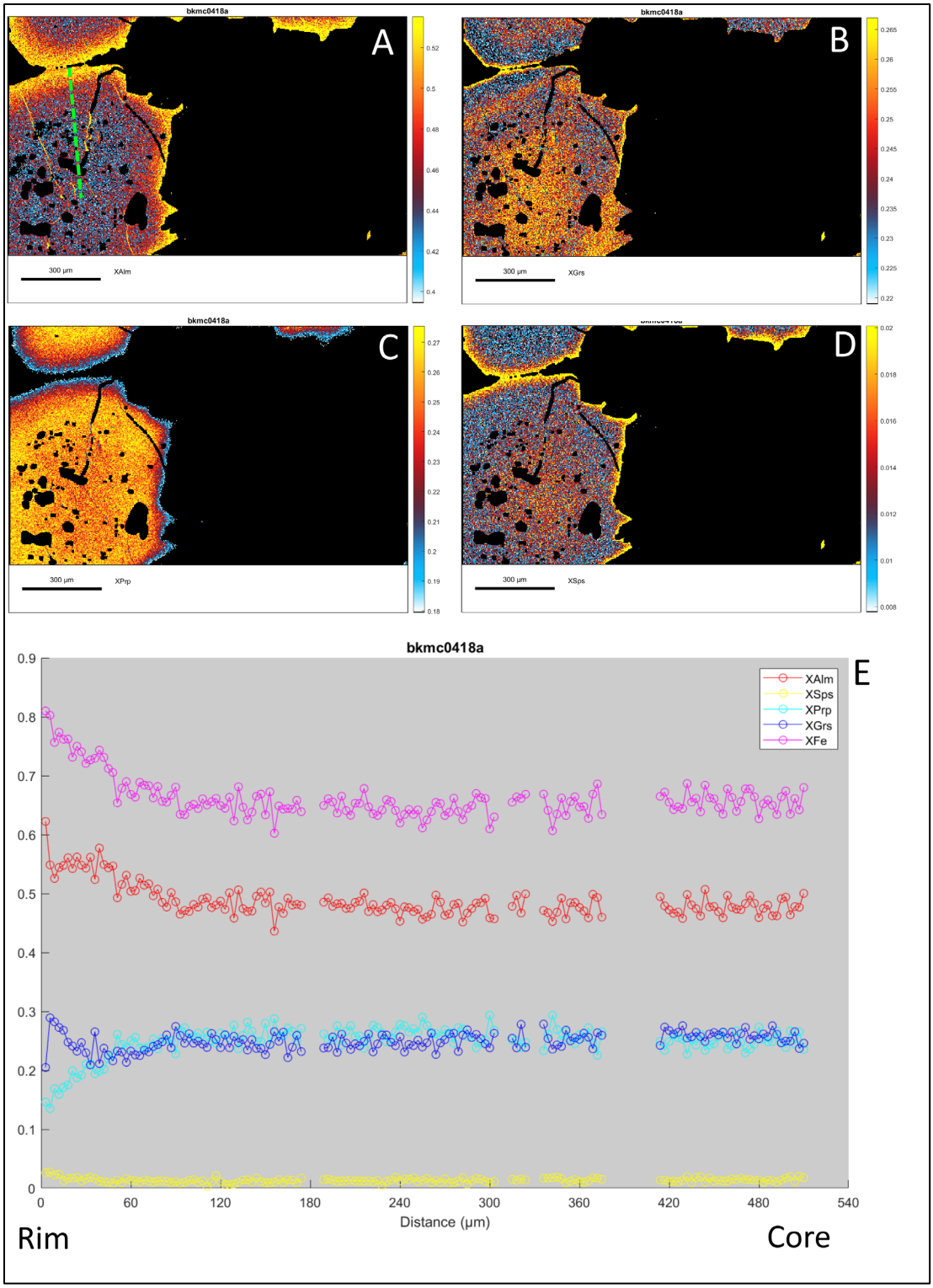

Figure 30: Garnet zoning maps and profiles for sample bkmc0418a. (A) almandine component (B) grossular component (C) pyrope component (D) spessartine component (E) component profiles corresponding to dashed green line in (A). Fuchsia= XFe; Red=XAlm; Blue=XGrs; Cyan=XPrp; Yellow=XSps

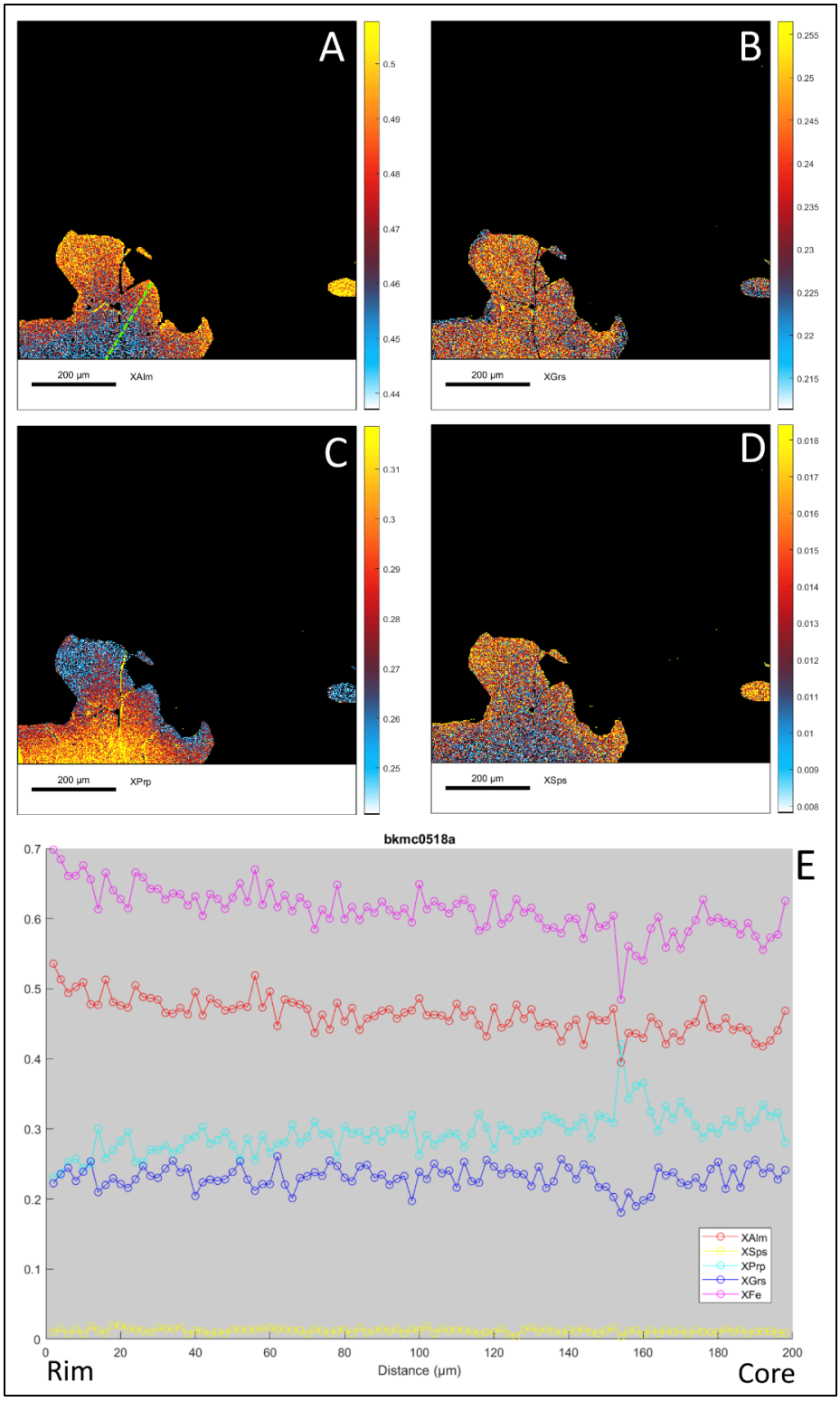

Figure 31: Garnet zoning maps and profiles from sample bkmc0518a. (A) almandine component (B) grossular component (C) pyrope component (D) spessartine component (E) component profiles corresponding to dashed green line in (A). Fuchsia= XFe; Red=XAlm; Blue=XGrs; Cyan=XPrp; Yellow=XSps

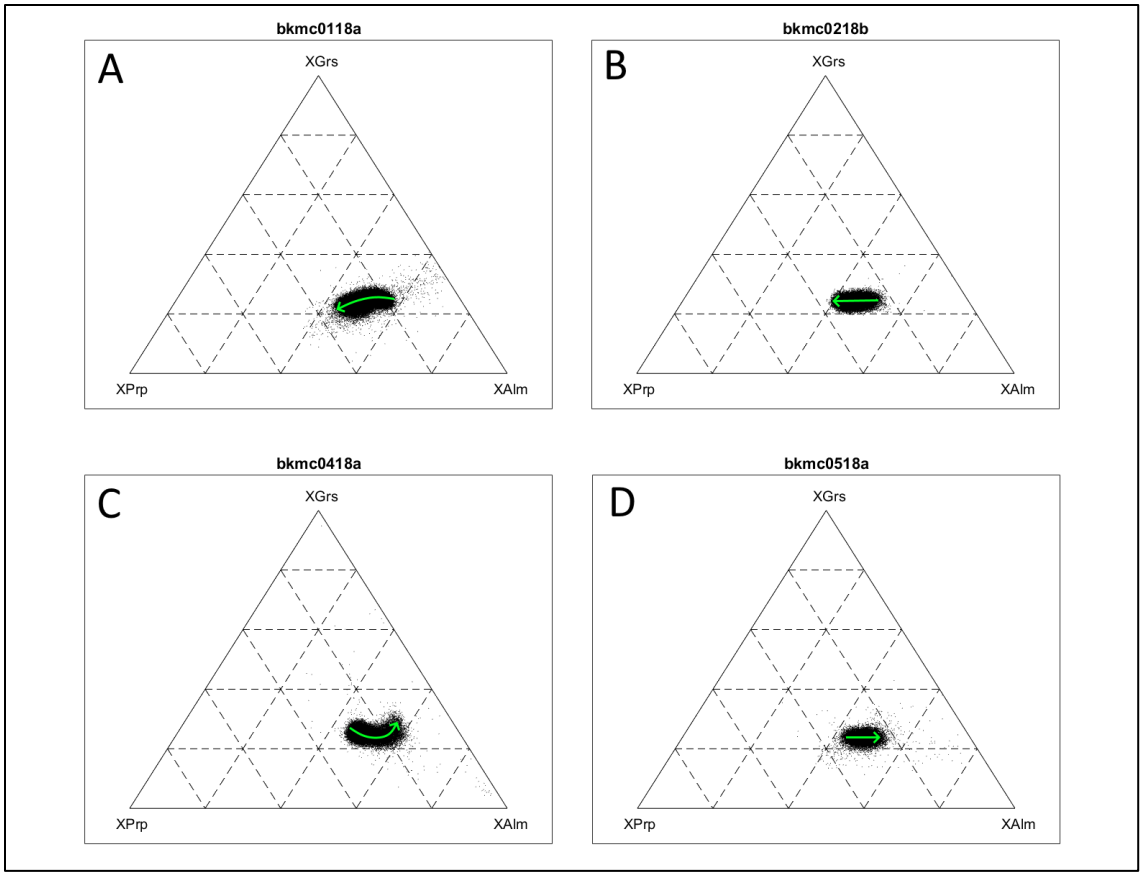

Figure 32: Ternary diagrams for aluminous garnet (Grew et al., 2013). Green arrows show general core-rim progression. Endmembers are pyrope (Prp), grossular (Grs), and almandine (Alm). A) sample bkmc0118a; B) sample bkmc0218b; C) sample bkmc0418a; D) sample bkmc0518a

4.5.2 Pyroxene

Clinopyroxene in the mapped area of sample bkmc0118a can be classified into two main groups: omphacite and diopside while a very small fraction classifies as aegirine-augite (Fig 33). Primary omphacite has a core composition $Di_{57}Jd_{25}Hd_{09}Ae_{05}Cats_{05}$ and an outer diopsidic rim ($Di_{67}Hd_{15}Jd_{07}Ae_{07}Cats_{07}$). Spongy clinopyroxene is diopsidic with an average composition $Di_{69}Hd_{14}Jd_{08}Ae_{05}Cats_{04}$ (Fig 34A). Coarser-grained regions within spongy Cpx have an intermediate composition between omphacite and diopside (Fig 34B).

In the mapped area of sample bkmc0218b, spongy Cpx is diopsidic overall (Fig 35). Coarser-grained regions within spongy clinopyroxene are more omphacitic (i.e., have a higher

jadeite component) ($Di_{61}Hd_{17}Jd_{11}Cats_{10}Ae_{04}$) than finer-grained regions ($Di_{71}Hd_{20}Cats_{05}Jd_{04}Ae_{04}$) (Fig 36).

No pyroxene was mapped in sample bkmc0418a.

Pyroxene in the mapped area of sample bkmc0518a is diopsidic (Fig 37) and ranges in composition from $Di_{79}Hd_{29}Cats_{10}Ae_{04}Jd_{06}$ to $Di_{67}Hd_{19}Cats_{14}Ae_{09}Jd_{04}$. This sample lacks the jadeite-enriched core regions seen in other samples. Interestingly, deficiencies in diopside component correspond with small enrichments in Calcium Tschermak's component ($CaAlAlSiO_6$) (Fig 38).

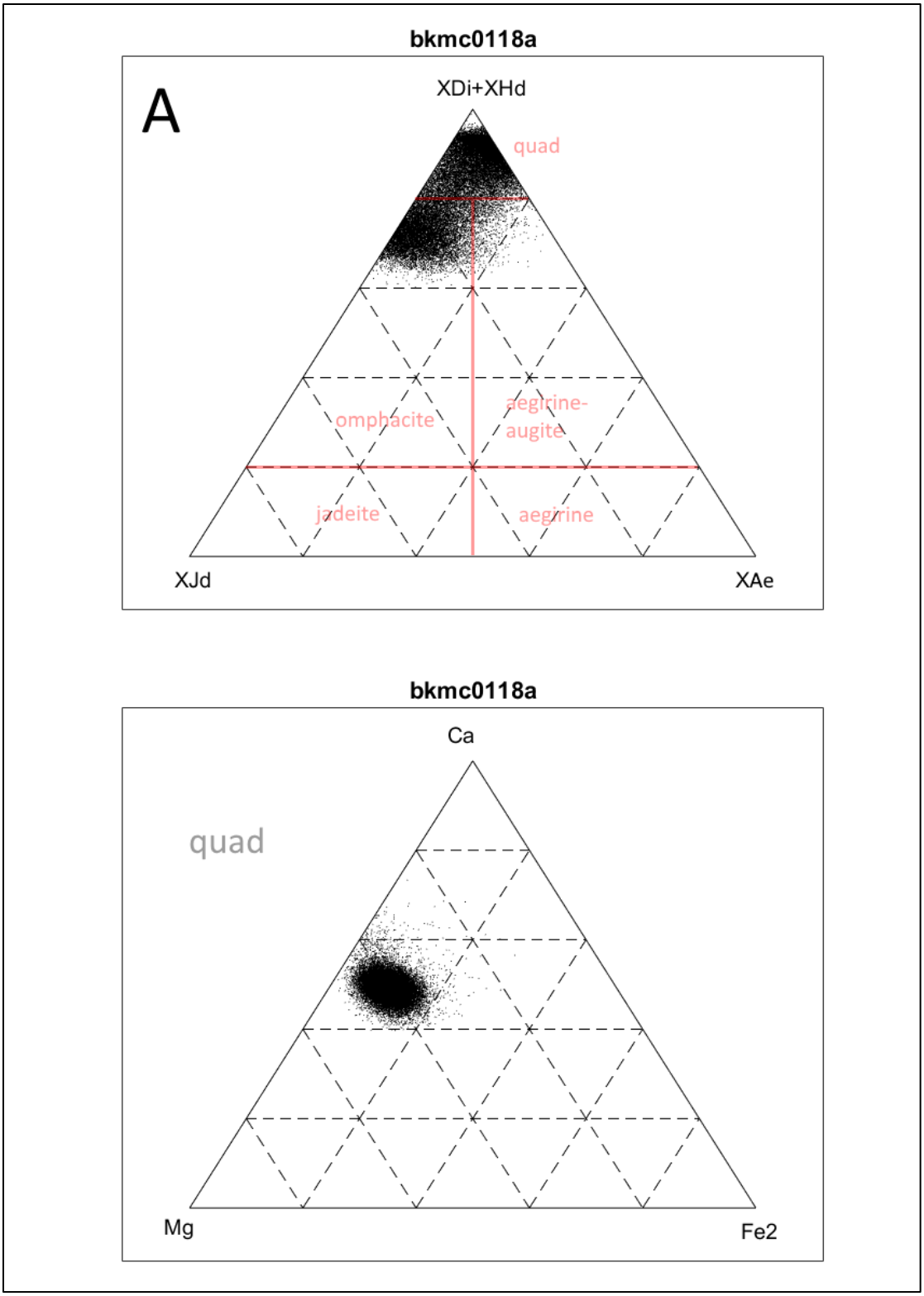

Figure 33: Pyroxene ternary diagrams for sample bkmc0118a (Morimoto, 1989). (A) Two distinct groups occupy the omphacite and quad fields that represent primary and symplectic CPX respectively. Jd=jadeite; Ae=aegirine; Di=diopside; Hd=hedenburgite. (B) Symplectic CPX plots as diopside.

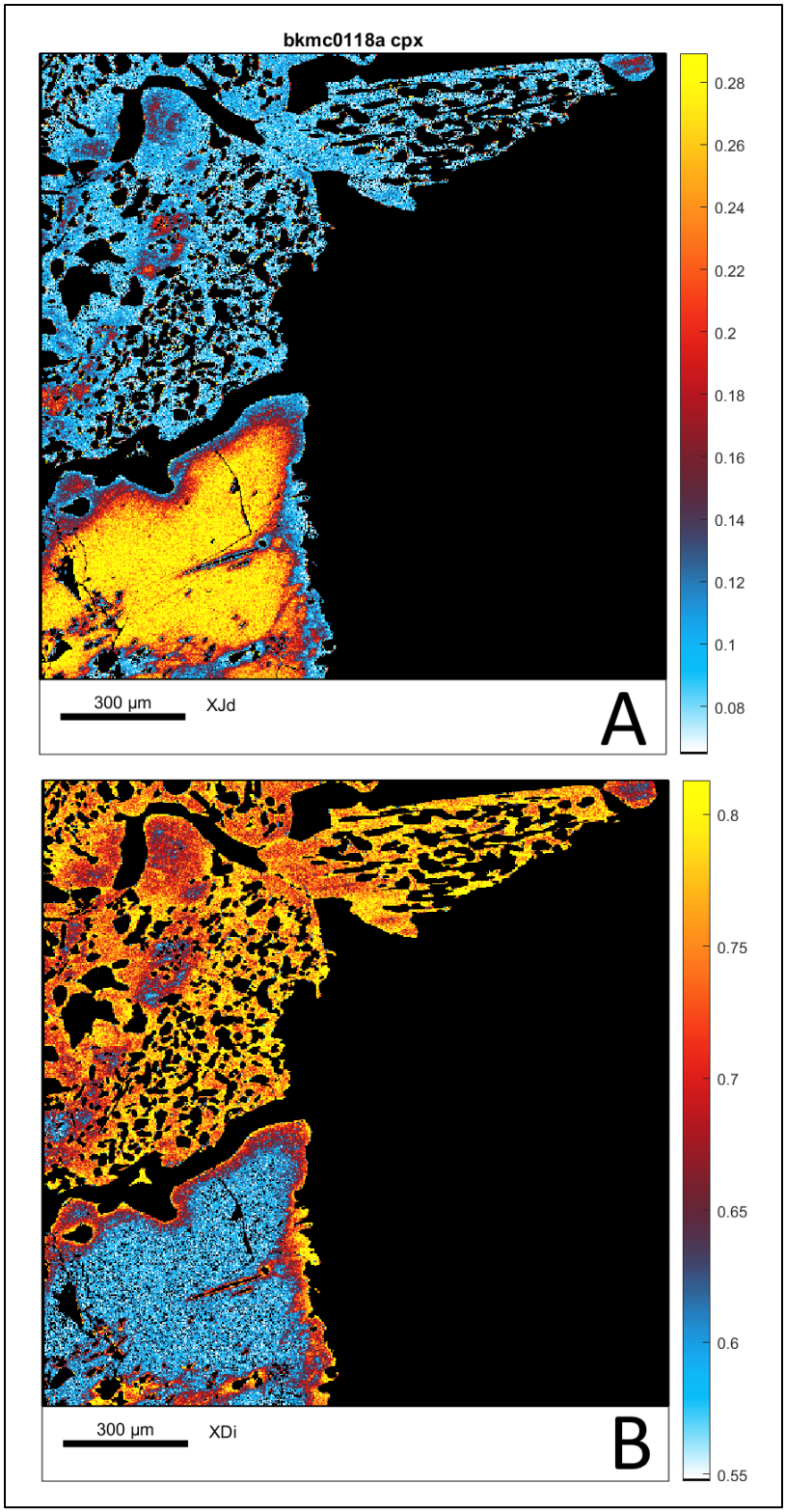

Figure 34: Mapped jadeite component (A) and diopside component (B) for clinopyroxene in sample bkmc0118a.

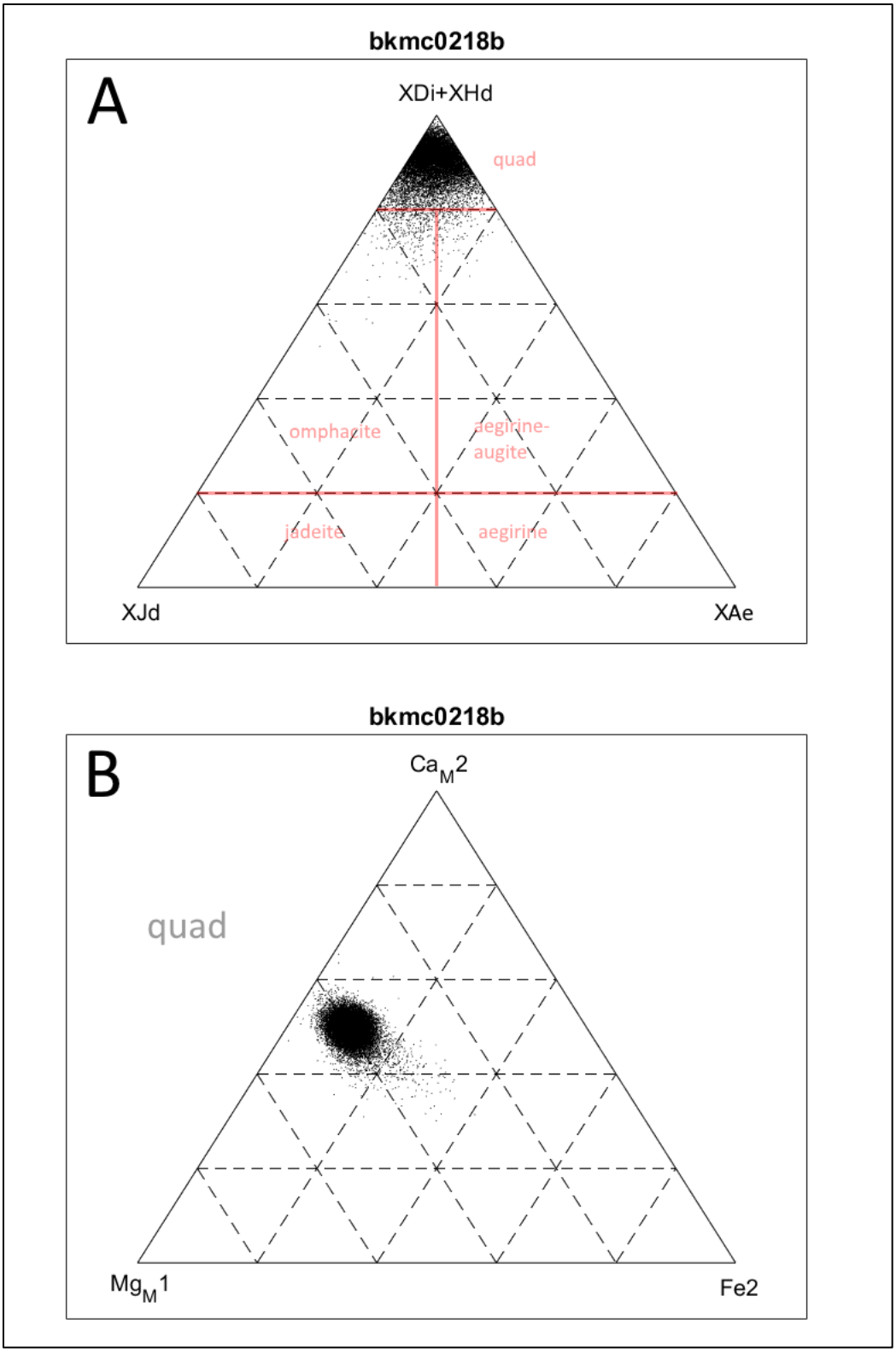

Figure 35: Pyroxene ternary diagrams for sample bkmc0218b (Morimoto, 1989). (A) has end members jadeite (Jd), aegirine (Ae), and diopside (Di) + hedenbergite (Hd) which make up the quad (B).

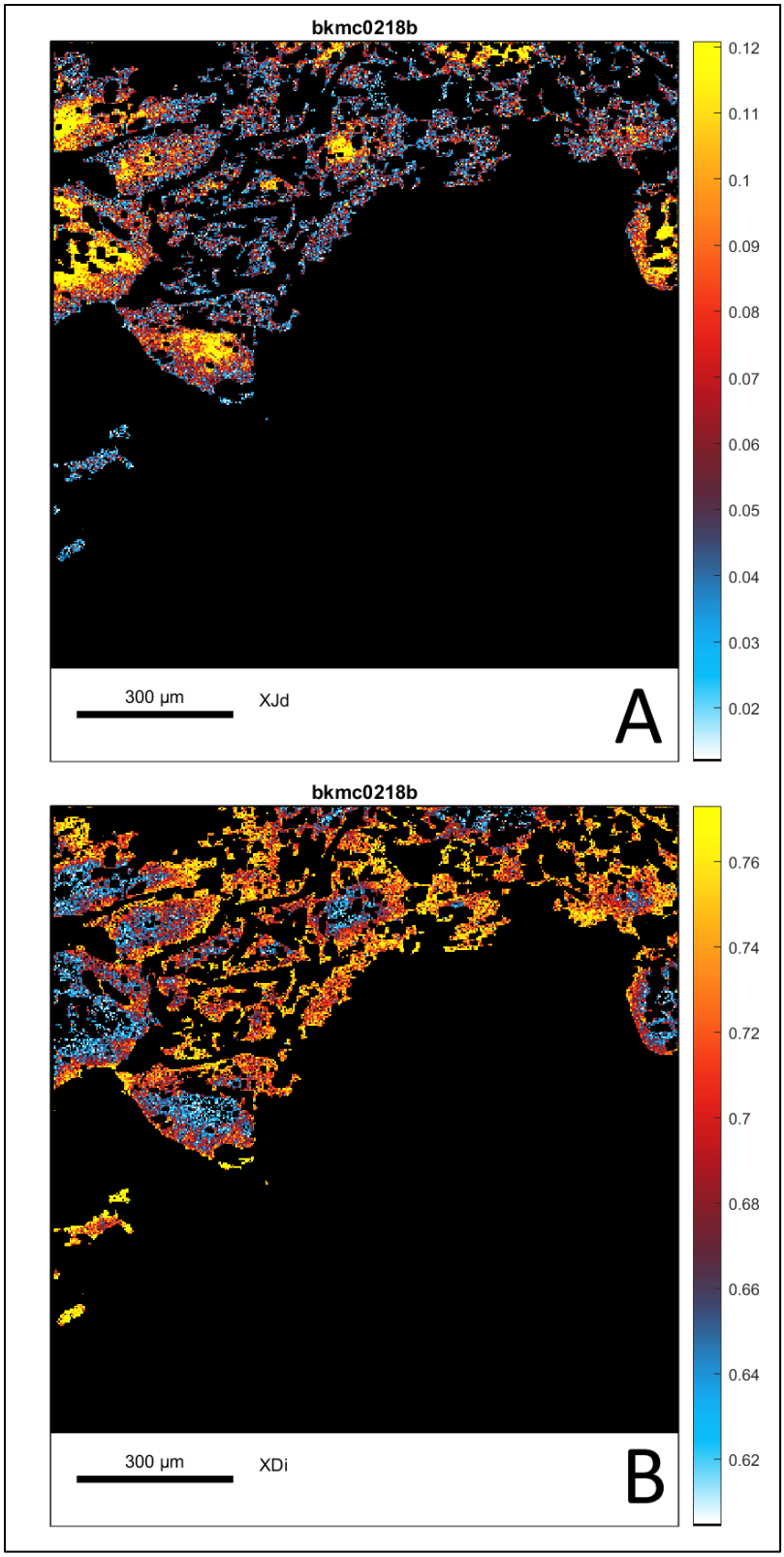

Figure 36: Mapped jadeite component (A) and diopside component (B) for clinopyroxene in sample bkmc0218b

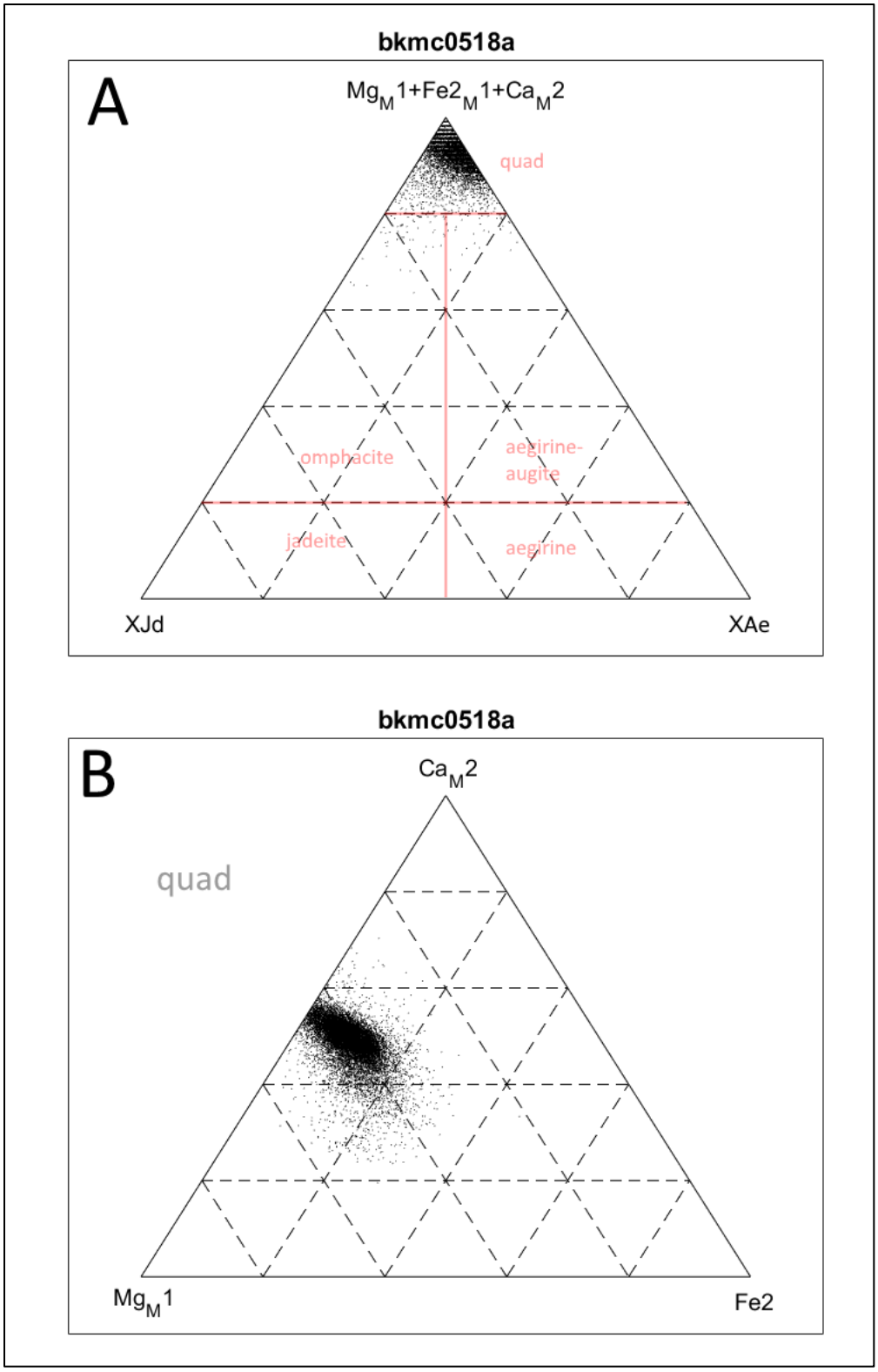

Figure 37: Pyroxene ternary diagrams for sample bkmc0518a (Morimoto, 1989). (A) has end members jadeite (Jd), aegirine (Ae), and diopside (Di) + hedenbergite (Hd) which make up the quad (B).

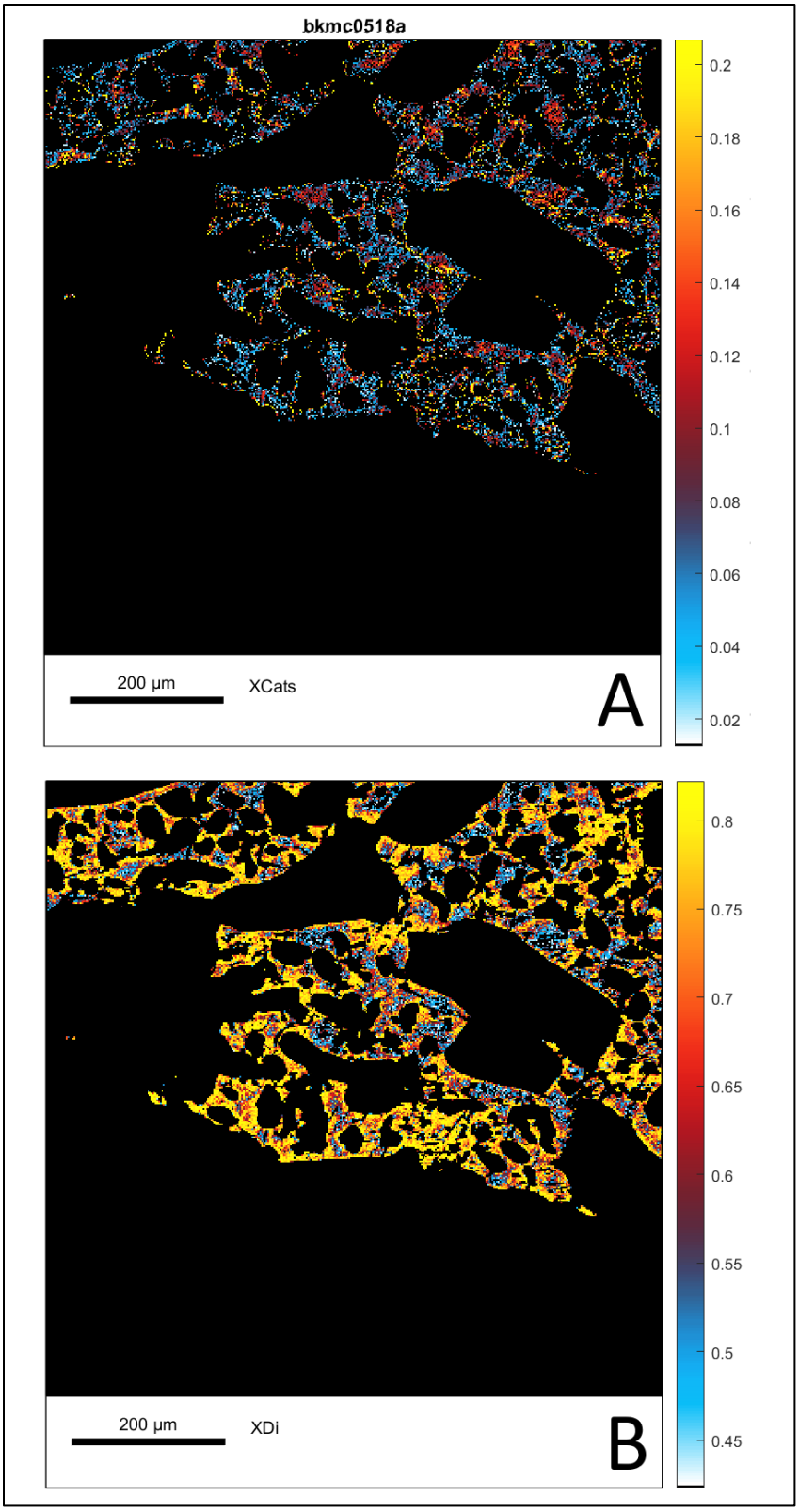

Figure 38: Mapped Calcium-Tschermak's component (A) and diopside component (B) for clinopyroxene in sample bkmc0518a

4.5.3 Amphibole

Amphibole in samples bkmc0118a and bkmc0218b largely classify as magnesiohastingsite (Figs 37A,B,C), while amphibole found in samples bkmc0418a and bkmc0518a have a greater Si/Al ratio and largely classify as edenite (Figs 39D,E).

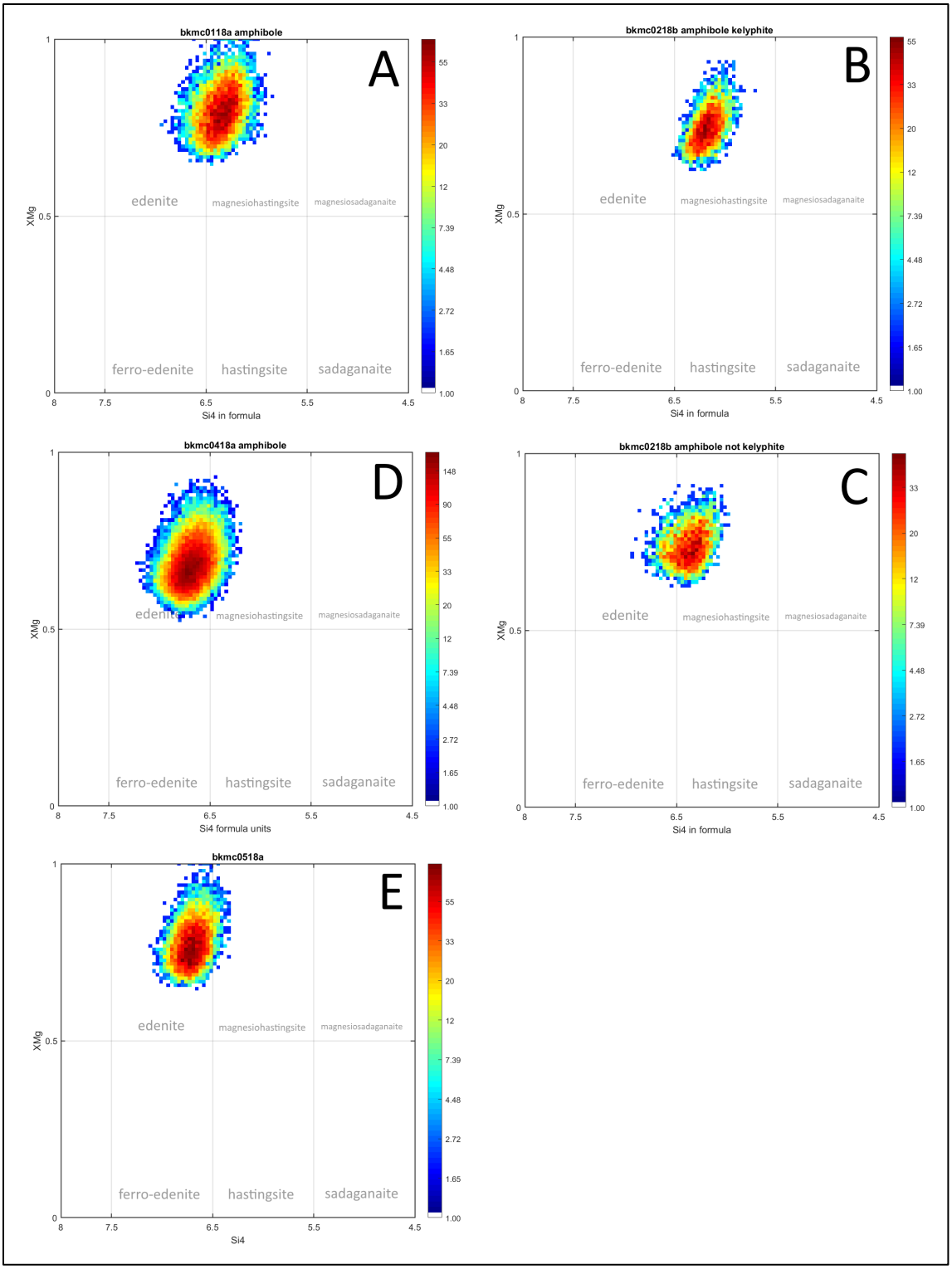

Figure 39: Frequency plots of amphibole compositions in Calcic amphibole nomenclature diagrams after Leake, et al., 1997 . (A) bkmc0118a; (B) bkmc0218b kelyphite; (C) bkmc0218b non-kelyphite; (D) bkmc0418a; (E) bkmc0518a

4.5.4 Feldspar

In the mapped area of sample bkmc0118a, feldspar occurs as sodic plagioclase with little-to-no K content and ranges in composition from oligoclase to andesine (Fig 40A). Plagioclase that outlines garnet and CPX has the average composition $Ab_{79}An_{20}Or_{01}$ and classifies as oligoclase. Plagioclase that occurs together with diopside in fine-grained symplectite and has the composition $Ab_{68}An_{31}Or_{00}$ and classifies as andesine (Fig 40B).

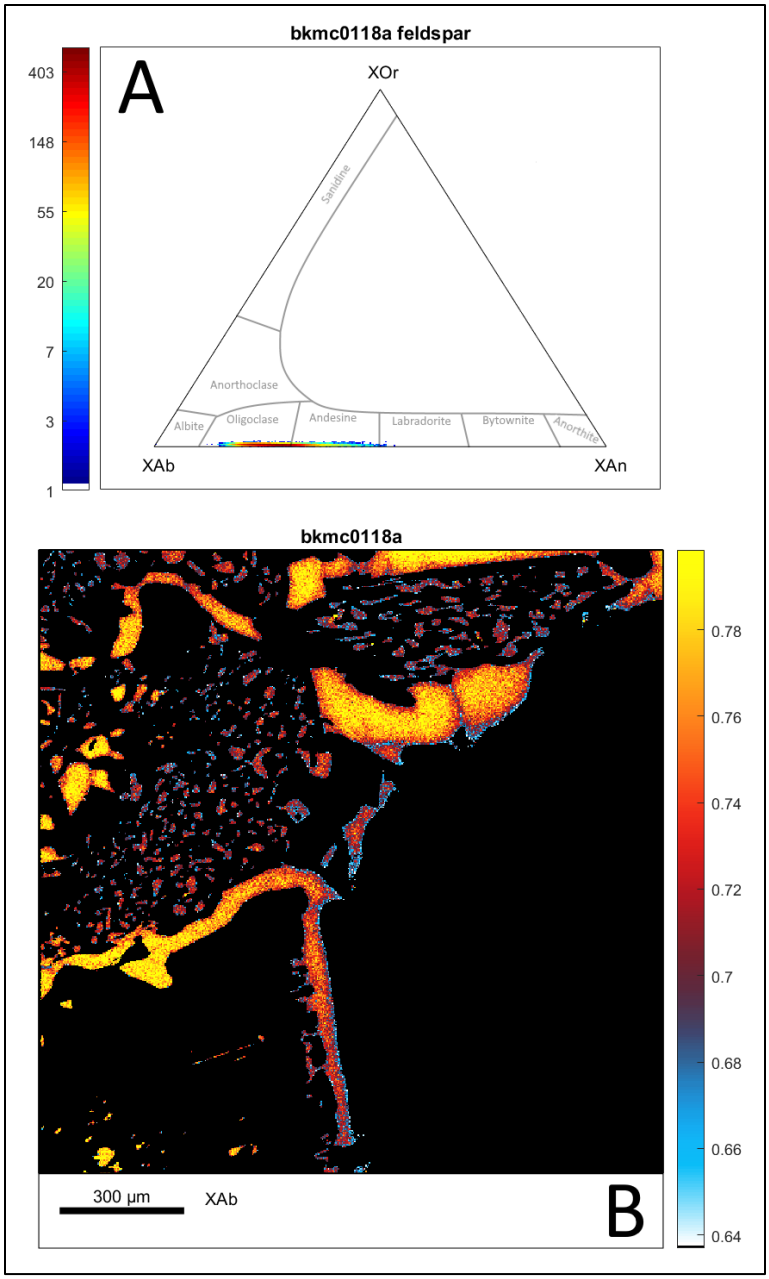

Figure 40: (A) Feldspar ternary diagram showing density plot of feldspar analyzed in sample bkmc0118a. (B) Mapped albite component fraction (XAb) in feldspar for sample bkmc0118a.

In the mapped area of sample bkmc0218b, two groups of plagioclase feldspar are recognized. Kelyphitic plagioclase has the average composition $An_{92}Ab_{08}Or_{00}$ and classifies as anorthite while symplectitc plagioclase has the average composition $Ab_{77}An_{23}Or_{00}$ and classifies as oligoclase (Fig 41A). Symplectic plagioclase becomes more calcic ($Ab_{60}An_{40}Or_{00}$) leading up to the contact with garnet and classifies as andesine (Fig 41B).

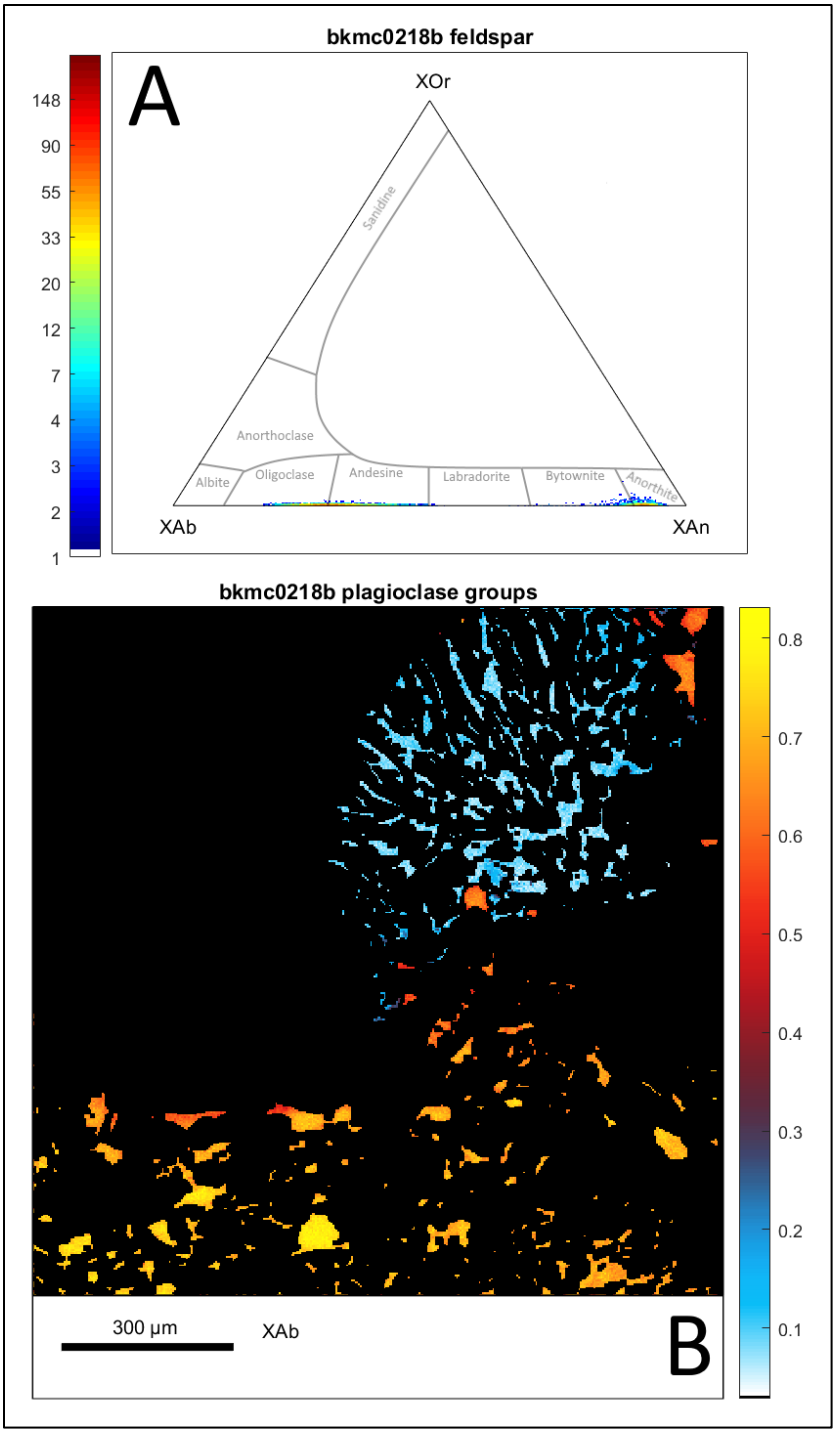

Figure 41: (A) Feldspar ternary diagram showing density plot of feldspar analyzed in sample bkmc0218b. (B) Mapped albite component fraction (XAb) in feldspar for sample bkmc0218b.

In the mapped area of sample bkmc0418a, three distinct groups of feldspar are recognized (Fig 40A). Group 1 largely classifies as bytownite plagioclase and has an average

composition $An_{81}Ab_{19}Or_{00}$. Group 2 largely classifies as labradorite plagioclase and has an average composition $An_{66}Ab_{34}Or_{00}$. Group 3 largely classifies as andesine plagioclase and has an average compositon $Ab_{64}An_{36}Or_{00}$ (Fig 40B).

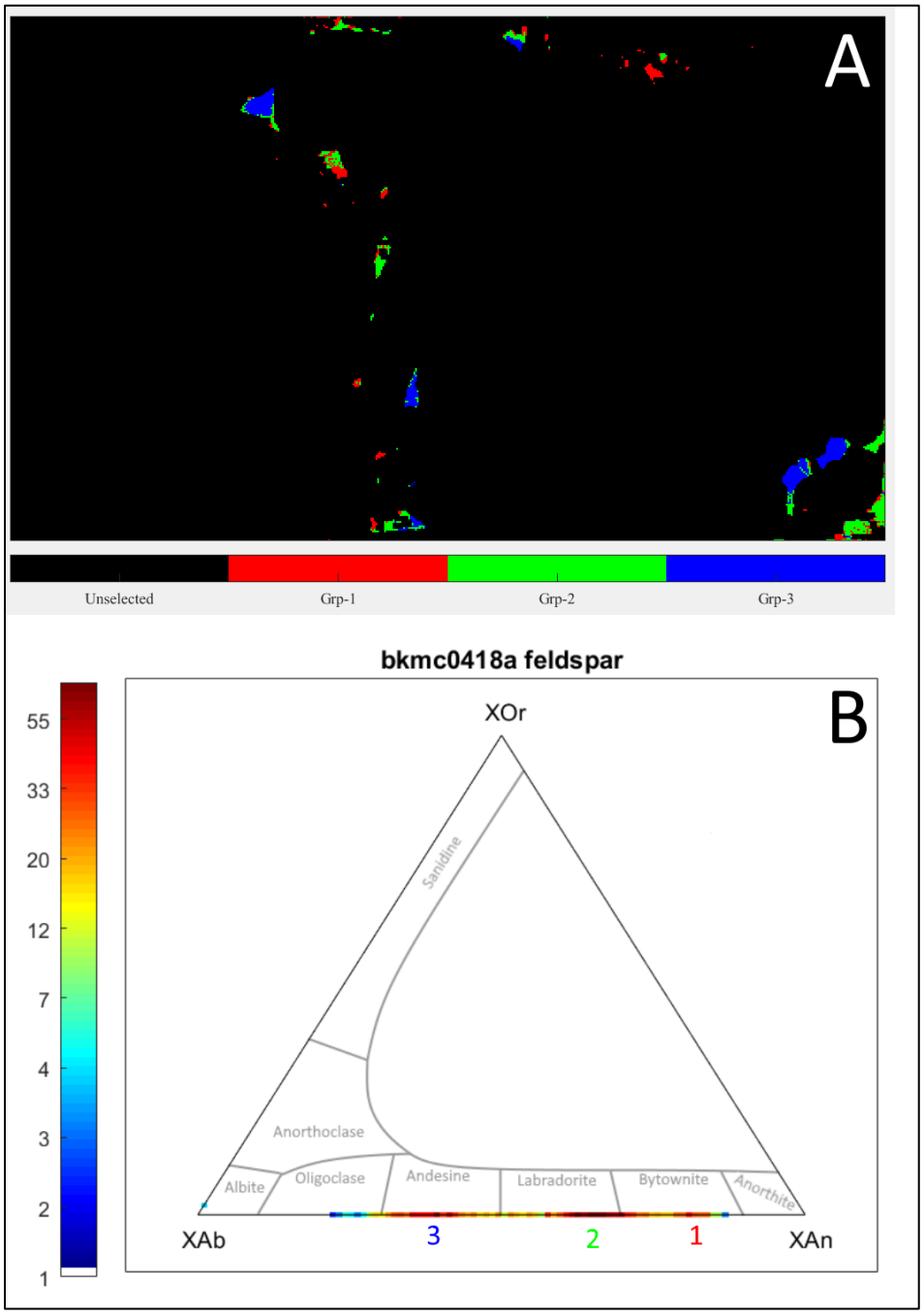

Figure 42: (A) Feldspar in mapped area of sample bkmc0418a occurs in three distinct groups. (B) Feldspar ternary diagram showing compositions of three groups of plagioclase that occur in mapped area of sample bkmc0418a. XAb=albite component; XAn=anorthite component

In the mapped area of sample bkmc0518a, feldspar is sodic and ranges from oligoclase to andesine plagioclase (Fig 43A). Moderately coarse grains have cores with an average composition $Ab_{78}An_{21}Or_{01}$ that become less sodic toward the rim. Symplectitc plagioclase is fine grained and has an average composition $Ab_{61}An_{38}Or_{01}$ (Fig 43B).

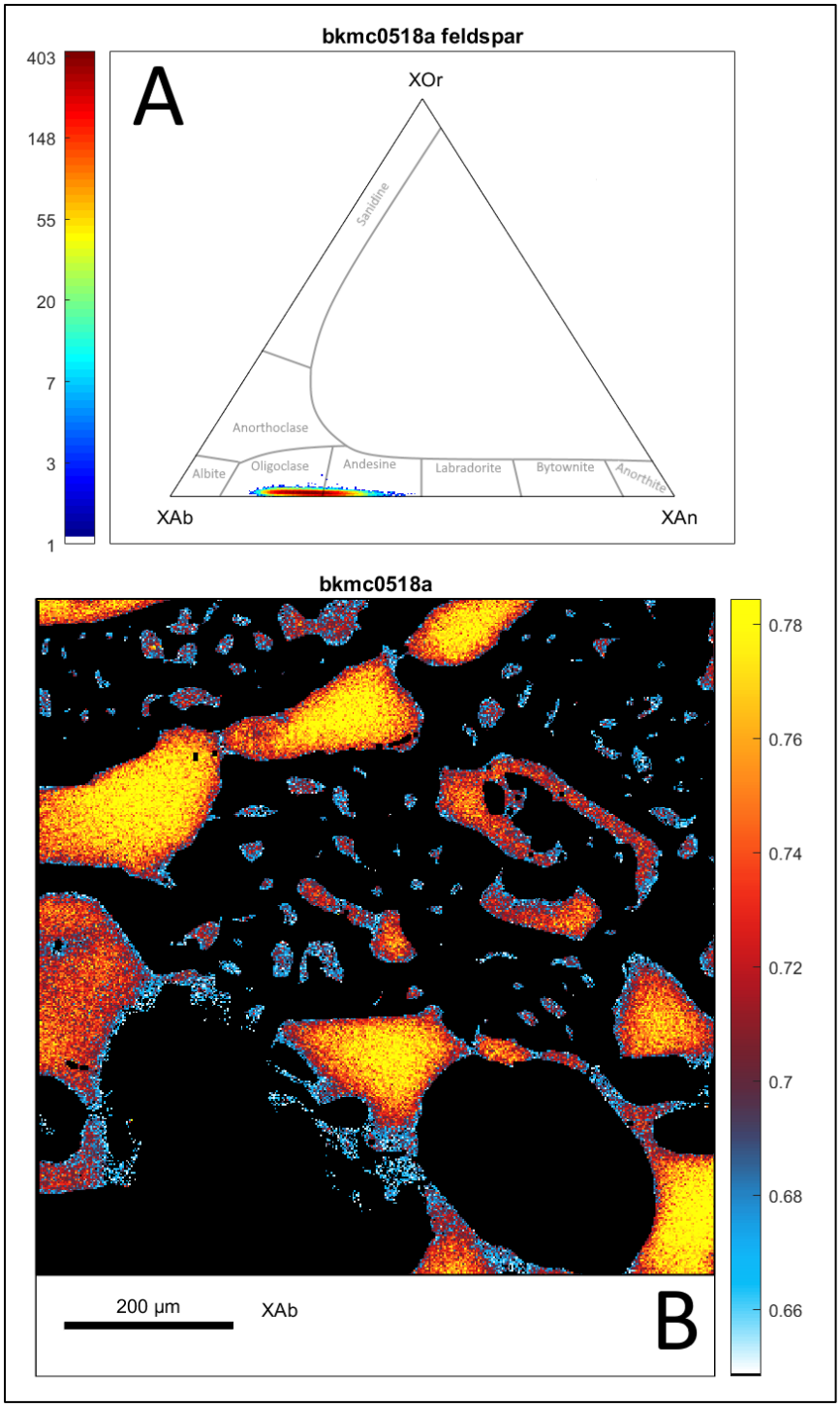

Figure 43: (A) Feldspar ternary diagram showing density plot of feldspar analyzed in sample bkmc0518a. (B) Mapped albite component fraction (XAb) in feldspar for sample bkmc0518a.

4.5.5 Allanite

In a backscatter electron image, allanite shows up bright compared to surrounding plagioclase and amphibole and displays faint concentric zoning (Fig 44). Approximately 16% oxide weight percent is not accounted for by the major element analysis (Table 5)

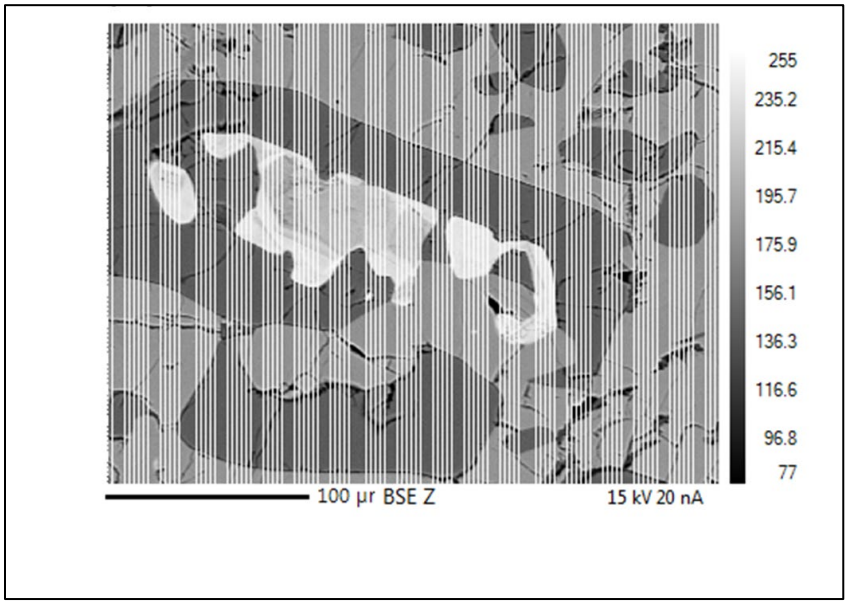

Figure 44: (A) backscatter electron (BSE) image of allanite grain. Brighter areas correspond to elements with higher atomic weights.

Table 5: Average wt% oxides of allanite from sample bkmc0518a

Allanite	
Oxide	wt%
Al_2O_3	19.9835
CaO	15.7829
Cr_2O_3	0.15709
FeO	10.0223
K_2O	0.021953
MgO	1.0336
MnO	0.097214
Na_2O	1.3669
SiO_2	34.9025
TiO_2	0.63303
Sum	84.0009

4.5.6 Phase u (*unidentified phase)*

In the mapped area of sample bkmc0418a, a phase occurs with plagioclase feldspar between garnet grains and between garnet and hornblende (Fig 45A). It has similar Si and Al content as feldspar but is lacking in Ca and Na (Fig 45B) and approximately 17% of its chemical composition is not accounted for by major element analysis (Table 6). Given its chemistry and intergranular occurrence, a likely candidate for this unidentified phase is pyrophyllite.

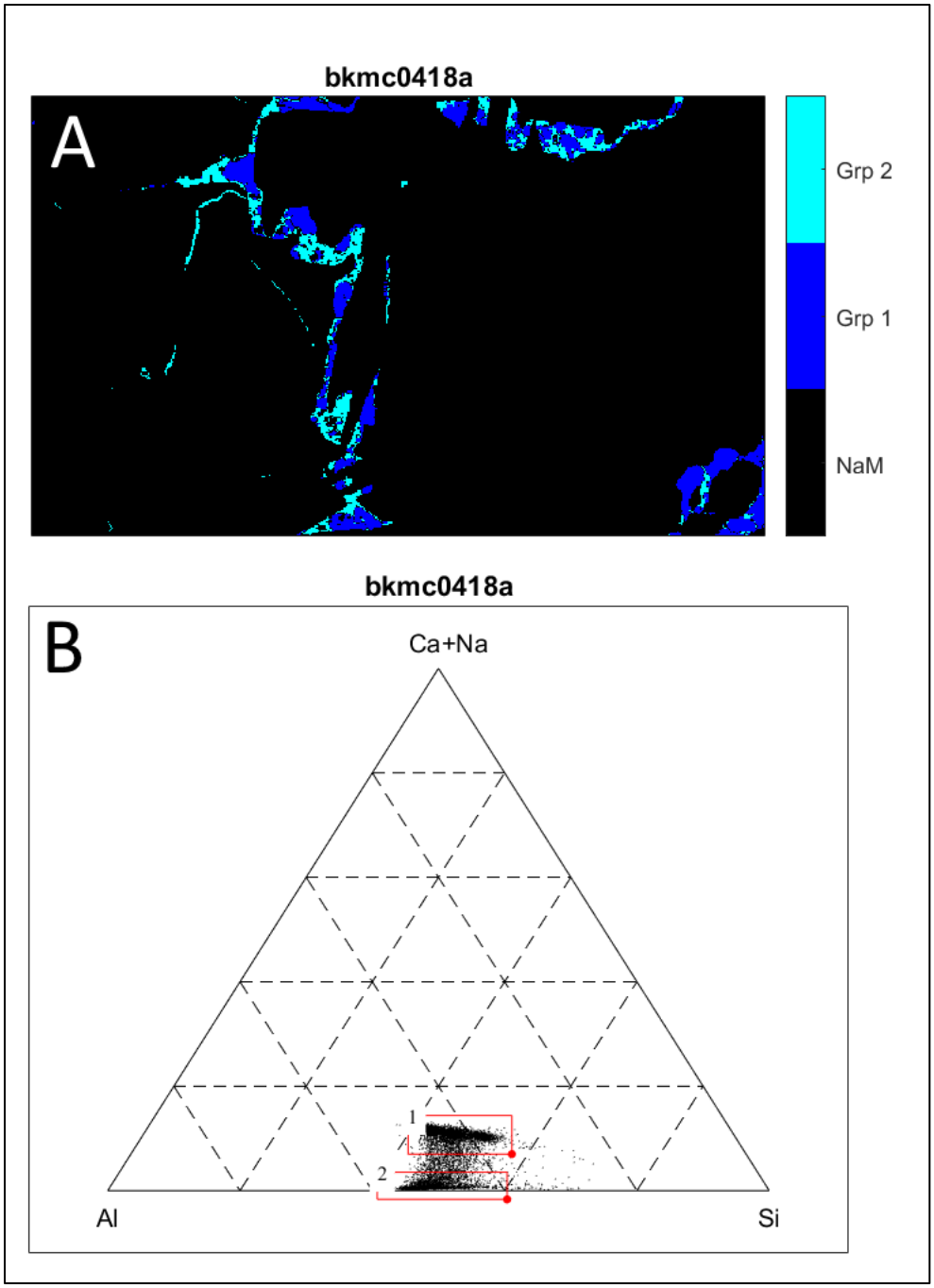

Figure 45: (A) Mapped area of sample bkmc0418a showing plagioclase feldspar (group 1) and unidentified phase (group 2). (B) Ternary diagram showing compositions of plagioclase (group 1) and unidentified phase (group 2).

Table 4: Table 6: Average wt% oxides for unidentified phase in sample bkmc0418a.

Phase *u*	
Oxide	wt%
Al_2O_3	32.0105
CaO	1.6283
Cr_2O_3	-
FeO	3.0998
K_2O	0.19098
MgO	0.22454
MnO	0.00587
Na_2O	0.63257
SiO_2	45.0826
TiO_2	0.01942
SUM	82.8946

4.6 Pressure-Temperature Estimates from Boone Samples

4.6.1 Sample bhcm418m1

Temperature estimates of garnet-hornblende pairs based on the calibration of Ravna (2000) are 591 ± 45 ºC for inclusions in garnet and 645 ± 48 ºC at garnet rim.

Pressure-temperature estimates, based on the assemblage amphibole-plagioclase-quartz, mapped to amphibole pixels range from approximately 620-730 ºC and 5.4-9.3 kbar. Hornblende surrounding garnet, and linear fractures in hornblende record higher pressures compared to the rest of mapped hornblende (Fig 46).

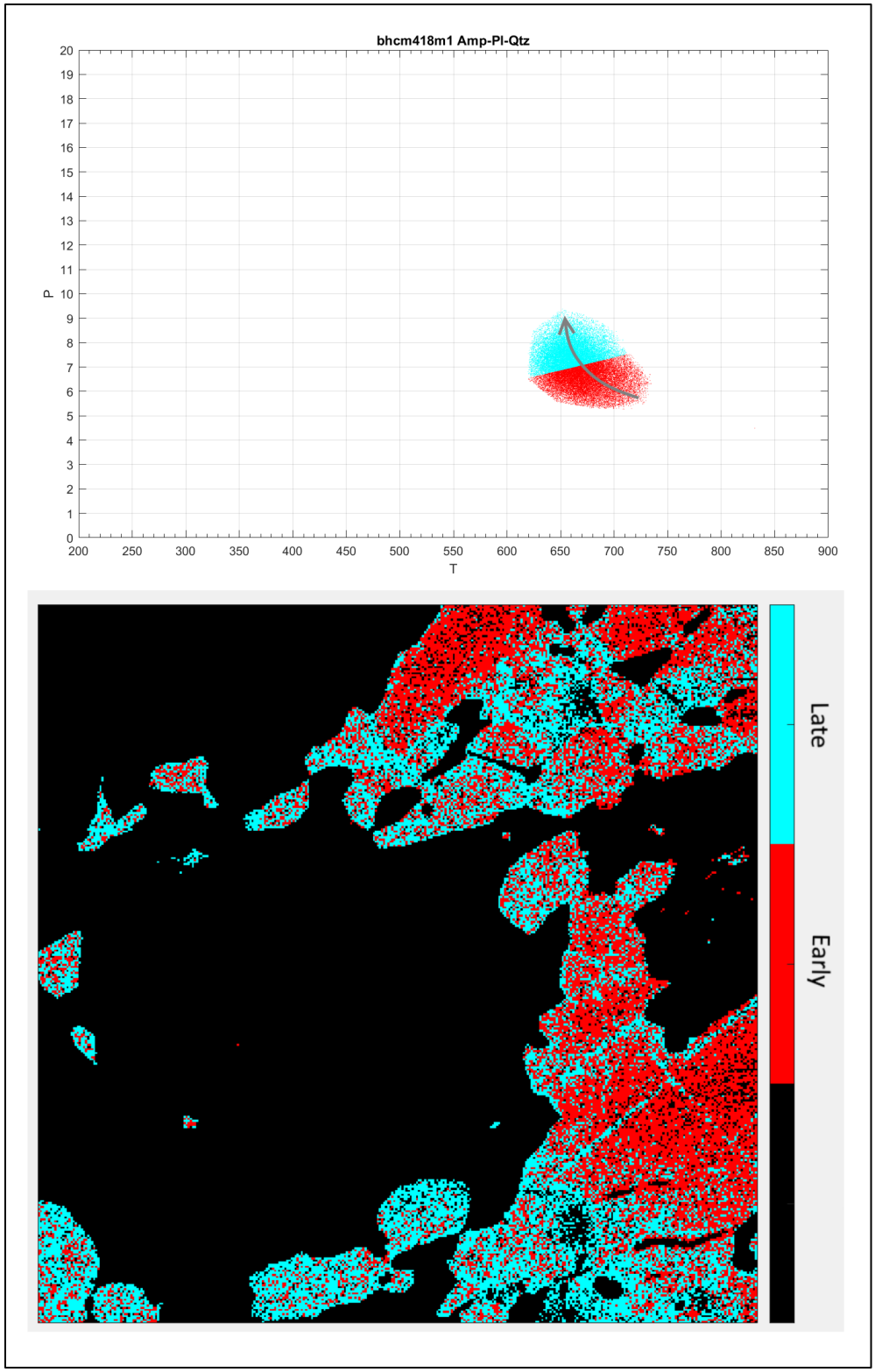

Figure 46: Pressure-temperature results based on the assemblage amphibole-plagioclase-quartz for sample bhcm418m1. A late increase in pressure is recorded in amphibole and is concentrated around garnet and at perpendicular linear fractures (lower right).

4.6.2 Sample bhcm418m2

Temperature estimates of hornblende-garnet pairs based on the calibration of Ravna (2000) yield different values depending on different areas selected (Fig 47). A temperature estimate of the formation of a hornblende inclusion in garnet is 601°C ±40 (Fig 47D). Estimates based on garnet-rim with matrix hornblende are warmer and range from 614°C ±42 to 705°C ±60 (Fig 47A-C).

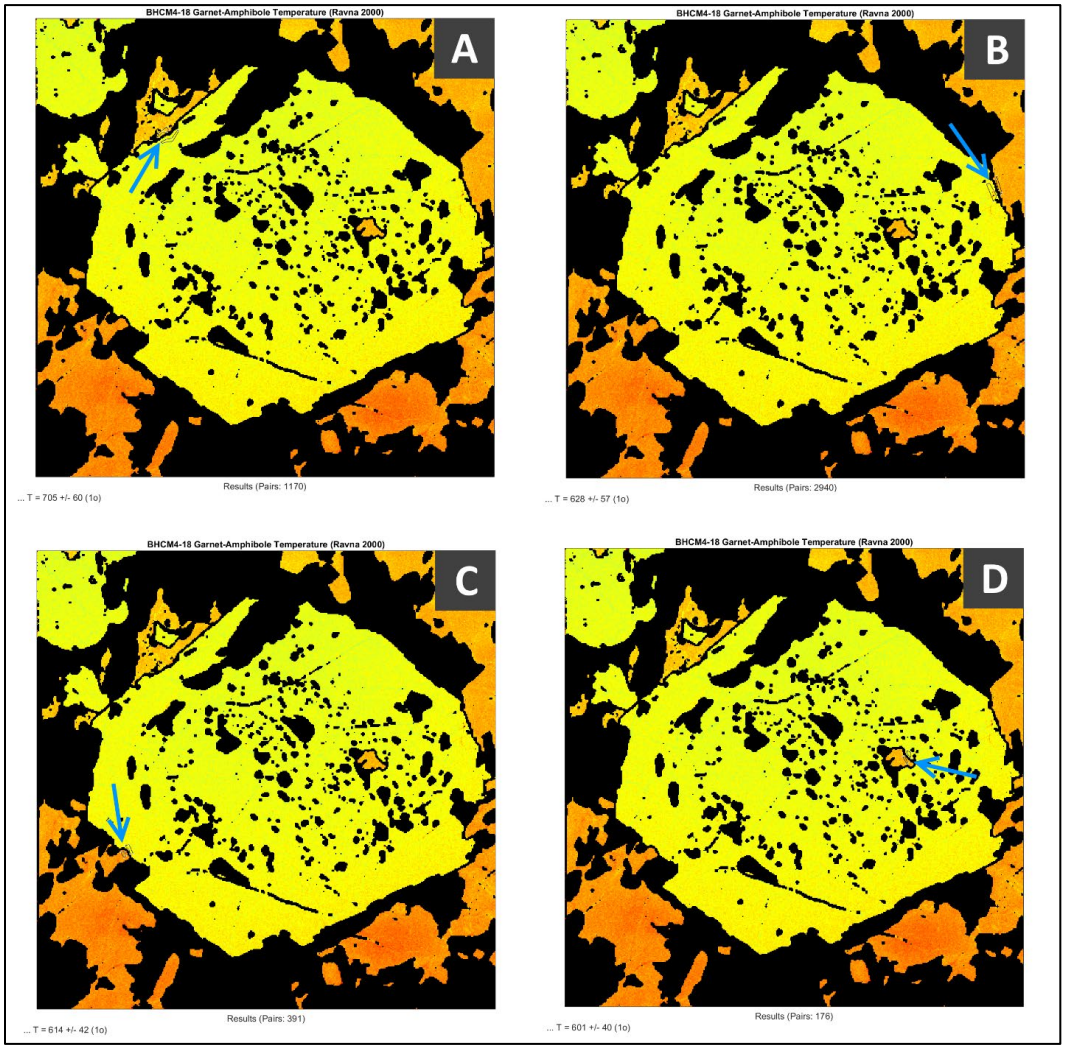

Figure 47: Four temperature estimates based on garnet (yellow) in contact with hornblende (orange) using the thermometer of Ravna (2000). Blue arrows point to mineral contacts. A) garnet rim-matrix hornblende 705°C ± 60. B) Garnet rim-matrix hornblende 628°C ± 57. C) Garnet rim-matrix hornblende 614°C ± 42. D) garnet-hornblende inclusion 601°C ± 40.

The presence of the late retrograde assemblage amphibole-plagioclase-quartz allowed for the use of the calibration of Holland and Blundy (1994) combined with the barometer of Schmidt (1992). Using a fixed composition of plagioclase allows for the estimation of a range of pressure and temperature that correspond to the varying composition of mapped amphibole pixels. Estimates obtained on the matrix assemblage range from approximately 560-800°C and 4.4-11 kbar (Fig 48) while those obtained on the same assemblage found as inclusions in garnet are similar and range from approximately 630-730°C and 6.5-8.9 kbar (Fig 49).

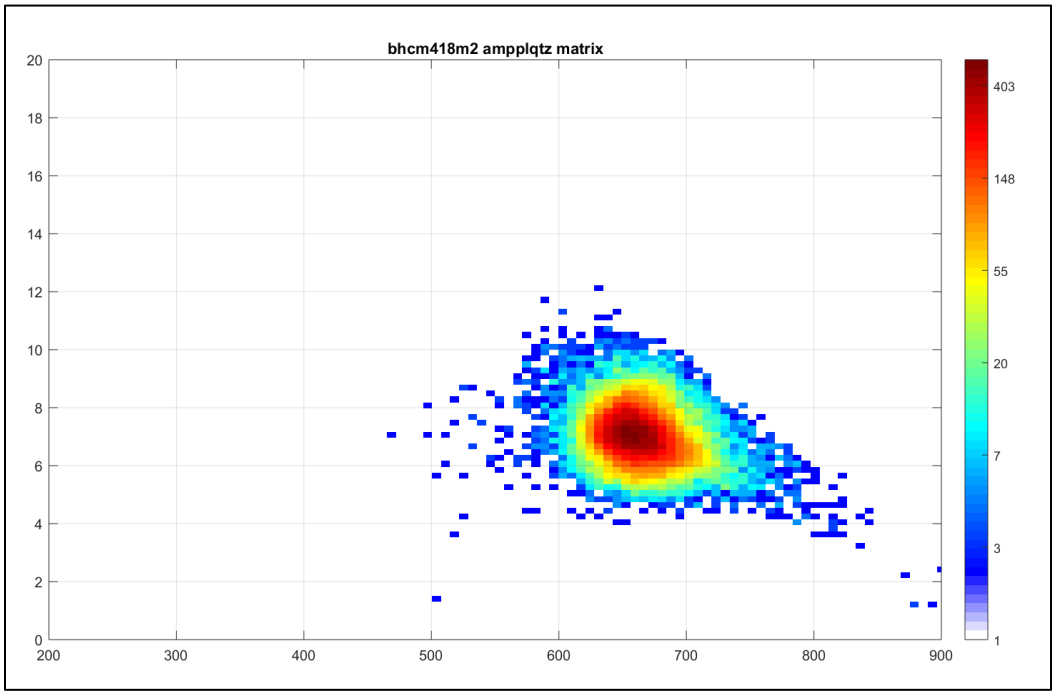

Figure 48: Pressure-temperature estimates of matrix assemblage hornblende-plagioclase-quartz in the mapped area of sample bhcm418m2. Color bar indicates number of datapoints.

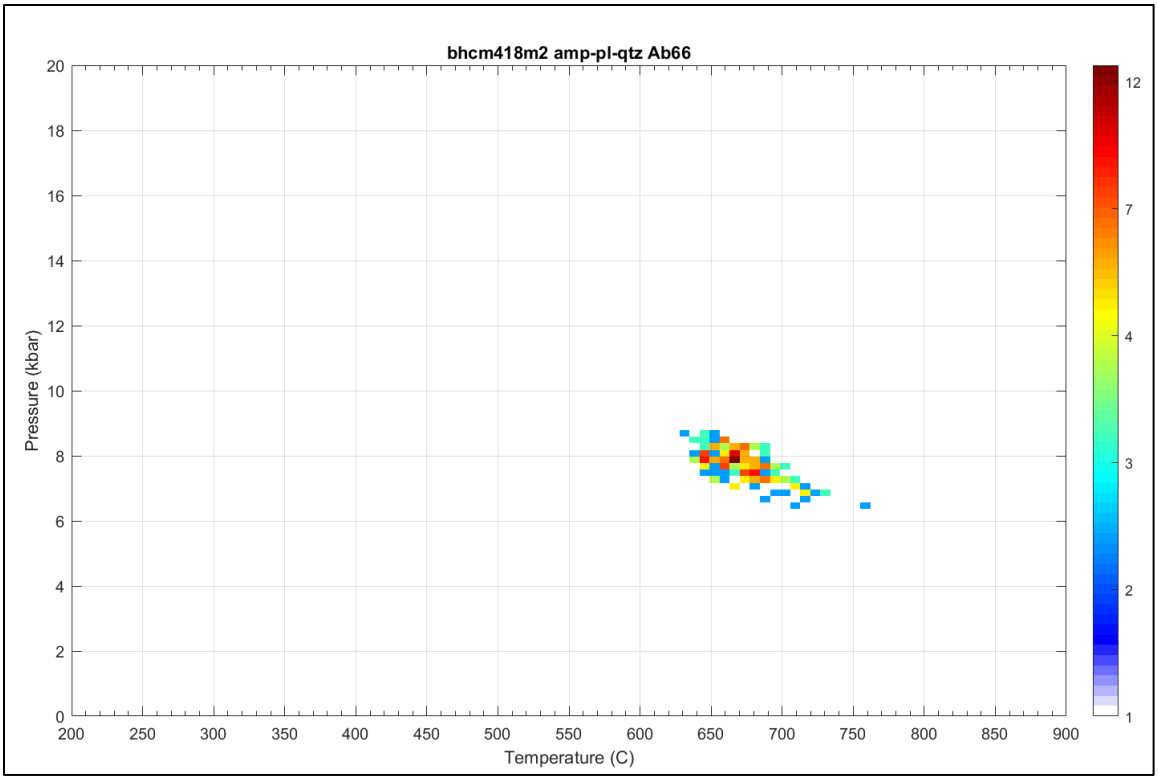

Figure 49: Pressure-temperature estimates of garnet-inclusion assemblage hornblende-plagioclase-quartz in the mapped area of sample bhcm418m2. Color bar indicates number of datapoints.

4.6.3 Sample bjm218b

Using the calibration of Ravna (2000), estimates based on adjacent garnet-clinopyroxene pairs (Fig. 50) range from 620± 63 at 4 kbar and 649 ± 63 at 12 kbar.

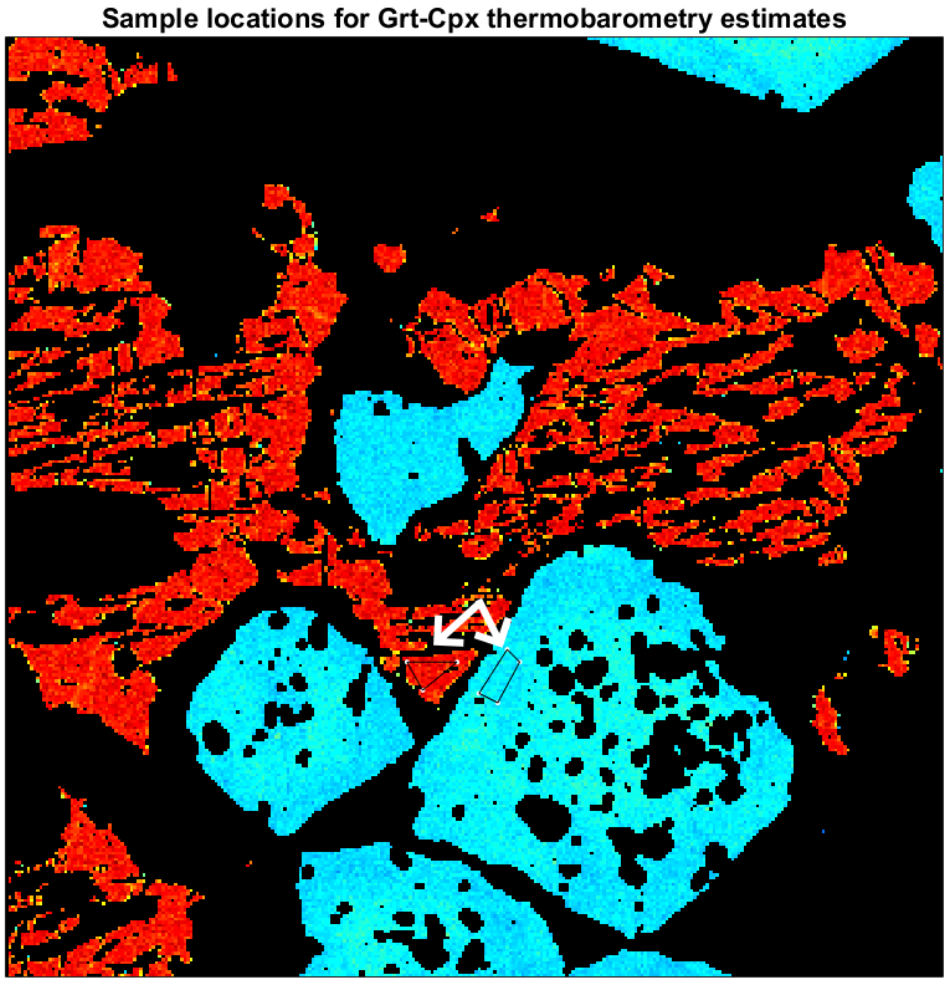

Figure 50: White arrows point to areas sampled for Grt-Cpx temperature estimates. Garnets depicted in cyan, Cpx depicted in red. Sample bjm218b.

4.7 Pressure-Temperature Estimates from Bakersville Samples

4.7.1 Sample bkmc0118a

Peak temperatures based on the distribution of Fe and Mg between garnet and omphacite using the thermometer of Ravna (2000) are estimated at 758°C ±39 and 18 kbar.

Retrograde temperatures based on the distribution of Na and Ca between plagioclase and hornblende using the edenite-ritcherite calibration of Holland and Blundy (1994) are estimated to range from 661°C ±112 to 702°C ±129 at 10 kbar. The lower estimate corresponds to plagioclase

and hornblende found between garnet and omphacite and the upper limit corresponds to plagioclase and hornblende found in symplectite.

Retrograde temperature using the garnet-hornblende thermometer of Ravna (2000) based on garnet rim in contact with hornblende is estimated at 694°C ±41.

Estimates based on the retrograde assemblage clinopyroxene-amphibole-plagioclase allowed for the use of the XMapTools function *cpx-pft* which is capable of yielding PT results of separate domains based on Na-content in clinopyroxene. Estimates on the formation of symplectite range from approximately 590-700°C and 1-16 kbar (Fig 51). Higher pressures are found on the rim of primary omphacite and at the cores of coarse-grained Di-Pl-Am symplectite while lower pressures are found in fine-grained Di-Pl-Am symplectite (Fig 52).

The presence of the late retrograde assemblage amphibole-plagioclase-quartz allowed for the use of the calibration of Holland and Blundy (1994) combined with the barometer of Schmidt (1992). Using a fixed composition of plagioclase allows for the estimation of a range of pressure and temperature that correspond to the varying composition of mapped amphibole pixels. Pressure estimates range from approximately 5-8 kbar and temperature estimates range from approximately 600-700°C (Fig 53)

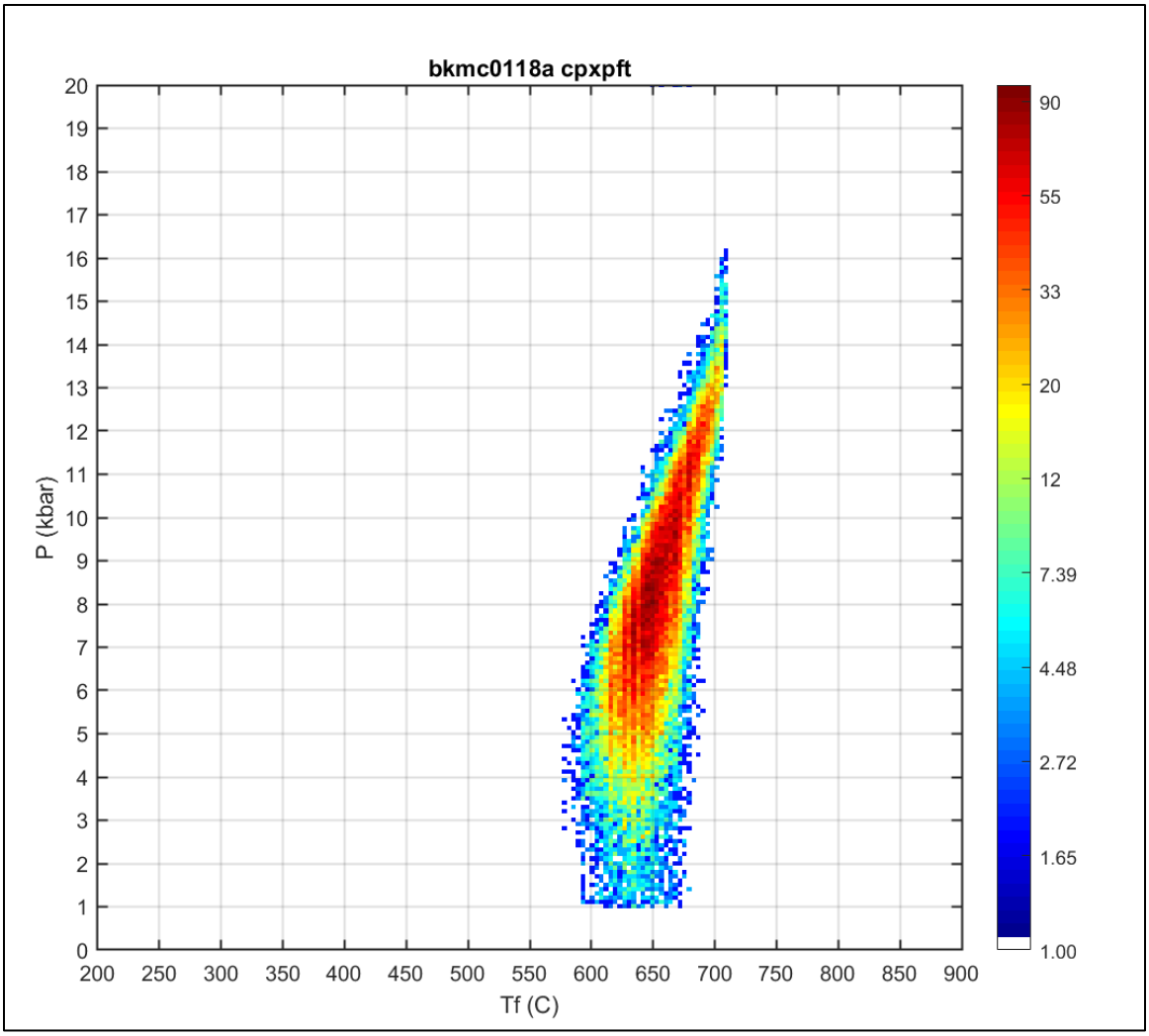

Figure 51: Pressure-temperature estimates based on the retrograde symplectic assemblage cpx-amphibole-plagioclase from the mapped area of sample bkmc0118a. Color bar indicates number of datapoints.

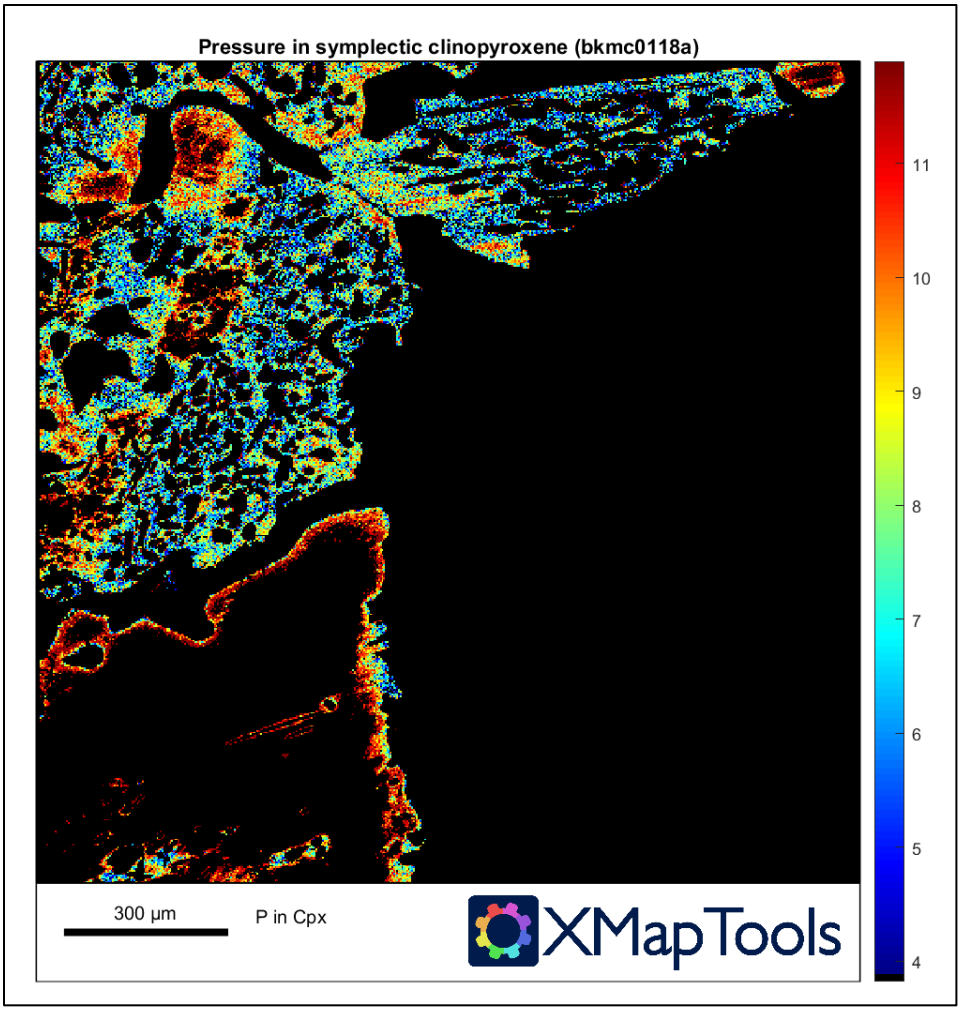

Figure 52: Map of pressure (kbar) in retrograde clinopyroxene from sample bkmc0118a.

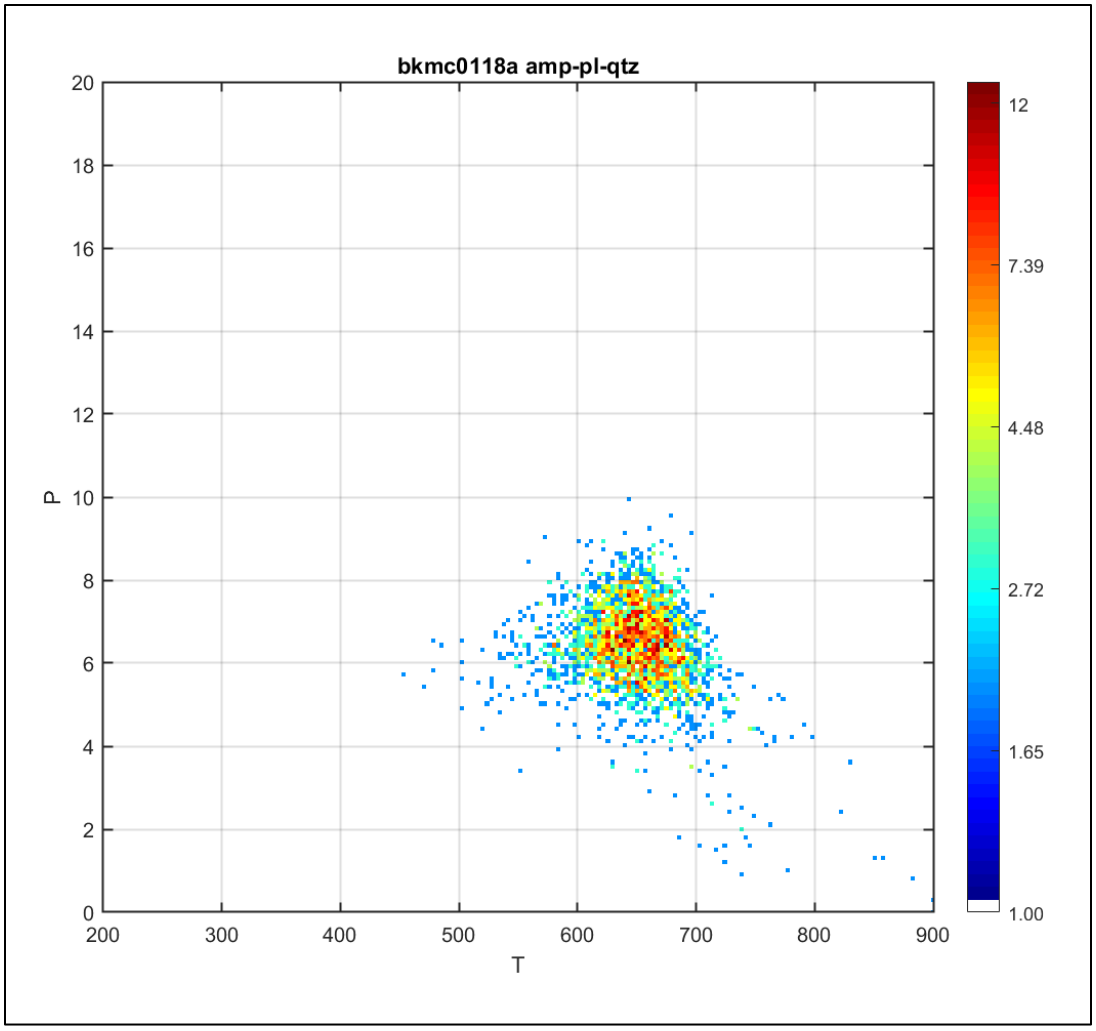

Figure 53: Pressure-temperature estimates based on the late retrograde assemblage amphibole-plagioclase-quartz in the mapped area of sample bkmc0118a. Color bar indicates number of datapoints.

4.7.2 Sample bkmc0218b

Temperature using the garnet-hornblende thermometer of Ravna (2000) based on garnet rim in contact with kelyphitic hornblende is estimated at 860°C ± 69. Using the same calibration of Ravna, estimates between garnet and non-kelyphitic hornblende are lower at 723°C ± 57.

Estimates using the calibration of Ravna (2000) between garnet rim and symplectitc clinopyroxene are 727°C ±41 and 15 kbar.

Estimates using the thermometer of Holland and Blundy (1994) on the hornblende-anorthite kelyphite are at 824°C ± 171 and10 kbar.

Using the XMapTools function that combines the calibration of Holland and Blundy (1994) with the barometer of Schmidt (1992), estimates of pressure and temperature were obtained from amphibole-plagioclase assemblages with and without quartz . Using a fixed composition of plagioclase allows for the estimation of a range of pressure and temperature that correspond to the varying composition of mapped amphibole pixels. Pressure-temperature estimates for the formation of the symplectic assemblage hornblende-plagioclase-quartz range from approximately 600-660°C and 7-10 kbar (Fig 54), while those of the kelyphitic assemblage, hornblende-anorthite are hotter at approximately 625-825°C and 5.5-10 kbar (Fig 55).

Estimates based on the assemblage clinopyroxene-amphibole-plagioclase allowed for the use of the XMapTools function *cpx-pft* which is capable of yielding PT results based on a range of Na-content in clinopyroxene. Estimates for clinopyroxene-plagioclase-amphibole symplectite formation range from approximately 600-700°C and 6-13 kbar (Fig 56).

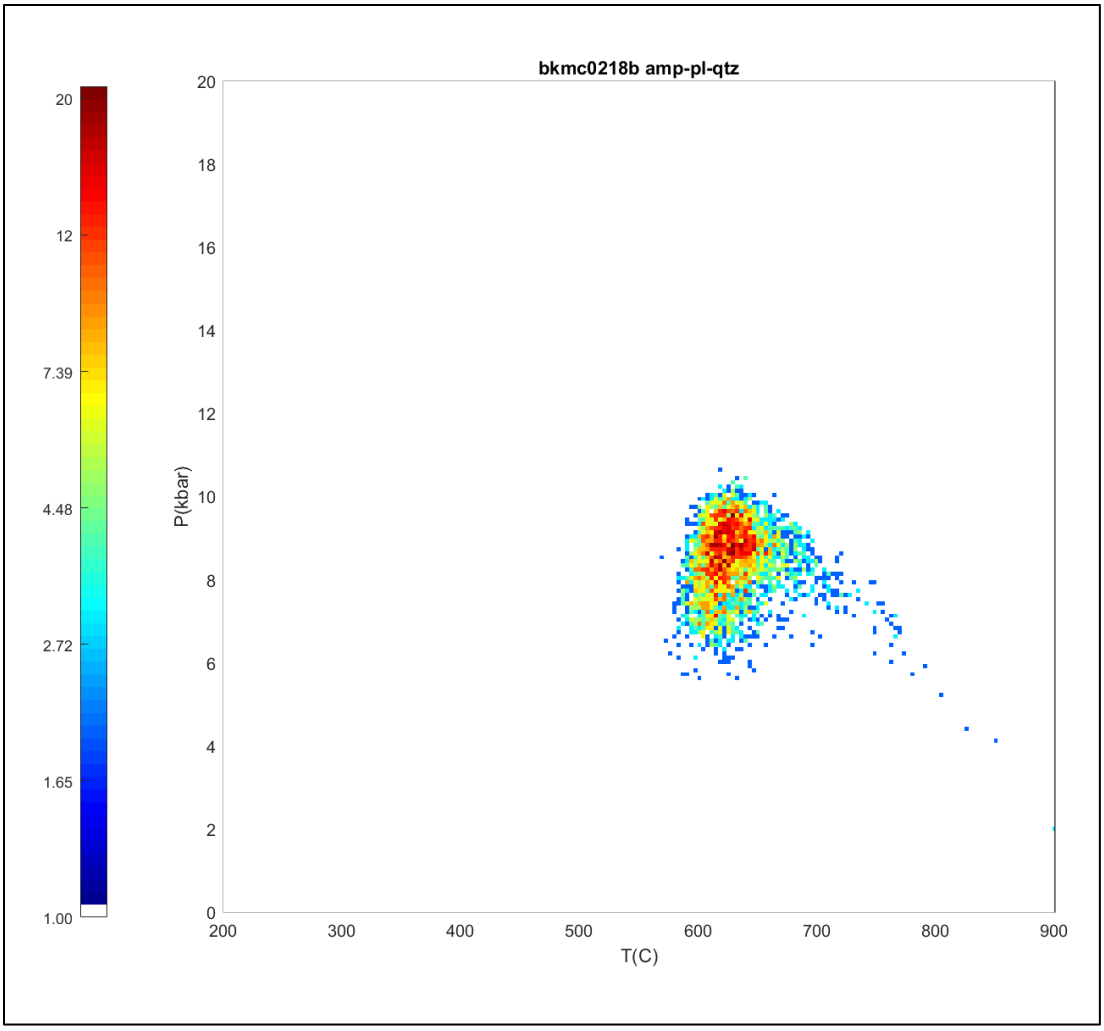

Figure 54: Pressure-temperature estimates of assemblage hornblende-plagioclase-quartz in the mapped area of sample bkmc0218b. Color bar indicates number of datapoints.

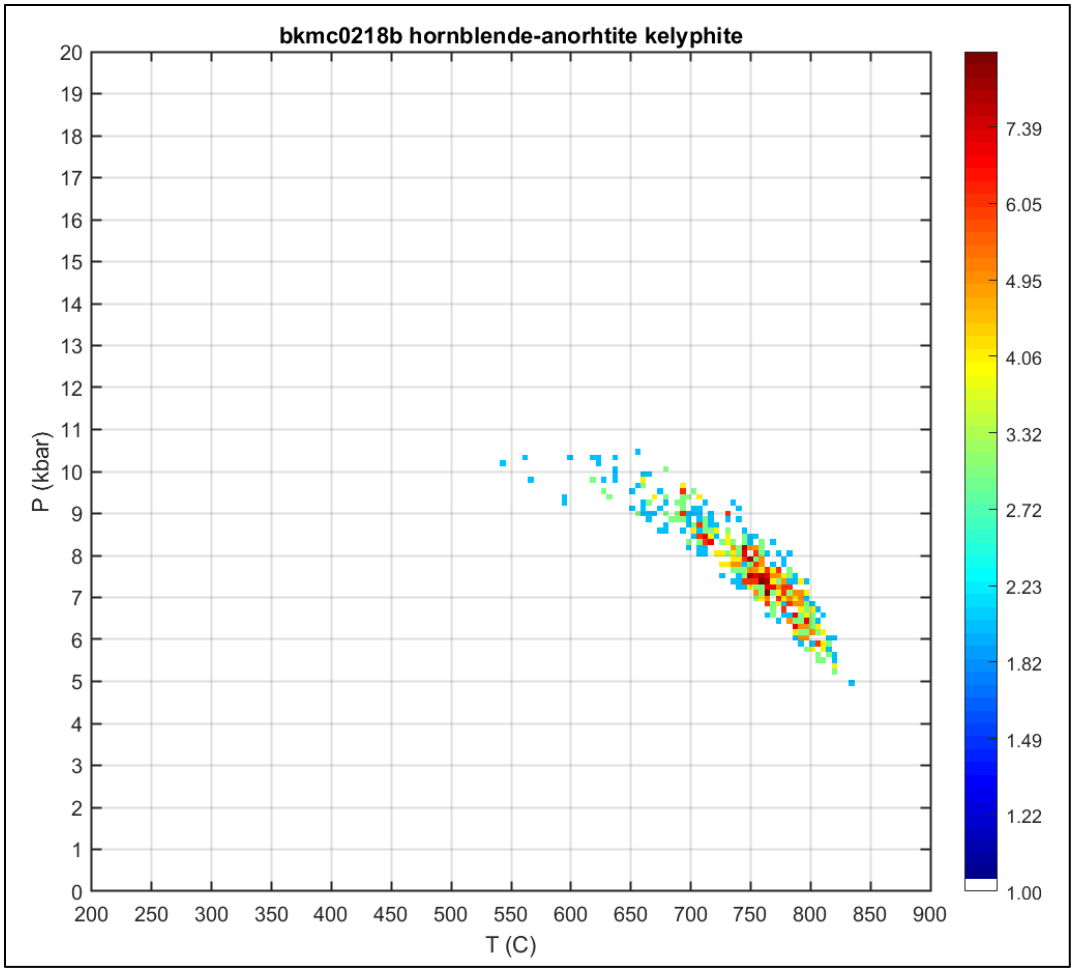

Figure 55: Pressure-temperature estimates of hornblende-anorthite kelyphite in the mapped area of sample bkmc0218b. Color bar indicates number of datapoints.

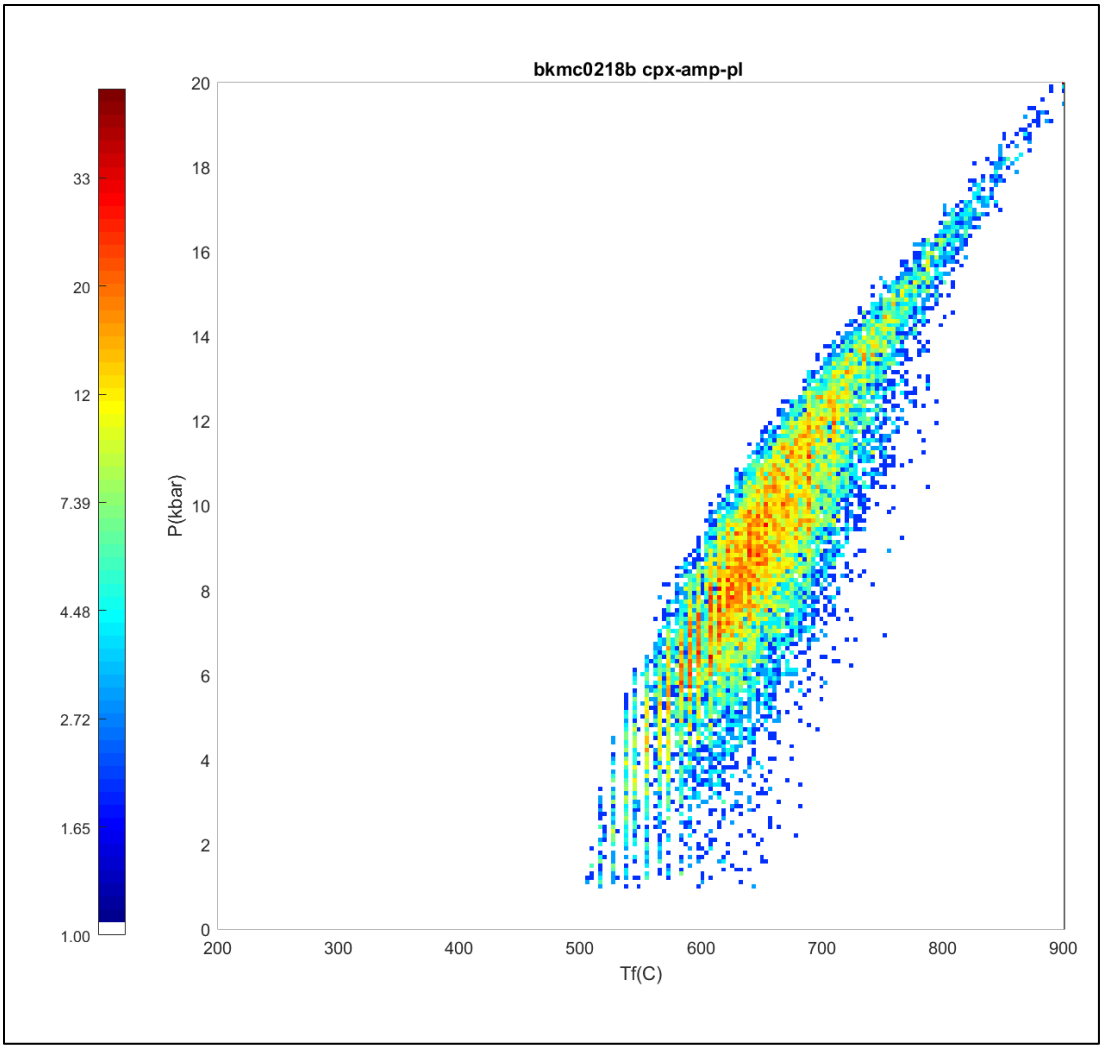

Figure 56: Sample bkmc0218b PT estimates for cpx-pl-amp symplectite formation. Color bar indicates number of datapoints

4.7.3 Sample bkmc0418a

Retrograde temperature using the garnet-hornblende thermometer of Ravna (2000) based on garnet rim in contact with hornblende is estimated at 713°C ±72.

The wide range of plagioclase compositions at apparent equilibrium with adjacent hornblende within the mapped area yield a corresponding range of temperature estimates using the thermometer of Holland and Blundy (1994). Estimates between hornblende and Na-rich plagioclase ($Ab_{64}An_{36}Or_{00}$) are at 678°C ± 138 and10 kbar while estimates between hornblende and Ca-rich plagioclase ($An_{81}Ab_{19}Or_{00}$) are higher at 737°C ± 169 and 10 kbar.

The presence of the late retrograde assemblage amphibole-plagioclase-quartz allowed for the use of the calibration of Holland and Blundy (1994) combined with the barometer of Schmidt (1992). Using a fixed composition of plagioclase allows for the estimation of a range of pressure and temperature that correspond to the varying composition of mapped amphibole pixels. Given the broad range of plagioclase composition in the mapped area, two sets of estimates were obtained using two different plagioclase compositions. Estimates using Ab_{64} yield a temperature range of 570-740°C and a pressure range of 4.5-8 kbar (Fig 57). Estimates using Ab_{19} yield a temperature range of 660-870°C and a pressure range of 1.5-6.5 kbar based on counts approximately greater than 4.5 (Fig 58).

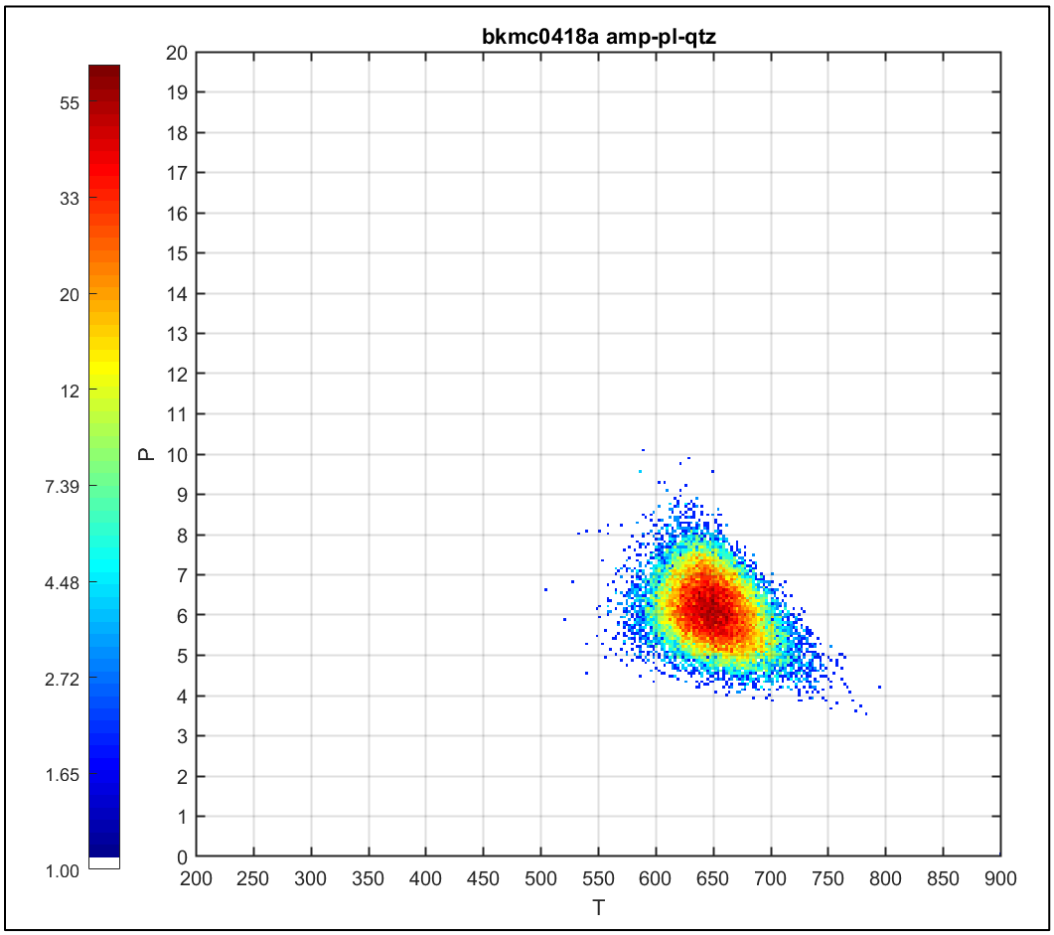

Figure 57: Pressure-temperature estimates based on the late retrograde assemblage amphibole-plagioclase (Ab_{64})-quartz in the mapped area of sample bkmc0418a. Color bar indicates number of datapoints.

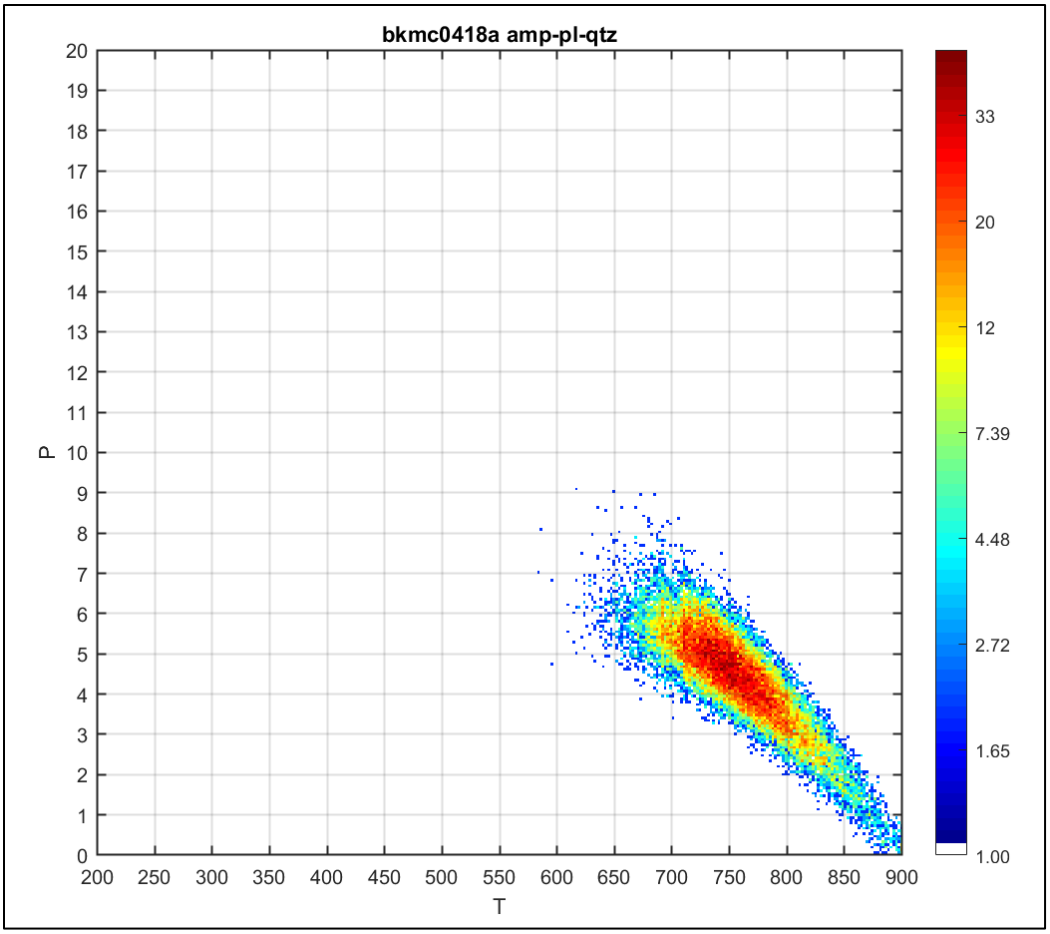

Figure 58: Pressure-temperature estimates based on the late retrograde assemblage amphibole-plagioclase (Ab_{19})-quartz in the mapped area of sample bkmc0418a. Color bar indicates number of datapoints.

4.7.4 Sample bkmc0518a

Retrograde temperature using the garnet-hornblende thermometer of Ravna (2000) based on garnet rim in contact with hornblende is estimated at 606°C ±37.

Retrograde temperatures based on the distribution of Na and Ca between plagioclase and hornblende using the calibration of Holland and Blundy (1994) are estimated at 637°C ±104 and 10 kbar.

5 INTERPRETATIONS AND DISCUSSION

5.1 Boone Metabasites Summary

Based on the results of this study, the Boone metabasites experienced peak granulite-facies conditions with a retrograde amphibolite-facies overprint. The inclusion assemblage found in garnet is nearly identical to that found outside of garnet with the exception of rare rutile, and the finding of plagioclase inclusions in garnet is new compared to previous studies (Anderson and Moecher, 2009). P-T estimates based on plagioclase and hornblende inclusions in garnet were not obtained, but they should be similar to retrograde estimates in granulite-facies based on the same assemblage from a previous study by Anderson and Moecher (2009). The common occurrence of plagioclase inclusions in garnet and conspicuous absence of omphacite suggests that the garnets are not eclogite-facies relics.

Additionally, the garnet zoning patterns suggest very little difference between prograde and retrograde conditions. The core-to-rim decrease of Mn and increase of Mg found in sample bjm718 from the southern outcrop is a record of prograde growth (Spear, 1991) while the contrary zoning found in northern samples is more characteristic of retrograde growth (Anderson and Moecher, 2009). These zoning patterns and similar mineralogy between outcrops suggest that prograde and retrograde conditions were similar. The flat zoning profiles of each is similar to those of the garnet-granulites from Winding Stair Gap (Moecher et al., 2004; Anderson and Moecher, 2009) and suggests homogenization due to slow cooling.

Previous interpretations for an eclogite-facies origin were based on the presence of Di-Pl symplectites, inferred to represent precursor eclogite-facies omphacite, and PT estimates derived from their reintegrations. An alternative explanation for the presence of the Di-Pl symplectites in the Boone high-pressure granulites involves the prograde alteration of amphibole, which may be possible under granulite-facies conditions. Hartel and Patterson (1996) proposed the following

reaction to explain the formation of migmatitic mafic granulites from the Kapuskasing Structural Zone in Ontario:

$$\text{Hbl} + \text{Pl}\ (+\text{Qtz?}) = \text{rt} + \text{Di} + \text{Ttn} + \text{Pl} + \text{Qtz} + \text{leucosome}$$

This reaction conveniently explains the formation of garnet with titanite inclusions, and also accounts for the highly cuspate texture of interstitial plagioclase (Fig 5), which has been recognized as a feature of partial melting (Holness et al., 2011; Peng et al., 2018). It should be noted that the absence of amphibole as a product reflects complete dehydration and doesn't explain the prevalence of amphibole observed in the Boone metabasites. This suggests a reaction under the influence of a relative abundance of water. In water-saturated dehydration experiments on amphibolite from the Smartville complex in Northern California, heating to 850-900 at 3kb, amphibole and quartz broke down to produce clinopyroxene (augitic) and melt that coexisted with a restite assemblage amphibole + magnetite +- Cpx +- plagioclase +- ilmenite (Beard and Lofgren, 1990). In order to test this hypothesis, more work is needed in modelling the melting temperature of amphibole in these rocks using both bulk and local chemistry and comparing that to the PT estimates.

The previous eclogite-facies P-T results derived from the reintegration of Di-Pl symplectites are valid assuming that they are isochemical with the omphacite they're assumed to have replaced. The isochemical nature of the omphacite decomposition reaction is questionable considering the pervasive amphibolite-facies overprint which suggests open system behavior.

5.2 Boone Pressure-Temperature Evolution

Given that the assemblage Grt-Hbl-Pl used to obtain retrograde in granulite facies from the most previous study is also found as inclusions in garnet from this study, it is suggested that these rocks cooled and decompressed from HP-GR facies (Fig 59. Gray shaded area #3) into amphibolite-facies conditions. Additionally, cracks in amphibole from northern sample bhcm418m1 suggest an increase in pressure in amphibolite-facies conditions (Fig 60).

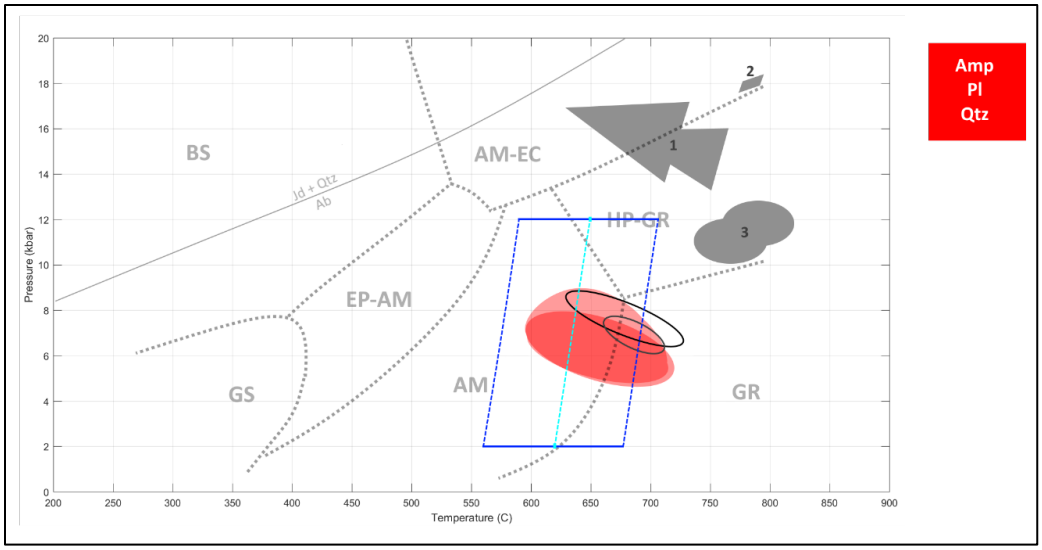

Figure 59: Summary of PT estimates based on southern outcrop samples. Red shaded regions represent matrix assemblage amphibole-plagioclase-quartz while black ellipses outline same assemblage as inclusion in garnet. Blue quadrilateral based on estimates from Garnet-Clinopyroxene pairs from sample bjm218b. Gray shaded regions show previous estimates (Anderson and Moecher, 2009). 1 and 3 derived from TWQ modelling. 2 derived from reintegrated Di-Pl symplectites. Metamorphic facies diagram after Liou et al., 2004.

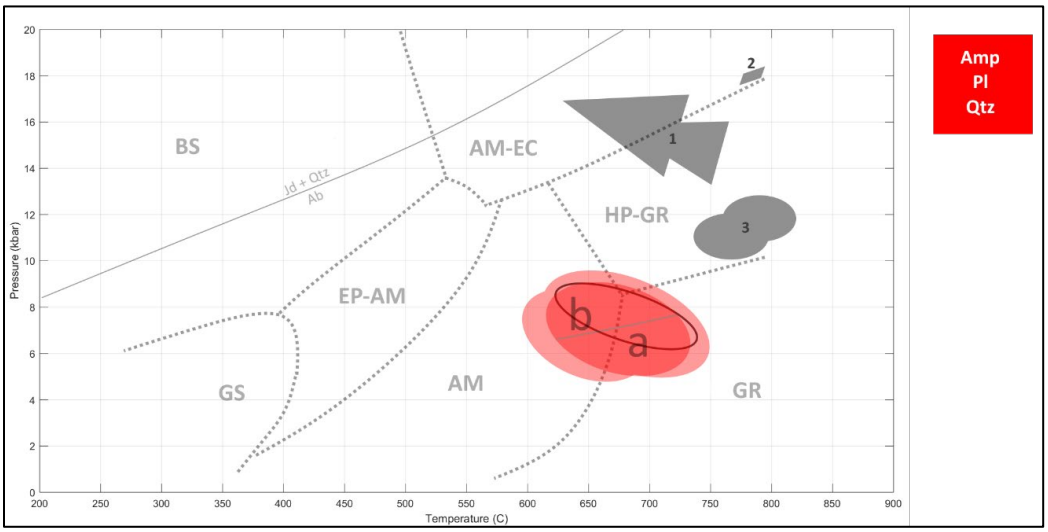

Figure 60: Summary of P-T estimates from Boone northern outcrop samples. P-T estimates from sample with resorbed garnet (bhmc418m1) show a transition from conditions recorded in amphibole core regions (a) to that occurring at fractures and surrounding resorbed garnet (b) . Numbered, gray-shaded areas represent estimates based previous studies (Anderson and Moecher 2009). 1) hornblende, quartz inclusions in garnet; 2) reintegrated omphacite and garnet; 3) garnet rim-plagioclase-hornblende. Metamorphic facies diagram after Liou et al., 2004.

5.3 Bakersville kelyphites

The fine-grained symplectitc alterations to garnet, (i.e., *partial kelyphites*) observed in the moderately altered eclogites (bkmc0218) differ from *true* kelyphites found in eclogites and mantle peridotites in that instead of completely surrounding garnet like a shell as their name suggests (Schrauf, 1882), they occur as distinct circular domains that seemingly originate from within garnet. Similar sub-kelyphitic textures (i.e., sculptured hummocky surfaces and etched pits) have been observed in kimberlites and it was determined that they formed from resorption processes in the range 600-900°C (Garvie and Robinson, 2012). The hydrous composition and discrete nature of the partial kelyphites of this study suggest that they are in-part controlled by limited, discrete sources of hydrous fluid. Reaction textures like symplectites and kelyphites that occur at grain boundaries are thought to have formed from grain-boundary diffusion with available aqueous fluid (Brady, 1983). The internal location of the partial kelyphites and spherical morphology suggest that the fluid source was internal as well which could have come from fluid inclusions or hydrous-phase inclusions (e.g., amphibole, epidote) that decomposed and released fluid upon heating and decompression through granulite facies conditions. Comparing partial kelyphite components, amphibole and anorthite, to an equivalent portion of garnet (Table 7) shows that there is more Fe in the garnet than any mixing proportion of the two components alone. This suggests that some of Fe from garnet may have contributed to the formation of the pyrite adjacent to the partial kelyphite. Additionally, there is less Ca in the garnet composition than the lowest Ca of either of the two components which suggests that an additional Ca-bearing phase played a part in the formation of kelyphite. This additional Ca could have come from surrounding Cpx, or from an epidote-group mineral. A breakdown of the latter could have also been a source of fluid for the breakdown reaction to take place. Further analysis using phase-stability modelling based on local composition is suggested to investigate the formation of kelyphites in this study.

Table 7: Comparison of kelyphite components to unaltered garnet composition

Oxide	Equivalent garnet	Kelyphite amphibole	Kelyphite anorthite
Al_2O_3	22.0507	14.8601	34.7347
CaO	8.9788	12.1589	18.7301
Cr_2O_3	0.33654	0.22022	-
FeO	21.4495	12.017	0.15838
K_2O	-	0.2024	-
MgO	8.2096	12.4356	-
MnO	0.58312	0.11782	-
Na_2O	0.042643	2.4734	0.96327
SiO_2	39.5023	41.9344	44.5117
TiO_2	0.028563	0.238	-
SUM	101.1827	96.6336	99.09815

5.4 Bakersville Garnet zoning

Prograde zoning patterns (i.e., a core-to-rim decrease in Fe and increase in Mg) were preserved in the least (bkmc0118a) and one of the moderately retrogressed samples (bkmc0218b) while zoning patterns (e.g., weak zoning, core-to-rim increase in Fe and decrease in Mg) that evoke slow cooling/long duration at high temperatures (Fernando et al., 2003) were observed in moderately and thoroughly retrogressed samples bkmc0518a and bkmc0418a respectively.

5.5 Bakersville Spongy Cpx

In mantle xenoliths (e.g., peridotites, pyroxenites), spongy Cpx is a feature of decompression associated with partial melting (Su et al., 2011, Pan et al., 2018) and metasomatic reactions (Misra et al., 2004), yet little is known about its formation in metabasites (e.g., eclogites, granulites).

In samples bkmc0118a and bkmc0218b, Cpx displays spongy textures wherein fine-grained blebs of sodic plagioclase and calcic hornblende reside in a reticular matrix of variable thickness composed of diopsidic clinopyroxene. Within the cpx matrix, coarser regions have cores that are enriched in Na and Al compared to thinner regions (Figs 34, 36). This relationship parallels with the example of the altered omphacite grain in sample bkmc0118a, wherein the core of primary omphacite is enriched in Na and Al compared to the secondary rim, and suggests that the coarser grained regions in spongy cpx equilibrated at higher pressures. The presence of hornblende in the spongy assemblage suggests that melting was induced by available water. The spongy cpx in this study shares several features with symplectites, such as a virtually identical assemblage and a connection to decompression being a cause of formation. Given these similarities, PT estimates were obtained using a method that has been applied to eclogitic symplectites (Lanari et al., 2013) and similarly shows a continuous retrograde path of decreasing pressure through granulite facies. The formative differences between vermicular-symplectitc and spongy textures are unknown and require further investigation.

5.6 Bakersville Pressure-Temperature Evolution

A suggested retrograde PT path from least retrogressed sample (bkmc0118a) recorded by the breakdown of omphacite, starts at approximately 700° C and 16 kbar and decompresses with

minor cooling through high-pressure granulite facies before cooling with minor decompression in amphibolite facies conditions at approximately 550° C and 6 kbar (Fig 61).

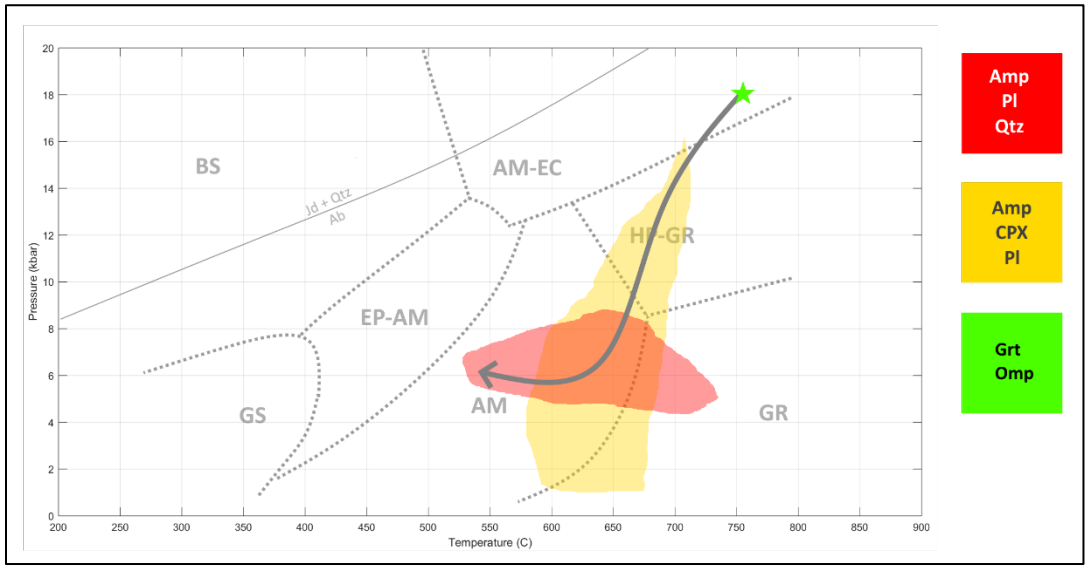

Figure 61: Suggested retrograde PT path for sample bkmc0118a. . Green star represents lower pressure estimate based on omphacite and garnet rim. Yellow shaded area represents Cpx-Pl-Hbl symplectite formation. Red shaded area represents formation of late retrograde assemblage Amp-Pl-Qtz. Facies diagram after Liou et al., 2004.

A suggested conservative retrograde path for moderately retrogressed eclogite, sample bkmc0218b, begins at 800° C and 16 kbar and decompresses in high-pressure granulite facies to end up in amphibolite facies at approximately 570° C and 7 kbar (Fig 62). An alternative path may follow the estimated stability field of hornblende-anorthite kelyphite wherein the temperature at approximately 10 kbar increases sharply to approximately 765° C and then returning back to the overlapping estimated stability fields of late symplectite evolution and formation of late assemblage amphibole-sodic plagioclase-quartz. In this manner, the formation of kelyphite may be the result of a local influx of heat along the decompression path.

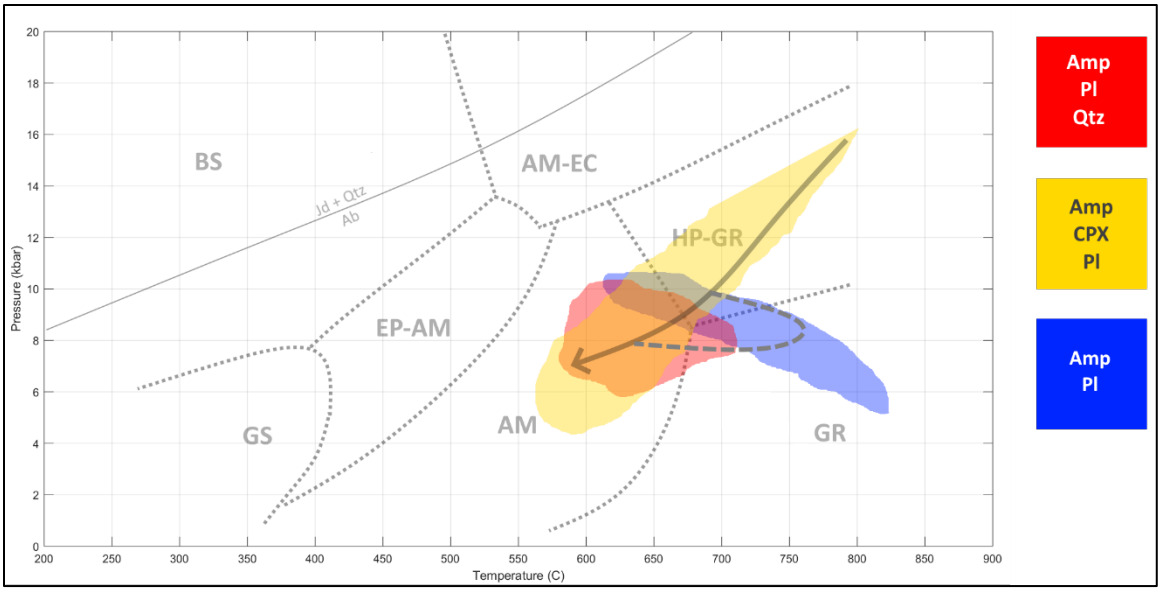

Figure 62: Proposed retrograde PT path for the mapped area of sample bkmc0218b. Yellow shaded area represents Cpx-Pl-Hbl symplectite formation. Blue shaded area represents hornblende-anorthite kelyphite formation. Red shaded area represents formation of late retrograde assemblage Amp-Pl-Qtz. Facies diagram after Liou et al., 2004.

5.7 Tectonic Implications

Subduction channels occur at the interface between the subducting slab and overriding plate and allow for materials to descend, ascend and move in a circulatory motion (Gerya et al., 2002). The oscillatory-zoned garnets of the Boone metabasites may be explained, in part by circulatory motion, as was the case for garnet amphibolites belonging to a subduction mélange from Cuba (Blanco-Quintero et al., 2011). Additionally, dehydration reactions deep below the mantle wedge may generate fluids that can travel up the subduction channel where they may serve to hydrate rocks they interact with (Ulmer and Trommsdorff, 1995). Such fluids may be the source of amphibolization found in the metabasites from Boone and Bakersville.

6: CONCLUSIONS

1. Of the Boone metabasites, the common occurrence of plagioclase as inclusions in garnet suggest that the garnets are not eclogite relics. Moreover, there is little variation between garnet inclusion assemblages and matrix assemblages, which suggests that there is little variation between prograde and retrograde granulite-facies conditions.
2. Newly determined late retrograde P-T estimates for Boone metabasites are estimated between 9.0-5.0 kbar and 750-600 °C that straddle granulite and amphibolite facies conditions.
3. Of the Bakersville metabasites, new P-T estimates based on symplectite formation adjacent to primary omphacite range from 700-550 °C and 16-6.0 kbar, which is in general agreement with previous studies. New P-T estimates based on spongy CPX with the same assemblage of symplectites after omphacite suggest a hotter decompression path ranging from 800-565 °C and 16-4.5 kbar.
4. New estimates of kelyphite formation in retrograde eclogite from Bakersville show that breakdown of garnet occurred in granulite-facies conditions in the ranges of 10-5.5 kbar and 825-625 °C.
5. Of the Bakersville metabasites, newly determined late retrograde P-T conditions are estimated between 9.0-4.5 kbar and 730-550 °C for a sample bearing primary eclogitic omphacite and garnet, and between 10.5-6.0 kbar and 715-575 °C for a sample with altered eclogitic garnet.

REFERENCES

Abbott, R.N., and Greenwood, J.P., 2001, Retrograde metamorphism of eclogite in the southern Appalachian Mountains, U.S.A.-A case involving seamount subduction? JMG Journal of Metamorphic Geology, v. 19, p. 433–443.

Abbott, R.N., and Raymond, L.A., 1984, The Ashe Metamorphic Suite, Northwest North Carolina; metamorphism and observations on geologic history: American Journal of Science American Journal of Science, v. 284, p. 350–375.

Anderson, E.D., and Moecher, D.P., 2009, Formation of high-pressure metabasites in the southern Appalachian Blue Ridge via Taconic continental subduction beneath the Laurentian margin: Tectonics, v. 28, p. n/a-n/a, doi:10.1029/2008TC002319.

Anderson, E., and Moecher, D., 2007, Omphacite breakdown reactions and relation to eclogite exhumation rates: Contributions to Mineralogy and Petrology, v. 154, p. 253,277.

Austrheim, H., 1987, Eclogitization of lower crustal granulites by fluid migration through shear zones: Earth and Planetary Science Letters, v. 81, p. 221–232, doi:10.1016/0012-821X(87)90158-0.

Beard, J.S., and Lofgren, G.E., 1991, Dehydration Melting and Water-Saturated Melting of Basaltic and Andesitic Greenstones and Amphibolites at 1, 3, and 6. 9 kb: Journal of Petrology, v. 32, p. 365–401, doi:10.1093/petrology/32.2.365.

Blanco-Quintero, I.F., García-Casco, A., and Gerya, T.V., 2011, Tectonic blocks in serpentinite mélange (eastern Cuba) reveal large-scale convective flow of the subduction channel: Geology, v. 39, p. 79–82, doi:10.1130/G31494.1.

Boland, J.N., and van Roermund, H.L.M., 1983, Mechanisms of exsolution in omphacites from high temperature, type B, eclogites: Physics and Chemistry of Minerals, v. 9, p. 30–37, doi:10.1007/BF00309467.

Brady, J.B., 1983, Intergranular diffusion in metamorphic rocks: American Journal of Science, v. 283, p. 181–200.

Eskola, P., 1921, On the eclogites of Norway: Рипол Классик.

Fernando, G.W.A.R., Hauzenberger, C.A., Baumgartner, L.P., and Hofmeister, W., 2003, Modeling of retrograde diffusion zoning in garnet: evidence for slow cooling of granulites from the Highland Complex of Sri Lanka: Mineralogy and petrology, v. 78, p. 53,71.

Garvie, O.G., and Robinson, D.N., 1984, The Formation of Kelyphite and Associated Sub-Kelyphitic and Sculptured Surfaces On Pyrope from Kimberlite, *in* KORNPROBST, J. ed., Developments in Petrology, Elsevier, v. 11, p. 371–382, doi:10.1016/B978-0-444-42273-6.50031-6.

Gerya, T.V., Stöckhert, B., and Perchuk, A.L., 2002, Exhumation of high-pressure metamorphic rocks in a subduction channel: A numerical simulation: Tectonics, v. 21, p. 6–1, doi:10.1029/2002TC001406.

Goldberg, S.A., 1997, Chronology of Paleozoic metamorphism and deformation in the Blue Ridge thrust complex, North Carolina and Tennessee: American Journal of Science, v. 297, p. 488,526.

Grew, E.S., Locock, A.J., Mills, S.J., Galuskina, I.O., Galuskin, E.V., and Halenius, U., 2013, Nomenclature of the garnet supergroup: The American mineralogist., v. 98, p. 785,811.

Hatcher, R.D., 2010, The Appalachian orogen: A brief summary, *in* From Rodinia to Pangea: The Lithotectonic Record of the Appalachian Region, The Geological Society of America, Memoir 206, p. 9, doi:10.1130/2010.1206(01).

Holland, T., and Blundy, J., 1994, Non-ideal interactions in calcic amphiboles and their bearing on amphibole-plagioclase thermometry: Contributions to Mineralogy and Petrology, v. 116, p. 433–447, doi:10.1007/BF00310910.

Holness, M.B., Cesare, B., and Sawyer, E.W., 2011, Melted Rocks under the Microscope: Microstructures and Their Interpretation: Elements, v. 7, p. 247–252, doi:10.2113/gselements.7.4.247.

Janák, M., O'Brien, P.J., Hurai, V., and Reutel, C., 1996, Metamorphic evolution and fluid composition of garnet-clinopyroxene amphibolites from the Tatra Mountains, Western Carpathians: Lithos, v. 39, p. 57–79, doi:10.1016/S0024-4937(96)00019-9.

Krogh Ravna, 2000, The garnet–clinopyroxene Fe 2+ –Mg geothermometer: an updated calibration: Journal of Metamorphic Geology, v. 18, p. 211–219, doi:10.1046/j.1525-1314.2000.00247.x.

Lanari, P., Riel, N., Guillot, S., Vidal, O., Schwartz, S., Pêcher, A., and Hattori, K.H., 2013, Deciphering high-pressure metamorphism in collisional context using microprobe mapping methods: Application to the Stak eclogitic massif (northwest Himalaya).: Geology, v. 41.

Lanari, P., Vidal, O., De Andrade, V., Dubacq, B., Lewin, E., Grosch, E.G., and Schwartz, S., 2014, XMapTools: A MATLAB©-based program for electron microprobe X-ray image processing and geothermobarometry: Computers & Geosciences, v. 62, p. 227–240, doi:10.1016/j.cageo.2013.08.010.

Leake, B.E. et al., 1997, Nomenclature of amphiboles; report of the Subcommittee on Amphiboles of the International Mineralogical Association Commission on New Minerals and Mineral Names: European Journal of Mineralogy, v. 9, p. 623–651.

Levine, J.S.F., Merschat, A.J., Mcaleer, R.J., Casale, G., Quillan, K.R., Fraser, K.I., and Bedell, T.G., 2018, Kinematic, Deformational, and Thermochronologic Conditions Along the Gossan Lead and Fries Shear Zones: Constraining the Western-Eastern Blue Ridge Boundary in Northwestern North Carolina: Tectonics, v. 37, p. 3500,3523.

Liou, J.G., Tsujimori, T., Zhang, R.Y., Katayama, I., and Maruyama, S., 2004, Global UHP Metamorphism and Continental Subduction/Collision: The Himalayan Model: International Geology Review, v. 46, p. 1–27, doi:10.2747/0020-6814.46.1.1.

Martin, C., 2018, P-T conditions of symplectite formation in the eclogites from the Western Gneiss Region (Norway): Geological Society, London, Special Publications, v. 478, p. SP478.18, doi:10.1144/SP478.18.

Martin, C., and Duchêne, S., 2015, Residual water in hydrous minerals as a kinetic factor for omphacite destabilization into symplectite in the eclogites of Vårdalsneset (WGR, Norway): Lithos, v. 232, p. 162,173.

McSween, Jr., Harry Y., Abbott, R.N., and Raymond, L.A., 1989, Metamorphic conditions in the Ashe Metamorphic Suite, North Carolina Blue Ridge: Geology, v. 17, p. 1140–1143, doi:10.1130/0091-7613(1989)017<1140:MCITAM>2.3.CO;2.

Miller, B., Stewart, K., and Whitney, D., 2010, Three tectonothermal pulses recorded in eclogite and amphibolite of the Eastern Blue Ridge, Southern Appalachians: GSA Memoirs, v. 206, p. 701,724.

Misra, K.C., Anand, M., Taylor, L.A., and Sobolev, N.V., 2004, Multi-stage metasomatism of diamondiferous eclogite xenoliths from the Udachnaya kimberlite pipe, Yakutia, Siberia: Contributions to Mineralogy and Petrology, v. 146, p. 696–714, doi:10.1007/s00410-003-0529-z.

Misra, K.C., and Conte, J.A., 1991, Amphibolites of the Ashe and Alligator Back Formations, North Carolina: Samples of Late Proterozoic-early Paleozoic oceanic crust.: Geological Society of America bulletin., v. 103, p. 737.

Moecher, D.P., Samson, S.D., and Miller, C.F., 2004, Precise Time and Conditions of Peak Taconian Granulite Facies Metamorphism in the Southern Appalachian Orogen, U.S.A., with Implications for Zircon Behavior during Crustal Melting Events: The Journal of Geology, v. 112, p. 289–304, doi:10.1086/382760.

Morimoto, N., 1989, Nomenclature of pyroxenes: Mineralogical Journal, v. 14, p. 198–221.

Obata, M., 1994, Material Transfer and Local Equilibria in a Zoned Kelyphite from a Garnet Pyroxenite, Ronda, Spain: Journal of Petrology, v. 35, p. 271–287, doi:10.1093/petrology/35.1.271.

Page, F.Z., Essene, E.J., and Mukasa, S.B., 2003, Prograde and retrograde history of eclogites from the Eastern Blue Ridge, North Carolina, USA: Journal of Metamorphic Geology, v. 21, p. 685–698, doi:10.1046/j.1525-1314.2003.00479.x.

Page, F.Z., Essene, E.J., and Mukasa, S.B., 2005, Quartz exsolution in clinopyroxene is not proof of ultrahigh pressures: Evidence from eclogites from the Eastern Blue Ridge, Southern Appalachians, U.S.A.: American Mineralogist, v. 90, p. 1092, doi:10.2138/am.2005.1761.

Pan, S., Zheng, J., Yin, Z., Griffin, W.L., Xia, M., Lin, A., and Zhang, H., 2018, Spongy texture in mantle clinopyroxene records decompression-induced melting: LITHOS, v. 320–321, p. 144,154.

Peng, Y., Li, S., Yu, S., Zhang, J., Sun, D., and Li, Y., 2018, Linking high-pressure mafic granulite, TTG-like (tonalitic- trondhjemitic) leucosome and pluton, and crustal growth during continental collision:, doi:10.1130/B31822.1.

Ravna, E.K., 2000, Distribution of Fe2+ and Mg between coexisting garnet and hornblende in synthetic and natural systems: an empirical calibration of the garnet–hornblende Fe–Mg geothermometer: Lithos, v. 53, p. 265–277, doi:10.1016/S0024-4937(00)00029-3.

Schmädicke, E., Okrusch, M., and Schmidt, W., 1992, Eclogite-facies rocks in the Saxonian Erzgebirge, Germany: high pressure metamorphism under contrasting P-T conditions: Contributions to Mineralogy and Petrology, v. 110, p. 226–241, doi:10.1007/BF00310740.

Schmidt, M.W., 1992, Amphibole composition in tonalite as a function of pressure: an experimental calibration of the Al-in-hornblende barometer: Contributions to Mineralogy and Petrology, v. 110, p. 304–310, doi:10.1007/BF00310745.

Schrauf, S., 1882, Beitrage zur Kenntnis des Assoziationskreises der Magnesiasilicate.: v. 6, p. 88.

Shervais, J.W., Dennis, A.J., Mcgee, J.J., and Secor, D., 2003, Deep in the Heart of Dixie: Pre-Alleghanian Eclogite and HP Granulite Metamorphism in the Carolina Terrane, South Carolina, USA: Journal of Metamorphic Geology, v. 21, p. 65–80, doi:10.1046/j.1525-1314.2003.00416.x.

Smyth, J.R., and Bell, D.R., 1991, Incorporation of hydroxyl in upper-mantle clinopyroxenes.: Nature, v. 351.

Spear, F.S., 1991, On the interpretation of peak metamorphic temperatures in light of garnet diffusion during cooling: Journal of Metamorphic Geology, v. 9, p. 379–388, doi:10.1111/j.1525-1314.1991.tb00533.x.

Spruzeniece, L., Piazolo, S., Daczko, N.R., Kilburn, M.R., and Putnis, A., 2017, Symplectite formation in the presence of a reactive fluid: insights from hydrothermal experiments: JMG Journal of Metamorphic Geology, v. 35, p. 281–299.

Stewart, K.G., Adams, M.G., Trupe, C.H., and Carolina Geological Society, 1995, Paleozoic Structure, Metamorphism, and Tectonics of the Blue Ridge of Western North Carolina: Carolina Geological Society Field Trip Guidebook, Banner Elk, North Carolina, September 26-28, 1997: Carolina Geological Society, https://books.google.com/books?id=xF0lkgEACAAJ.

Su, B.-X. et al., 2011, The origin of spongy texture in minerals of mantle xenoliths from the Western Qinling, central China: Contributions to Mineralogy and Petrology, v. 161, p. 465–482, doi:10.1007/s00410-010-0543-x.

Trupe, C.H., Stewart, K.G., Adams, M.G., Miller, B.V., Waters, C.L., and Hewitt, L.K., 2003, The Burnsville fault: Evidence for the timing and kinematics of southern Appalachian Acadian dextral transform tectonics: GSA Bulletin, v. 115, p. 1365–1376, doi:10.1130/B25256.1.

Ulmer, P., and Trommsdorff, V., 1995, Serpentine stability to mantle depths and subduction-related magmatism (P. Ulmer, Ed.): Science (Washington), v. 268, p. 858–858.

Vallis, F., and Scambelluri, M., 1996, Redistribution of high-pressure fluids during retrograde metamorphism of eclogite-facies rocks (Voltri Massif, Italian Western Alps): LITHOS, v. 39, p. 81–92, doi:10.1016/S0024-4937(96)00012-6.

Vermeesch, P., 2006, Tectonic discrimination of basalts with classification trees: Geochimica et Cosmochimica Acta, v. 70, p. 1839–1848, doi:10.1016/j.gca.2005.12.016.

Willard, R.A., and Adams, M.G., 1994, Newly discovered eclogite in the southern Appalachian orogen, northwestern North Carolina: Earth and Planetary Science Letters, v. 123, p. 61–70, doi:10.1016/0012-821X(94)90257-7.

Yang, T.N., 2004, Retrograded textures and associated mass transfer: evidence for aqueous fluid action during exhumation of the Qinglongshan eclogite, Southern Sulu ultrahigh pressure metamorphic terrane, eastern China: Journal of Metamorphic Geology, v. 22, p. 653,669.

APPENDIX A: OXIDE ANALYSES

Table 1: Average Pyroxene Compositions from Boone location (profiles within mapped areas)

	Matrix symplectite with plagioclase							
	north		south					
	Bhcm418m1	Bhcm418m2	Bjm218b	Bjm518m1	Bjm518m2	Bjm618b	Bjm718	*Inclusion in grt (Anderson, 2011)*
SiO_2	52.1713	51.9762	52.3212	52.00749	51.7097	52.2380	51.7264	*50.85*
TiO_2	0.1060	0.1037	0.1571	0.09180	0.1170	0.0711	0.1171	*0.26*
Al_2O_3	2.2443	2.0595	2.3038	1.81680	2.1446	1.9352	2.0510	*2.36*
FeO	9.8059	9.8880	10.3346	11.13978	10.5873	9.7141	10.0710	*6.70*
MnO	0.1035	0.1108	0.0397	0.06557	0.0805	0.0914	0.1164	*0.14*
MgO	11.8209	11.9797	11.7243	11.52520	11.8548	12.3632	11.8685	*11.52*
CaO	23.1932	22.9436	22.4095	21.91257	21.8117	22.4842	22.8884	*22.92*
Na_2O	0.7903	0.8852	1.1405	1.03599	1.1294	0.8935	0.9107	*0.93*
K_2O	0.0042	0.0027	0.0025	0.00651	0.0050	0.0054	0.0015	*0.00*
Cr_2O_3	0.0147	0.0222	0.0160	0.01988	0.0397	0.1287	0.0116	*X*
Total	100.2543	99.9716	100.4491	99.62160	99.4798	99.9247	99.7627	*101.43*
n	6	9	14	12	4	7	8	

Table 2: Average Amphibole Compositions from Boone location (profiles within mapped areas)

	matrix								Garnet inclusion
	north			south					
	Bhcm518*	Bhcm418m1	Bhcm418m2	Bjm218b	Bjm518m1	Bjm518m2	Bjm618b	Bjm718	Bjm718
SiO_2	43.6273	43.4418	42.1520	43.9298	43.2369533	45.8565	45.2284	43.6914	42.2748
TiO_2	0.7911	0.7347	1.0041	1.1948	1.10228667	0.89438	0.9892	1.2011	1.6907
Al_2O_3	12.1798	12.3952	13.3911	11.0399	11.3700767	12.46524	10.3630	11.1752	11.6601
FeO	18.3662	16.9925	17.7688	17.9122	17.8388633	14.01304	15.4357	17.1612	19.9193
MnO	0.3463	0.0879	0.0614	0.0356	0.05106333	0.08083	0.0926	0.1075	0.1451
MgO	9.2956	10.0485	9.5653	9.9192	9.98537333	9.58909	11.3685	10.4333	8.5007
CaO	11.0226	11.7401	11.6111	11.3724	11.2446833	10.54147	11.7381	11.4155	11.3184
Na_2O	2.0707	1.9293	2.1279	2.1720	2.41701	3.52181	1.9030	2.1914	2.3086
K_2O	0.1552	0.1547	0.2353	0.0405	0.18895667	0.15192	0.1097	0.1301	0.1167
Cr_2O_3	0.0806	0.0457	0.0197	0.0277	0.02723333	0.03571	0.1380	0.0377	0.0500
Total	97.9353	97.5705	97.9367	97.6441	97.4625067	97.14999	97.3662	97.5443	97.9845
n	33	25	17	12	3	1	18	51	11

Table 3: Chemical analysis of two amphibole groups in sample bhcm418m1 (Boone). Component abbreviations: Tr=tremolite; Ftr=ferrotremolite; Ts=Tschermakite; Prg=pargasite; Gln=gluacophane

Amphibole Composition (bhcm418m1)			
Site	Occupying Cation	Early (formula units)	Late (formula units)
T1	Si	6.5513	6.5206
T2	Al^{IV}	1.3630	1.3907
M2	Al^{VI}	0.7421	0.8017
	Mg	0.6948	0.6328
	Fe	0.5595	0.5617
M13	Mg	1.7022	1.6773
	Fe	1.3705	1.4894
M4	Ca	1.9115	1.8117
	Na	0.0885	0.1883
A	Na	0.4989	0.3666
	[]	0.5011	0.6334
XTr		0.1516	0.1115
XFtr		0.1219	0.0985
XTs		0.1921	0.3295
XPrg		0.4989	0.3666
XGln		0.0442	0.0942

Table 4: Average Garnet Compositions from Boone location (*representative spot analysis) compared to those of previous study (Anderson, 2011)

	north				south					Anderson, 2011	
	Bhcm418 m1	Bhcm418 m2	Bhcm418 m2 (core)*	Bhcm418 m2 (rim)*	Bjm218 b	Bjm318m 2	Bjm518m 1	Bjm618 b	Bjm718	core	rim
SiO_2	38.38282	38.1739	38.17369	38.25589	38.1888	37.4958	37.7974	37.8597	38.2136	38.04	37.69
TiO_2	0.13369	0.1931	0.1048	0.04856	0.0701	0.0557	0.0643	0.1086	0.1112		
Al_2O_3	22.86250	21.3858	21.33483	21.38173	21.3203	21.2947	21.1998	20.8959	21.0077	21.54	21.55
FeO	20.60411	27.4874	28.77669	27.07249	28.0892	27.8570	27.4500	26.5443	25.5166	25.29	25.14
MnO	0.87616	0.9549	0.69807	1.08399	0.6038	0.8640	0.6196	1.1212	1.4556	1.90	1.19
MgO	2.41554	3.4560	3.60124	3.27318	3.6026	3.8040	3.6470	3.7195	2.4251	2.80	3.04
CaO	14.62257	9.7943	8.70565	10.03858	9.4923	9.1439	10.1902	10.1819	12.0818	10.61	10.78
Na_2O	0.01841	0.0198	0.00001	0.01874	0.0177	0.0195	0.0154	0.0159	0.0226		
K_2O	0.00260	0.0021	0.00103	0.00001	0.0006	0.0031	0.0016	0.0015	0.0021		
Cr_2O_3	0.05347	0.0206	0.01608	0.04188	0.0087	0.0279	0.0211	0.0508	0.0135		
Total	99.97186	101.4878	101.4121	101.215	101.3939	100.5655	101.0066	100.4993	100.8498	100.17	99.38
n	30	37	1	1	19	10	14	24	25		

Table 5: Average Feldspar Compositions from Boone location (profiles within mapped areas)

	north			south					
	Bhcm518*	Bhcm418m1	Bhcm418m2	Bjm218b	Bjm318m2	Bjm518m1	Bjm518m2	Bjm618b	Bjm718
SiO_2	65.7190	58.4620	58.5214	61.1364	60.6939	61.6300	61.3663	66.4788	60.9437
TiO_2	0.0174	0.0070	0.0043	0.0119	0.0064	0.0070	0.0043	0.0080	0.0054
Al_2O_3	21.4895	26.3609	25.9952	24.2944	23.6136	23.4487	23.9726	20.0767	24.4775
FeO	0.3555	0.3038	0.2140	0.5775	0.3808	0.4600	0.2423	0.2243	0.2474
MnO	0.0137	0.0100	0.0143	0.0153	0.0000	0.0085	0.0221	0.0055	0.0091
MgO	0.0000	0.0016	0.0087	0.0439	0.0072	0.0042	0.0031	0.0054	0.0049
CaO	2.3721	8.3788	7.9495	5.9648	5.4849	5.4480	5.2759	1.4093	6.1902
Na_2O	10.5924	7.1205	7.5786	8.5527	9.1499	9.0726	9.1027	11.1225	8.3384
K_2O	0.0376	0.0170	0.0151	0.0085	0.0140	0.0390	0.0433	0.0434	0.0216
Cr_2O_3	0.0153	0.0056	0.0090	0.0078	0.0102	0.0086	0.0053	0.0078	0.0070
Total	100.6125	100.6672	100.3102	100.6133	99.3609	100.1265	100.0381	99.3816	100.2452
n	3	20	14	15	2	7	2	4	16

Table 6: Average Accessory Phase Compositions from Boone location (profiles within mapped areas)

	north		south	
	epidote			Prehnite*
	Garnet inclusion	Matrix	Garnet inclusion	matrix
	Bhcm418m1	Bhcm418m2	Bjm718	Bjm618b
SiO_2	38.3503	38.0571	37.6019	42.8337
TiO_2	0.1445	0.1384	0.1889	0.0513
Al_2O_3	26.1627	24.7520	25.7079	22.7786
FeO	8.9758	11.1620	9.6172	1.4878
MnO	0.0900	0.0672	0.0362	0.0197
MgO	0.0665	0.0823	0.0247	0.0139
CaO	23.5513	23.2662	23.5586	26.9500
Na_2O	0.0050	0.0062	0.0136	0.0142
K_2O	0.0040	0.0023	0.0028	0.0026
Cr_2O_3	0.0799	0.0240	0.0153	0.0106
Total	97.4299	97.5575	96.7671	94.1624
n	10	15	3	23

Table 7: Average garnet compositions from Bakersville

	Bkmc0118a		Bkmc0218b		Bkmc0418a		Bkmc0518a	
	Core	rim	Core	rim	core	rim	core	rim
SiO_2	39.5125	38.2994	38.3092	39.6209	38.2905	36.9286	39.5981	39.634
TiO_2	0.095399	0.0570	0.0395	0.0208	0.95993	0.33558	0.0464	0.05369
Al_2O_3	21.4306	21.6198	22.341	21.8108	21.8615	21.9412	21.7468	21.4647
FeO	24.7429	22.4686	22.323	22.6662	22.6621	25.1357	21.8752	23.3397
MnO	1.4183	0.32655	0.69128	0.91489	0.68098	0.74501	0.52292	0.6616
MgO	5.7223	8.1406	7.4674	7.1723	6.7901	5.4122	8.5185	6.9861
CaO	8.8925	8.4939	9.044	8.8734	9.6582	8.7057	9.0734	8.8806
Na_2O	0.0313	0.032448	0.041196	0.0408	0.0119	0.011429	0.0127	0.0140
K_2O	0.007	0.00687	0.00	0.00	0.0056	0.0057	0.01169	0.015
Cr_2O_3	0.23441	0.19338	0.11531	0.41708	0.0484	0.051461	0.15009	0.1878
Total	102.0876	99.6388	100.3728	101.5382	100.9692	99.2726	101.5557	101.2376

Table 8: Average pyroxene compositions from Bakersville

	Bkmc0118a			Bkmc0218b	Bkmc0518a
	Omph core	Omph rim	Spongy cpx	Spongy cpx	Spongy cpx
SiO_2	54.1923	51.8535	49.9279	51.64	52.2177
TiO_2	0.301	0.3297	0.31806	0.27605	1.103
Al_2O_3	8.8231	7.8394	4.5171	5.275	3.2656
FeO	5.5135	6.3686	7.9131	7.6191	7.0695
MnO	0.095654	0.10843	0.05237	0.1696	0.072381
MgO	10.6609	11.2673	12.928	12.8309	13.5967
CaO	17.4878	19.1517	22.0556	22.2797	22.5734
Na_2O	3.8332	2.6073	1.0716	1.3166	0.98797
K_2O	0.0056	0.005	0.1403	0.15444	0.011626
Cr_2O_3	0.0784	0.085	0.0907	0.18372	0.043053
Total	100.9915	99.617	99.0148	101.745	100.9408

Table 9: Average amphibole compositions from Bakersville

	Bkmc0118a	Bkmc0218b		Bkmc0418a	Bkmc0518a
		Kelyphite			
SiO_2	43.7366	41.9344	43.8709	45.2634	45.0061
TiO_2	0.99413	0.2138	0.49981	0.55728	1.0931
Al_2O_3	11.2165	14.8601	13.3342	10.6823	9.9763
FeO	10.7286	12.017	11.8967	14.7257	11.3345
MnO	0.04062	0.11782	0.11462	0.09955	0.15147
MgO	13.7793	12.4356	12.8727	11.5591	13.8213
CaO	11.6148	12.1589	11.9341	11.8136	11.9497
Na_2O	6.91	2.4734	2.3695	1.3973	1.8893
K_2O	0.33215	0.2024	0.1741	0.0323	0.4748
Cr_2O_3	0.39633	0.22022	0.22436	0.0689	1.1977
Total	99.749	96.6336	97.291	96.1995	96.6943

Table 10: Average feldspar compositions for Bakersville

	Bkmc0118a		Bkmc0218b		Bkmc0418a			Bkmc0518a
	spongy	Interstitial	Kelyphite		1	2	3	
SiO_2	59.9874	61.9324	44.7631	60.3538	47.2077	51.0596	57.2892	61.6297
TiO_2	0.0643	0.032472	0.22609	0.0099	0.026959	0.024045	0.018627	0.051906
Al_2O_3	22.9039	23.2455	34.1984	24.2409	32.0739	30.0438	26.6895	23.282
FeO	0.628	0.56935	0.63502	0.59436	2.3668	5.5162	1.7754	0.26563
MnO	0.05339	0.055477	0.068086	0.01478	0.0111	0.012019	0.011468	0.039868
MgO	0.22047	0.097205	0.48205	0.062049	0.076737	0.0888	0.078361	0.034303
CaO	6.2907	5.7048	17.8691	6.5956	15.468	12.0587	6.2323	5.6456
Na_2O	7.7276	8.0019	1.0008	7.7314	2.0364	3.1287	5.9599	8.3024
K_2O	0.11781	0.11507	0.13021	0.053084	0.010996	0.016812	0.0009	0.19193
Cr_2O_3	0.014332	0.01365	0.20839	0	0.022507	0.023855	0.02686	0.00
Total	98.0092	99.7679	99.5813	99.6562	99.3012	101.97	98.09	99.4476

APPENDIX B: SELECTED BAKERSVILLE AMPHIBOLE COMPOSITION MAPS

In the mapped area of sample bkmc0118a, amphibole shows higher concentration of Al (13 wt%) where it is in contact with garnet (Fig 1A). Amphibole between garnet and primary omphacite is high in Mg (15.5 wt%) (Fig 1B), and amphibole between garnet and clinopyroxene is low in Ti (0.8 wt%) compared to fine-grained symplectitc amphibole (1.2 wt%) (Fig 1C).

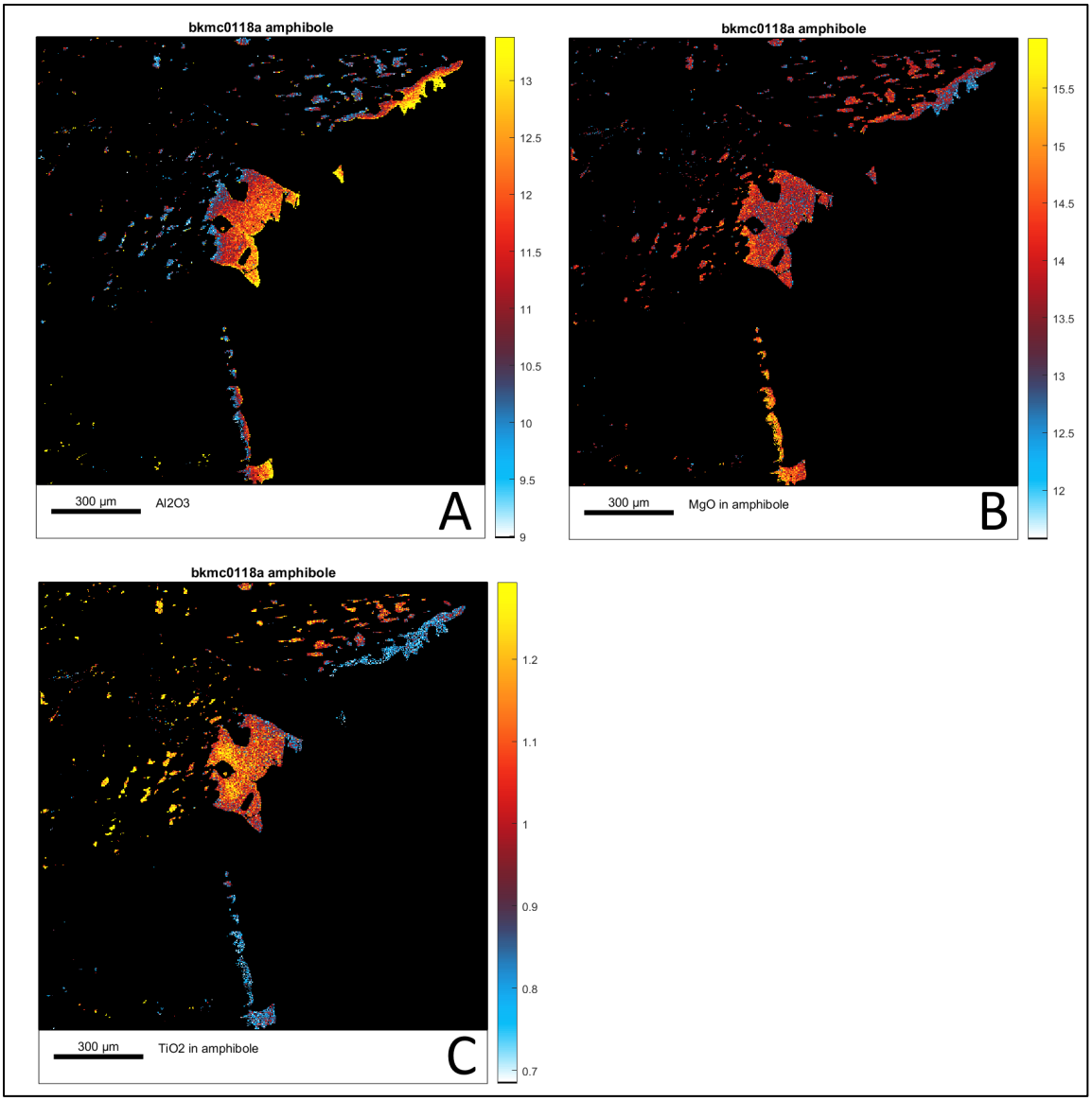

Figure 1: Selected oxide concentration spatial distributions in amphibole for sample bkmc0118a. A) Al_2O_3; B) MgO; C) TiO_2.

In the mapped area of sample bkmc0218b, amphibole occurs as semicircular kelyphite that intrudes into garnet, at the edge of garnet, and as symplectite together with calcic CPX and sodic Plagioclase. The highest concentration of Al is found in the kelyphite (15.5 wt%) and the lowest at the interface with CPX (~13 wt %) (Fig 2A). K and Na are slightly higher in kelyphite compared to symplectite (Fig 2B, D). TiO_2 is lowest in kelyphite while high concentrations are found in coarse grains adjacent to CPX and pyrite (Fig 2C).

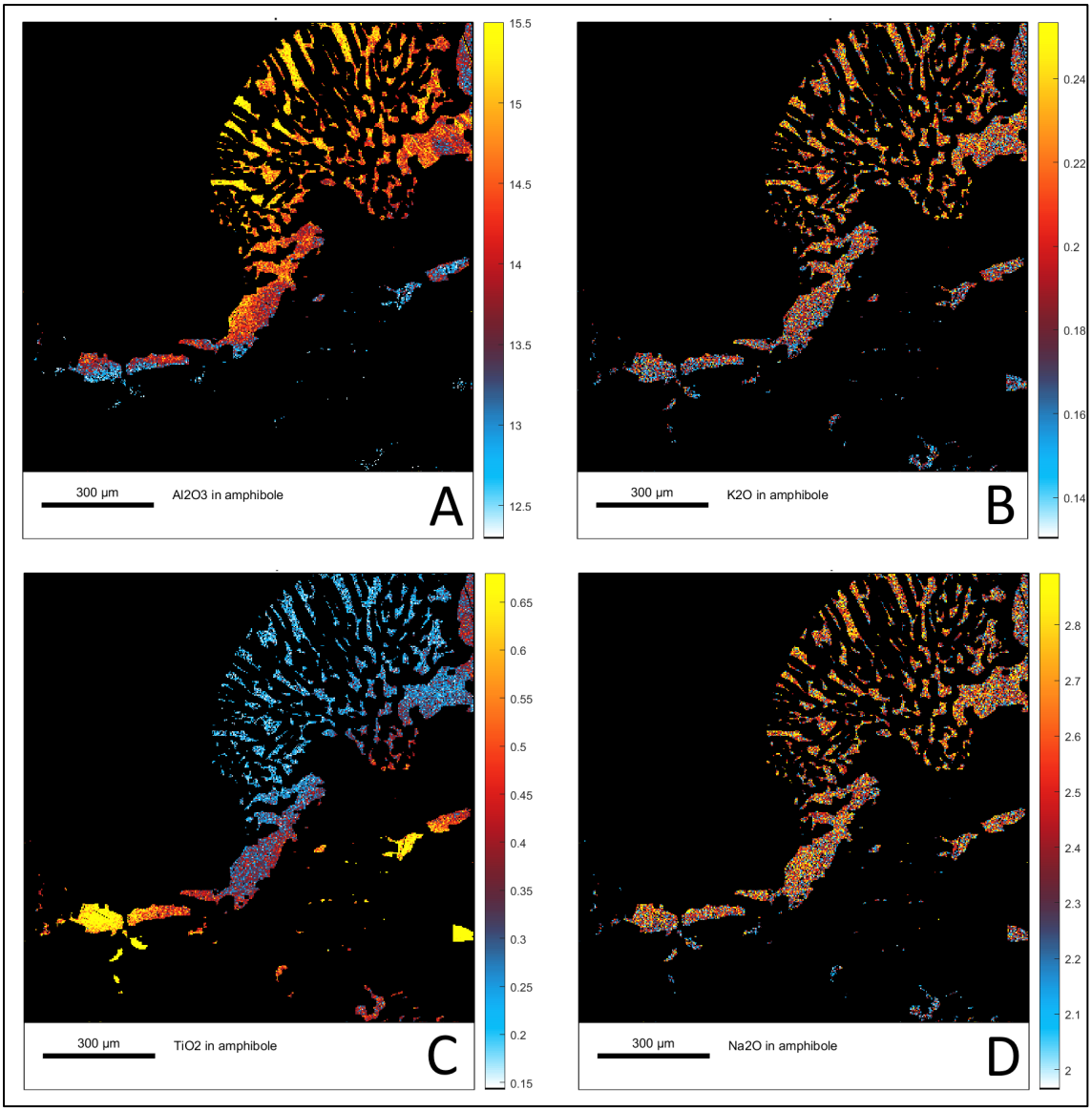

Figure 2: Selected oxide percent spatial distributions in amphibole for sample bkmc0218b. A) Al_2O_3; B) K_2O; C) TiO_2; D) Na_2O

In the mapped area of sample bkmc0418a, high concentrations of Al (>= 11.5Wt%) occur around rutile and radiate outwards from garnet (Fig 3). The highest concentrations of Ti (>= 0.8 wt%) are directly adjacent to rutile and decrease with distance (Fig 3). High concentrations of Mg >=12.6 are patchy while moderate concentrations (~11.6-12.4 wt%) occur where amphibole has a sieve-like texture with quartz inclusions (Fig 3).

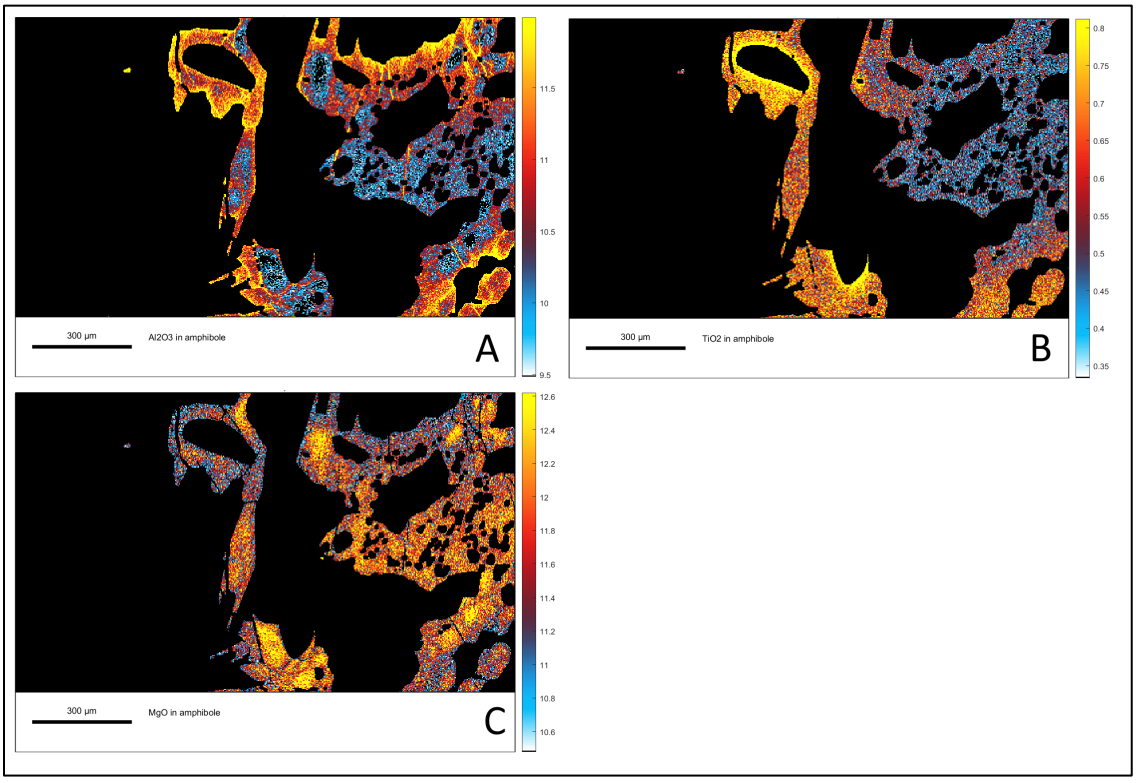

Figure 3: Selected oxide concentration spatial distributions in amphibole for sample bkmc0418a. A) Al_2O_3; B) TiO_2; C) MgO

In the mapped area of sample bkmc0518a, high concentrations of Al around 11 wt% oxide occur adjacent to plagioclase feldspar and garnet (Fig 4A). The highest concentrations of Ti (>= 1.4 oxide wt%) occur in symplectitc amphibole away from garnet (Fig 4B). Interestingly, high concentrations of Cr comparable to those of Ti are found adjacent to garnet (Fig 4C).

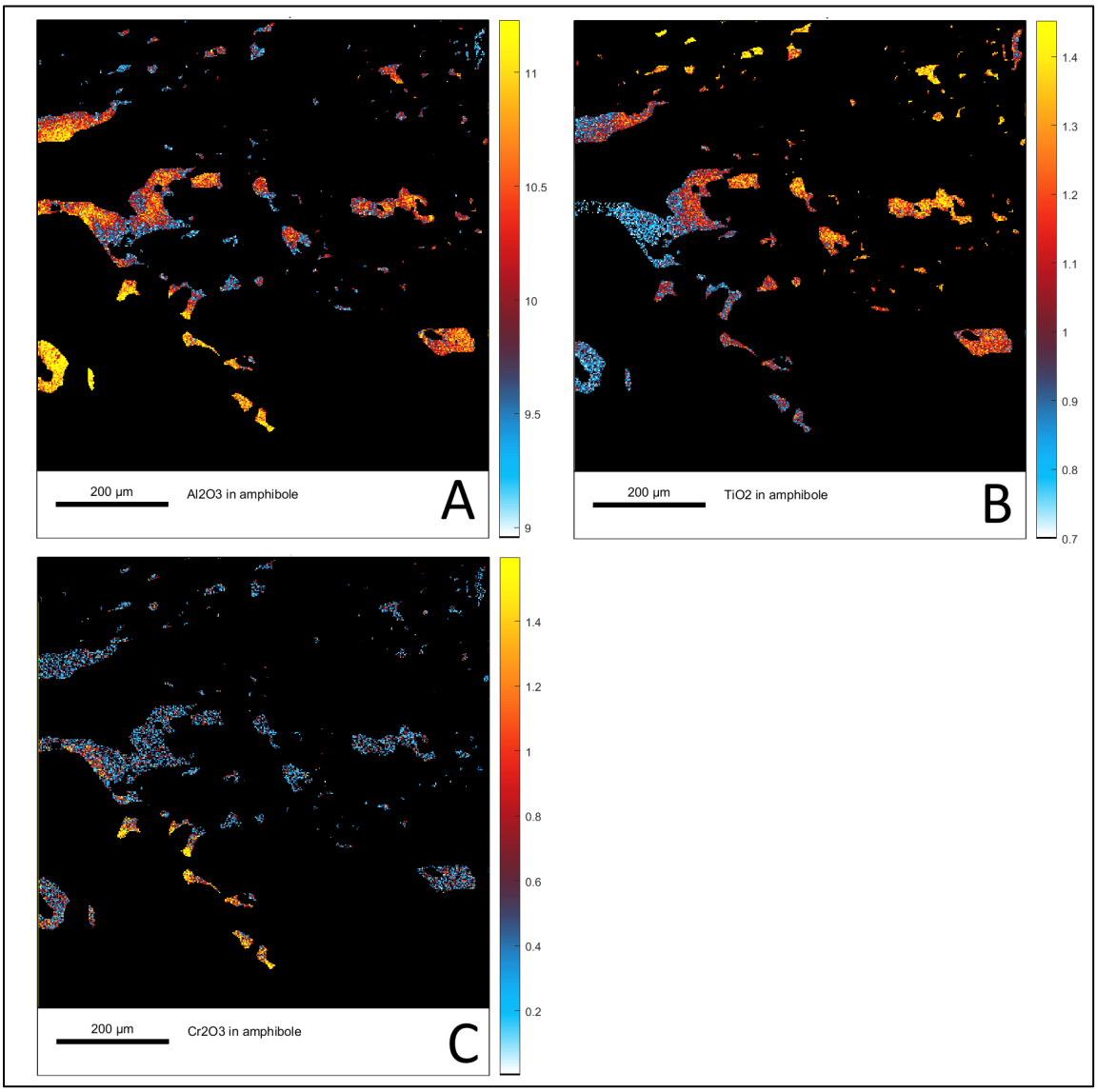

Figure 4: Selected oxide concentration spatial distributions in amphibole for sample bkmc0518a. A) Al_2O_3; B) TiO_2; C) Cr_2O_3

APPENDIX C: BOONE GARNET GROWTH ZONES

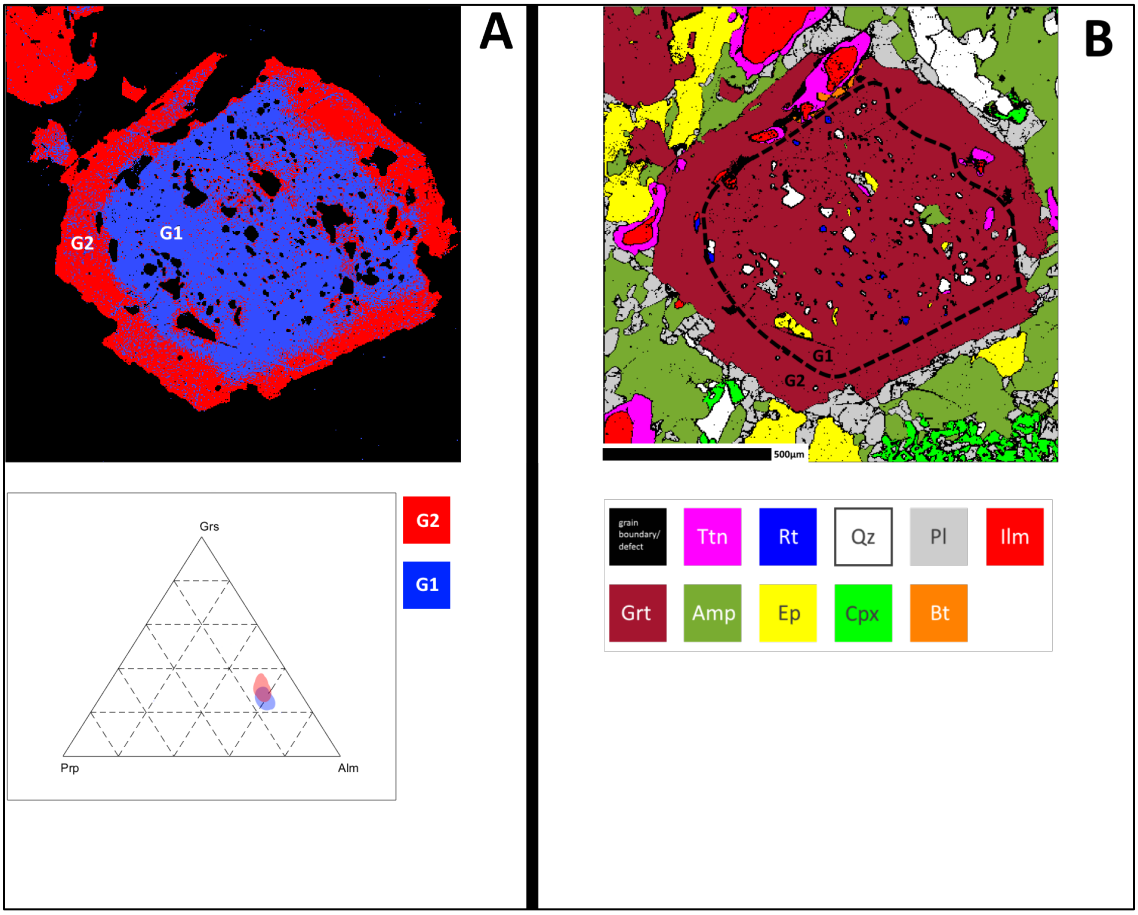

Figure 5: Description of growth zones in garnet from sample bhcm418m2. (A) Two growth zones in garnet. . (B) Compared to G1, G2 has less inclusions overall and lacks rutile, hornblende, quartz, and epidote but gains ilmenite and biotite.

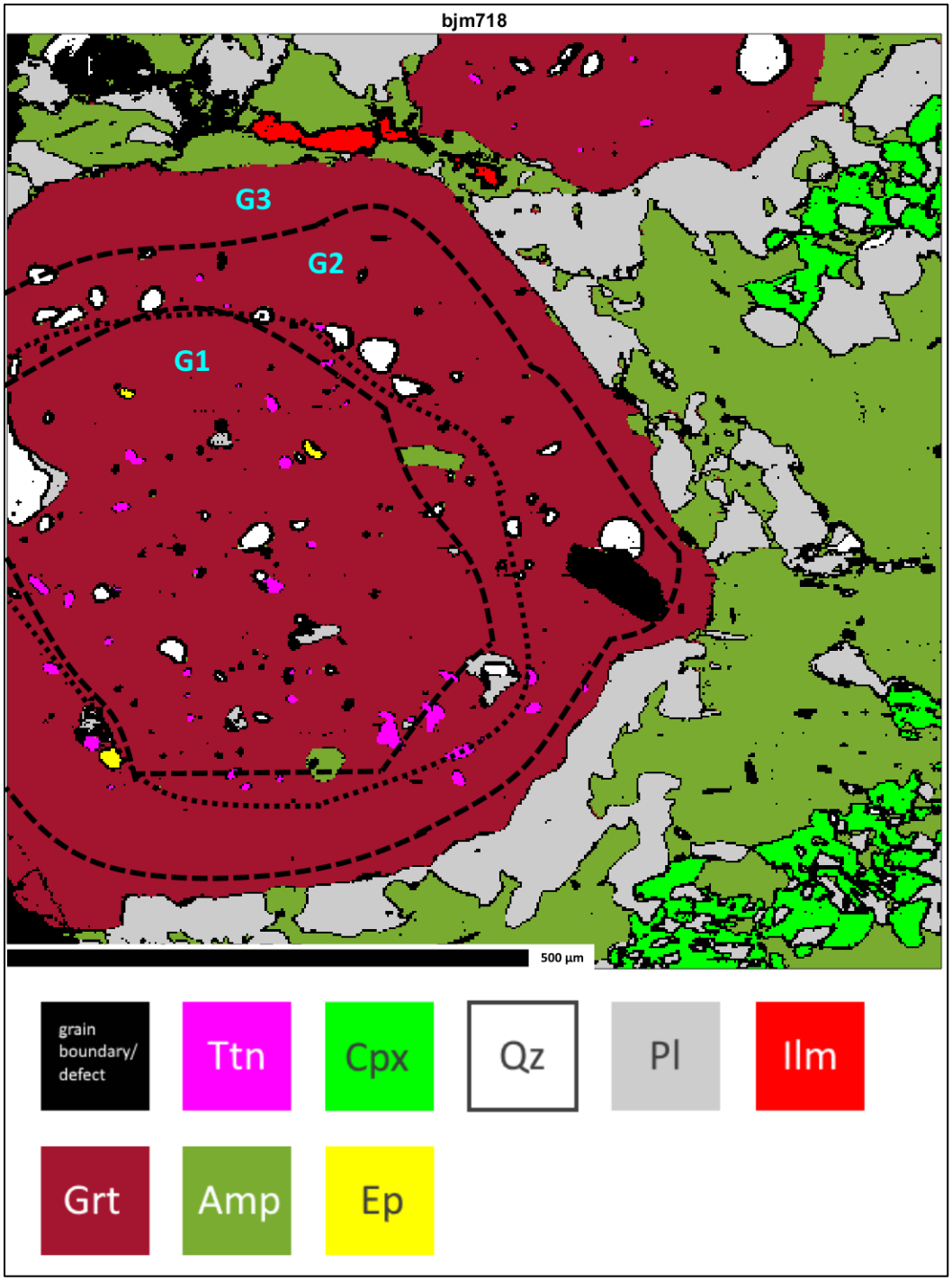

Figure 6: Description of growth zones in garnet from sample bjm718. Three growth zones in garnet from southern sample bjm718. G1 is core comprised of high Mn (short dashed line) and moderate Ca that nearly coincide and contains most of the inclusions. G2 is a zone of high Ca and begins where the Mn-rich core ends, is marked by the absence of epidote and the appearance of amphibole, and has less inclusions overall compared to G1. G3 is a thin rim of low Ca that is devoid of inclusions.

APPENDIX D: BOONE PYROXENE AND AMPHIBOLE COMPOSITIONS

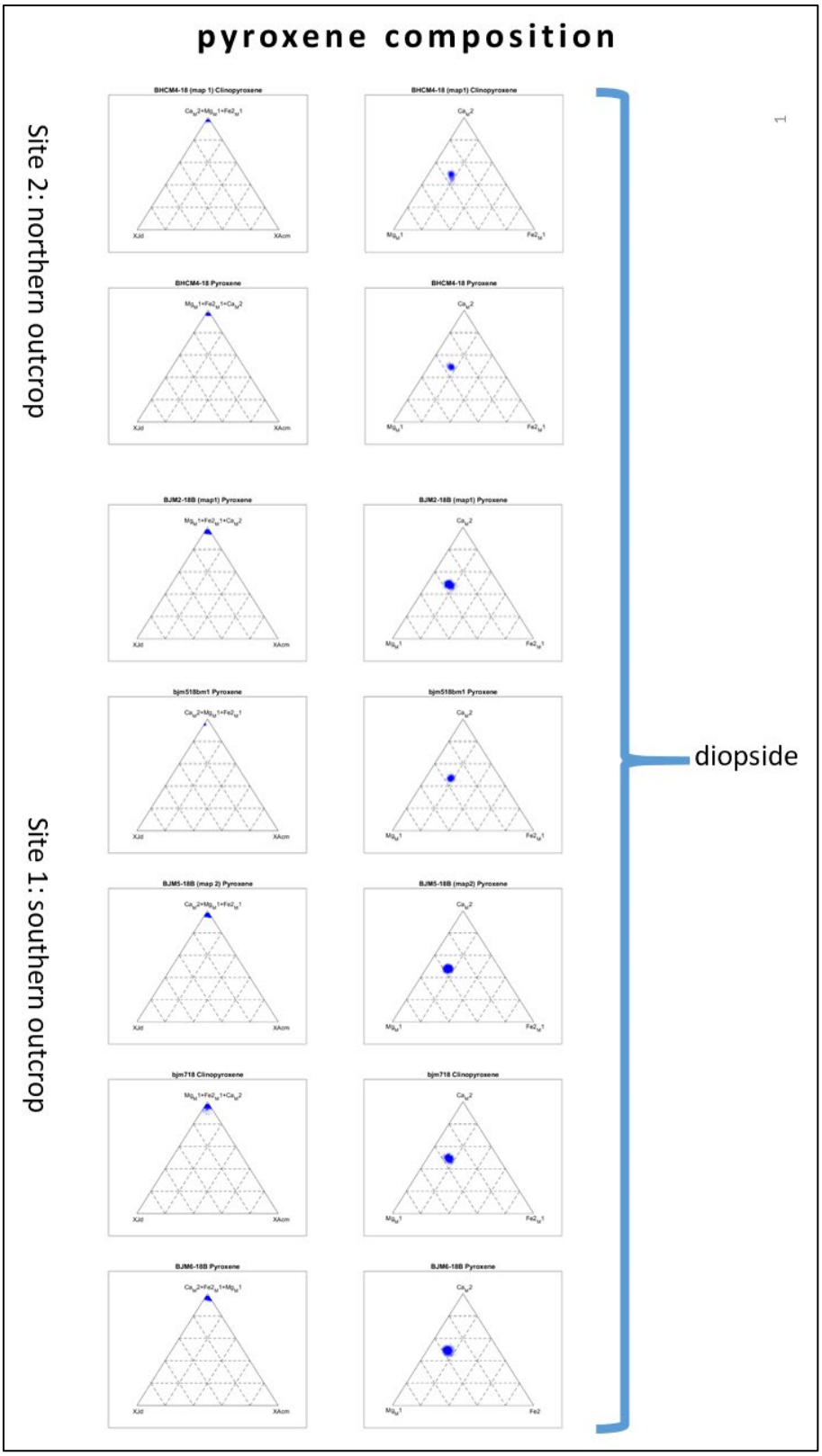

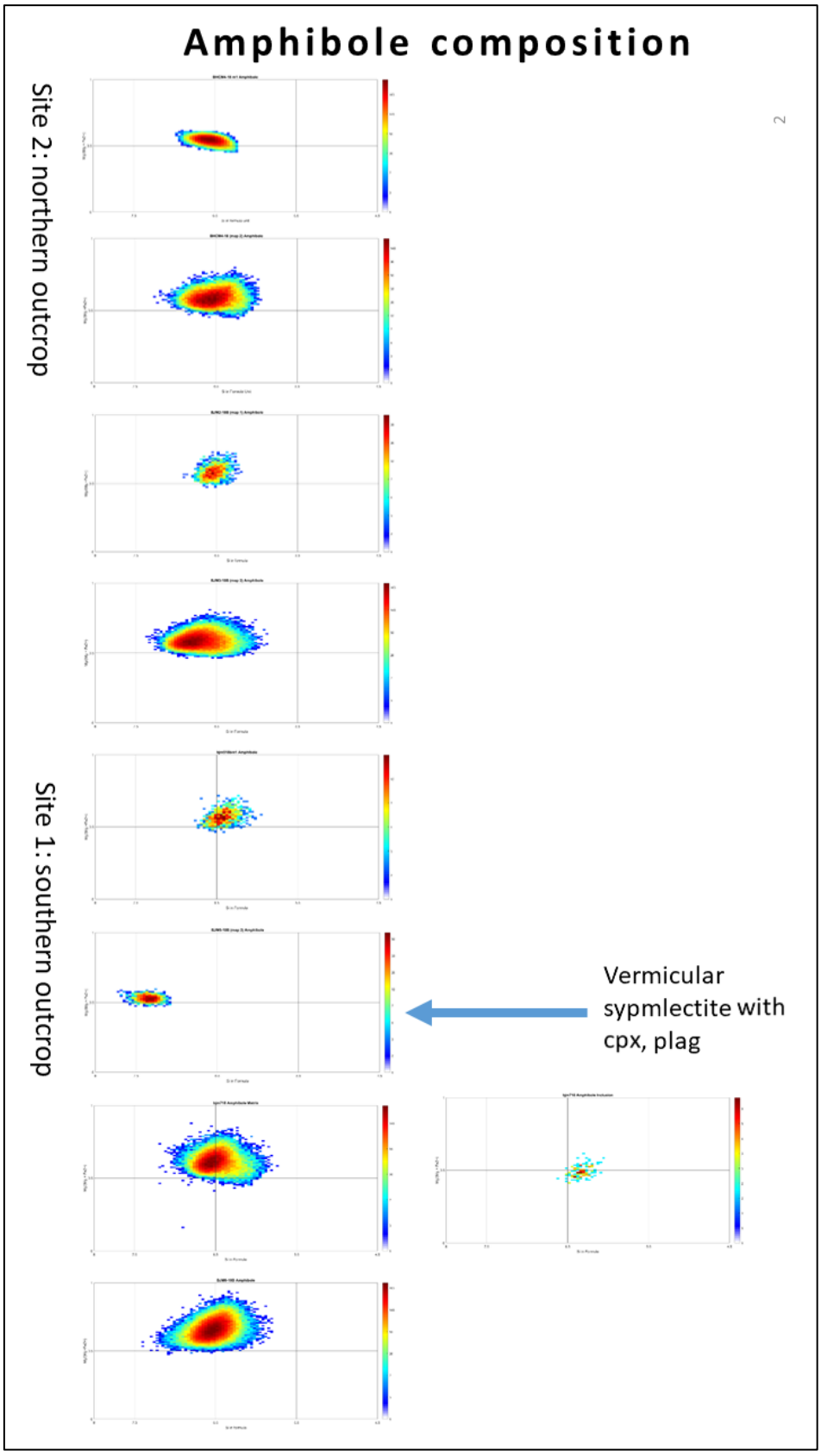
Amphibole composition
Site 2: northern outcrop
Site 1: southern outcrop
Vermicular sypmlectite with cpx, plag